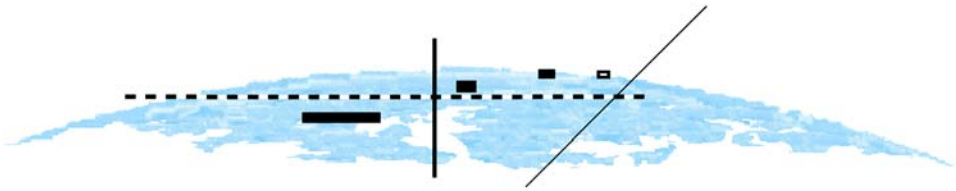

GeoForschungsZentrum Potsdam

STIFTUNG DES ÖFFENTLICHEN RECHTS

Scientific Technical Report

ISSN 1610-0956

GFZ - STR07/06

Aus der Sektion 3.3 – Klimadynamik und Sedimente am GeoForschungsZentrum Potsdam

---

Microfacies and isotope analyses of the varved Piànico lake sediment profile for high-resolution reconstruction of interglacial climate dynamics

Dissertation
zur Erlangung des akademischen Grades
"doctor rerum naturalium"
(Dr. rer. nat.)
in der Wissenschaftsdisziplin "Geologie"

eingereicht an der
Mathematisch-Naturwissenschaftlichen Fakultät
der Universität Potsdam

von

Clara Mangili

Potsdam, im November 2006

DOI: 10.2312/GFZ.b103-07065

In all things of nature there is something of the marvelous

Aristotle

DOI: 10.2312/GFZ.b103-07065

Table of Contents

DOI: 10.2312/GFZ.b103-07065

DOI: 10.2312/GFZ.b103-07065

DOI: 10.2312/GFZ.b103-07065

Abstract

Understanding the climate system and the natural processes that lead to its changes is fundamental when trying to evaluate and assess the human influence on climate variability. Human activities characterised most of the Holocene time period, so that palaeoclimate sequences of the last 8,000 years recorded both climate change and human impact. In order to study natural climate variability, we have to investigate past interglacial climate records, when human impact was none.
Amongst many palaeoclimate archives, lacustrine varved sequences are invaluable records that allow high resolution palaeoclimate reconstruction.
The interglacial lake deposits of Piànico (Southern Alps) consist of ca 15,500 biochemically precipitated calcite varves. The goal of my research is the sedimentological, geochemical and isotopical study at seasonal/decadal resolution of climate variability as recorded in this sequence. The chronology obtained from varve counting constitutes a floating chronology of an interglacial period; the recovery of two tephra layers allowed to fix the floating chronology to the interglacial centred at 400 ka BP, thus corresponding to MIS 11.
I studied the upper 5,900 varves at seasonal resolution, using a multi proxy approach. The thickness of summer layers is the proxy for productivity and spring-summer temperature, whereas detrital layers indicate extreme precipitation events; $\delta^{18}O$ has been used as a proxy for temperature and/or air masses circulation. I developed a new sampling technique for isotope analyses, in order to ensure the sampling of endogenic calcite, avoiding detrital contamination; this method also allowed me to quantify the effect of Triassic dolomite in bulk carbonate samples.
The 15.5 ka of interglacial conditions in Piànico are characterised by short-term climate change. At least four rapid climatic oscillations and a climatic deterioration at the very end of the 15,500 years are recorded. The main climatic oscillation is a 1000 years long cold period that took place after ca 10,000 years of interglacial conditions.
This type of climate oscillation has not been recorded in the Holocene yet. This implies that, so far, the Holocene has not experienced all the possible range of interglacial climate changes.

DOI: 10.2312/GFZ.b103-07065

Zusammenfassung

Um die anthropogenen Einflüsse auf das Klimasystem verstehen zu können sind Kenntnisse über ablaufende Prozesse und Mechanismen in diesem System von grundlegender Bedeutung.
Spätestens seit dem Holozän greift der Mensch in das Klimasystem ein, demzufolge enthalten paläoklimatische Sequenzen der letzten 8.000 Jahre Signale des anthropogenen Einflusses sowie der natürlichen Klimavariabilität.
Um Aussagen über die natürliche Klimavariabilität treffen zu können ist es deshalb notwendig, frühere Warmzeiten zu untersuchen und mittels objektiver Parameter (Proxies) zu beschreiben. Jahreszeitlich geschichtete lakustrine Sedimente (Warven) erweisen sich hierbei als sehr gutes Archiv und erlauben paläoklimatische Rekonstruktionen mit höchster Auflösung.
Die fossilen, warmzeitlichen Ablagerungen des Piànico-Sees in den südlichen Alpen bestehen aus 15.500 biochemisch gefällten Kalzit-Warven. Forschungsgegenstand dieser Arbeit ist eine Analyse der saisonalen und dekadischen Klimavariabilitäten in dieser Sequenz, deren Chronologie auf Warvenzählung basiert. Eine absolute zeitliche Einordnung konnte mit Hilfe zweier Tephralagen erreicht werden, denen zufolge der untersuchte Bereich im marinen Isotopenstadium 11 (~ 400 ka BP) liegt.
Bei der Untersuchung der obersten 5.900 Warven wurde beobachtet, dass die Mächtigkeit der Sommerlage als Anzeiger für biologische Produktivität und die Wassertemperatur nutzbar ist. Enthaltene detritische Lagen sind als Ergebnis extremer Niederschlagsereignisse zu werten. Darüber hinaus ermöglicht die Messung stabiler Sauerstoffisotope ($\delta^{18}O$) die Rekonstruktion von Temperatur und atmosphärischer Zirkulation. Für diese Isotopenmessungen wird eine neue Methode vorgestellt, mit deren Hilfe eine saubere, jede Verunreinigung durch detritische Komponenten vermeidende Beprobung des endogenen Kalzits durchgeführt werden kann.
Die Ergebnisse dieser Arbeit zeigen, dass der 15.500 Jahre lange interglaziale Zeitraum in Piànico durch kurzfristige klimatische Schwankungen gekennzeichnet ist. Mindestens vier rapide und deutlich kältere Intervalle sowie eine generelle Abkühlung zum Ende des Interglazials konnten identifiziert werden.
Die markanteste Unterbrechung warmzeitlicher Bedingungen bildet hierbei eine etwa 1.000 Jahre lange Periode ca. 10.000 Jahre nach Beginn des Interglazials.
Da solche Schwankungen für das Holozän unbekannt sind, ist anzunehmen, dass die bis heute andauernde Warmzeit bisher nicht den vollen Umfang möglicher, natürlicher Variabilität erfahren hat.

DOI: 10.2312/GFZ.b103-07065

Acknowledgements

My first thanks are for the supervisor of my Ph.D. project, Achim Brauer. His continuous availability and constant presence during the three years of project were invaluable and nowadays so rare to find in our rushing world. All his efforts for guiding and teaching me the know-how of science are also gratefully acknowledged.

Special thanks also to Gerald Haug for supporting the project and for always caring that everything was running smooth.

This study would have not been possible without the help of many people; to all of them my thanks. Birgit Plessen performed the isotope analyses and Petra Meier helped with the samples preparation. Peter Dulski ran the µ-XRF measurements. Gabi Arnold, Michael Köhler and Dieter Berger prepared high-quality thin sections. Rudolf Naumann carried out the XRD analyses. Helga Kemnitz and Juliane Herwig taught me how to use the S.E.M. and helped during S.E.M. analyses. Andreas Hendrich and Manuela Dziggel drew many of the figures used in the publications. Christine Gerschke helped me untangling from the labyrinth of bureaucracy. Thanks also to the other members of the Section 3.3 of GFZ for the suggestions I received and for the constructive discussions we had in these years.

I am very grateful to Andrea Moscariello for his wise advices and for his encouragement.

Finally, I would like to thank Gergana Yancheva, Susanne Blumberg, Olga Kwiecien, Iris Kristen, Sebastian Breitenbach and Christian Wolff; they have been my family for the last three years.

DOI: 10.2312/GFZ.b103-07065

1. Introduction

Weather and climate are part of the daily experience of human beings. A lot of concern arises on the prospect of human-induced climate changes. In particular, the debate is on the role played by humans on the climate system and whether the system has already undergone human-induced climate changes (IPCC, 2001). In order to evaluate the human influence on climate, one has to understand the climate system and the processes that lead to climate variability (IPCC, 2001). Rapid climate changes in interglacial periods have a particular relevance as nowadays a sudden change in climatic conditions could affect the billions of people living on the Earth.

We are currently living in an interglacial period, the Holocene, which has been lasting for at least 10,000 years. During this time interval, the Earth climate has been characterised by mild temperatures and by a relative stability, if compared to the millennial-scale oscillations recorded, for example, in the last glacial period (i.e. Dansgaard et al., 1993; Grootes et al., 1993). During the Holocene, only few climate oscillations have been recorded. At 8.2 ka B.P. a rapid cooling is recorded in the ice cores and on the continents (e.g. Alley et al., 1997; von Grafenstein et al., 1998; Tinner and Lotter, 2001; Veski et al., 2004; Prasad et al., 2006). This cool period lasted 180-200 years and was characterised by a drop in temperatures of ca 2.8°C in Greenland and of ca 1.7°C in central Europe (von Grafenstein et al., 1998). During this period, that is recorded as the most prominent Holocene climate event in Greenland ice-core proxies (Alley et al., 1997), decrease in temperature was already enough to induce vegetation changes in Europe (e.g. Ralska-Jasiewiczowa et al., 1998; Tinner and Lotter, 2001).

The other period of the Holocene in which major changes in climate are recorded lasted from ca 1350 to ca 1850 A.D. and is known as “Little Ice Age” (e.g. Stuiver et al., 1995). These centuries were characterised by high climate variability (e.g. Pfister, 1994; Barlow, 2001) and prolonged periods of climate deterioration that causes, for example on the Alps, readvance pulses of the glaciers. Extreme climatic conditions were reached more frequently and they severely affected human beings by causing, e.g. famine and floods (e.g. Le Roy Ladurie, 1971; Fagan, 2000). During the “Little Ice Age”, human impact was already considerable; the palaeoclimate records of the time are already a combination of natural climate and human impact (e.g. Kienel et al., 2005).

Traces of human activities were observed in palaeoclimate records starting from the 8.2 ka event (Edwards et al., in press) and steadily increased from 8000 years BP (Ruddiman; 2005b). Almost the whole Holocene climate was then affected by human impact, so that study of the natural climate dynamics is not possible. In order to disentangle natural climate signal and human impact, we have to study previous interglacial periods, when human impact was none.

In particular, the last five climatic cycles show stronger variations between the glacial and interglacial periods if compared to the glacial/interglacial cycles between 800 ka BP and 430 ka BP (i.e. +20% δD amplitude in Antarctica; Fig. 1.1; EPICA community members, 2004). The last five interglacials are therefore interpreted to have been warmer than the previous ones (EPICA community members, 2004).

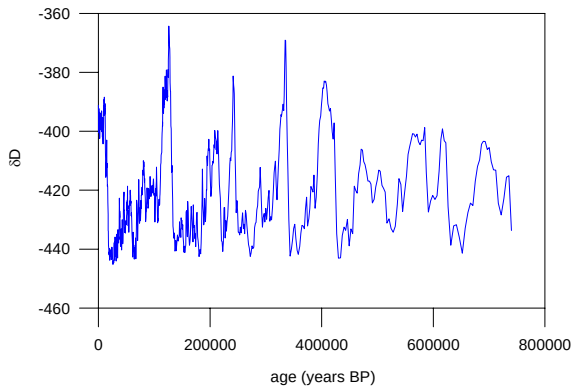

Fig. 1.1: δD record from EPICA Dome C (Antarctica), showing the last eight glacial/interglacial cycles (data from EPICA community members, 2004). Note the change in δD amplitude before and after 430 ka BP.

DOI: 10.2312/GFZ.b103-07065

Records of previous interglacials are usually extracted from marine sediments (e.g. Shackleton et al., 1990; McManus et al., 1999; Lisiecki and Raymo, 2005), ice caps (e.g. Petit et al., 1999; EPICA community members, 2004; North Greenland Ice Core Project members, 2004; Rasmussen et al., 2006) and continental records (e.g. Miyoshi et al., 1999; Ding et al., 2000; Kashiwaya et al., 2001; Dykoski et al., 2005). On land, lakes are one of the archives that can preserve long sediment sequences spanning many climatic cycles (e.g. Wijmstra and Smit, 1976; Follieri et al., 1988; Reille et al., 2000). From these records, information on the general climate trends and on the alternations between glacial and interglacial periods is obtained. Usually, the longer the sequence is, the lower is the sedimentation rate. Sediments from Lake Baikal, for example, span the last 12 Ma and the mean sedimentation rate is 0.05 mm/year (calculated using the data in Kashiwaya et al., 2001). For this sequence, in a sampling carried out at 2 cm intervals, each sample includes ca 500 years (Khursevich et al., 2001).
In contrast, varved records allow reconstructing palaeoclimate at seasonal to annual resolution. Different types of varves form under different environmental conditions: clastic varves occur typically in arctic or high-alpine lakes, biogenic varves (i.e. diatomaceous, calcite and iron-rich varves) are common in temperate climate zones while evaporitic varves are related to arid climates (Brauer, 2004). Annually laminated sequences are mostly known from the Holocene (e.g. Anderson, 1993; Brauer et al., 2001) and the Lateglacial (e.g. Goslar, 1998; Brauer et al., 1999). Varved records from past interglacials are rare (e.g. Müller, 1974; Nitychoruk et al., 2005). The longest varve records are from Suigetsu Lake, Japan (45,000 years; Kitagawa and van der Plicht, 1998) and from Lake Holzmaar, Germany (23,000 years; Brauer et al., 1994; Zolitschka et al., 2000).

1.1. Goal of research

The goal of my research is the study at seasonal/decadal resolution of climate variability as recorded in the ca 15,500 varves of the Piànico sequence. The varved sequence of Piànico is outcropping along a riverbed and represents an isolated interglacial record. The approach used to study this sequence includes two types of dating: the creation of a floating chronology based on varve counting, and the use of absolute/numerical dating to anchor the floating chronology. Absolute/numerical dating of the sequence of Piànico is complicated, as suitable dating methods are lacking.
A multi proxy approach was chosen to study the sequence. For the first time, the study of the varves is carried out at seasonal resolution. The summer layer thickness of varves is used as proxy for summer temperature and lake productivity while the number of calcite sub-layers within a single summer layer is the proxy for temperature at time of calcite precipitation and for the length of the productive season. Detrital layers, sometimes present within single varves, are the proxy for extreme precipitation events. The position of the detrital layers within single varves was used to infer the season in which the extreme precipitation events took place.
$\delta^{18}O$ data are proxies for summer temperature and atmospheric circulation, μ-XRF and XRD data for productivity and detrital influx.

The highest resolution (seasonal) study was concentrated on the topmost 5,900 varves of the sequence. Due to the huge amount of work that this type of study requires, it would have been impossible to study the whole 15,500 years record at seasonal resolution within a 3 years Ph.D. project. Isotope analyses have been carried out on samples including five varves each and span the whole 15,500 years interval, with higher sampling frequency in the upper 9,350 years and lower in the remnant part of the sequence.

DOI: 10.2312/GFZ.b103-07065

1.2. Studied site

1.2.1. Geographical, geological and stratigraphical settings

The Piànico-Sèllere Basin (45° 48' N, 10° 02' E; elevation: 280-350 m a.s.l.) is located in the Borlezza River Valley (Southern Alps, Italy; Fig. 1.2), which is a western tributary of Lake Iseo. The Borlezza Valley is bounded by steep slopes reaching 1460 m a.s.l. The catchment area of the Borlezza River (39 km^2) is entirely located within the Calcareous Southern Prealps. The Upper Triassic bedrock is formed almost entirely by dolomitic rocks of the Dolomia Principale and subordinately by limestone of the Calcare di Zorzino Formation.
The Quaternary geological evolution of the Borlezza Valley has been driven by the multiple glacier advances in the Camonica Valley. Glacial deposits and moraines distribution in the Piànico-Sèllere area indicate that a lateral branch of the Oglio glacier flowed into and up the Borlezza Valley and maybe dammed the river to form a lake (e.g. Stoppani, 1873, 1880).
The Piànico palaeolake was ca 3 km long and 500-800 m wide (Casati, 1968); its topmost deposits are outcropping at an altitude of ca 350 m a.s.l. The presence of varves indicates meromictic deep water conditions.

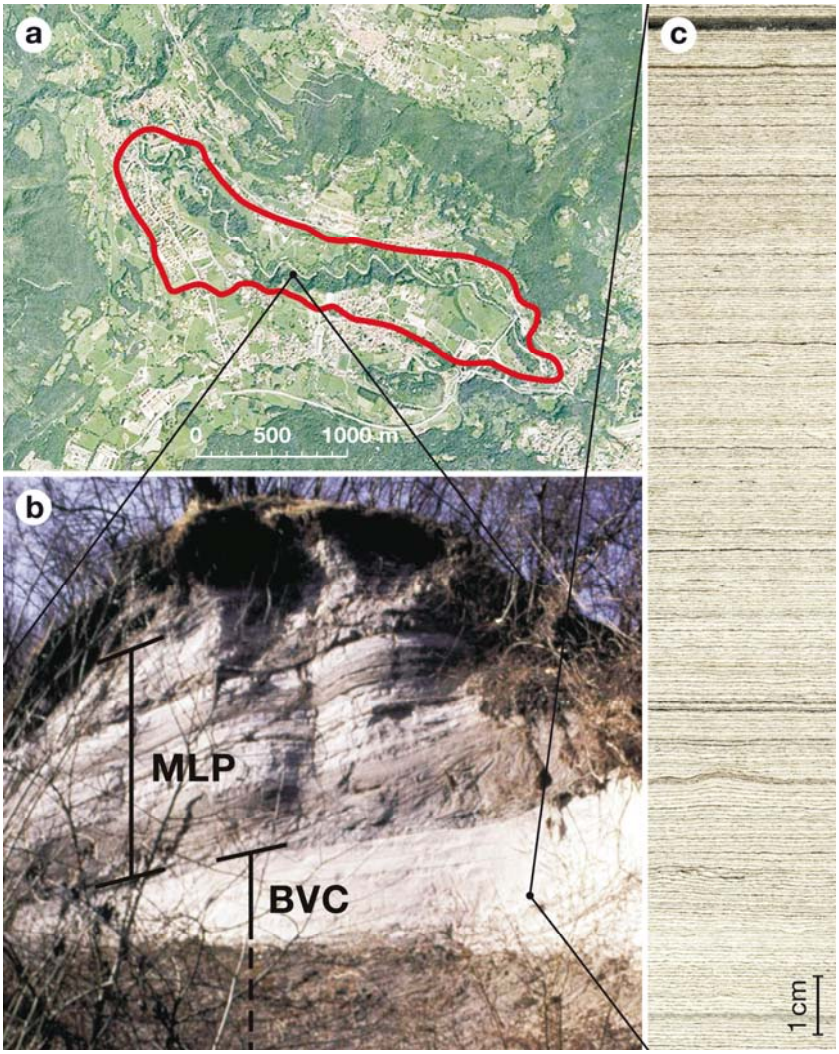

Fig. 1.2: a) Aerial picture of the lower part of the Borlezza Valley (photo courtesy of Regione Lombardia - CGR IT 2000). The red line marks the maximum extension of the palaeolake according to Casati (1968). b) Sediments of the Pianico palaeolake outcropping at the Main Section. c) Varves as they appear in the field.

DOI: 10.2312/GFZ.b103-07065

Probably during the Lateglacial, the Borlezza River cut a deeply incised gully in the Piànico palaeolake sediments, resulting in exceptional exposures of glacial, fluvioglacial and lacustrine sediments on both sides of the river (Moscariello et al., 2000). In the northeastern part of the palaeolake basin, long sequences of lacustrine sediments, known as the Piànico Formation, are outcropping (Moscariello et al., 2000). The Piànico Formation is 48 m thick and has been subdivided into four units of partly finely laminated sediments (from the bottom to the top): BTB (Banco Torbiditico Basale), SAB (Silt e Argille Basali), BVC (Banco Varvato Carbonatico) and MLP (Membro di La Palazzina). The BTB unit is formed by an assemblage of mud turbidites deposited in a peri/proglacial lacustrine environment. The SAB unit consists of non-periodic heterogeneous horizontally laminated mud. These sediments are thought to represent a transition from periglacial to temperate limnic conditions represented by the BVC unit. The BVC represents a long period of interglacial climate as revealed by the continuous formation of at least 15,500 biochemically precipitated calcite varves (Brauer et al., submitted) and by vegetation reconstructions (e.g. Lona and Venzo, 1956; Moscariello et al., 2000; Rossi, 2003). The lithological transition to the overlying MLP unit is sharp and reflects threshold effects of regional glacial processes. The MLP unit exhibits an intercalation of endogenic calcite and detrital intervals reflecting highly variable environmental conditions at the glacial inception. The lithological change at the BVC/MLP boundary allows defining 15,500 years of peak interglacial conditions (BVC unit) and a sequence of millennial scale climate fluctuations (MLP unit).

1.2.2. Previous investigations

The Pianico Basin has been known since the middle of 19th century for its very nicely preserved fossils both of animals and plants (i.e. Stoppani, 1857; Picozzi, 1859; Sordelli, 1873; Curioni, 1877; see Moscariello et al., 2000 for an extensive summary). The floristic assemblage of the varved interval indicates warm interglacial conditions: the species identified are almost all still present in the area, except for some elements that are now typical of the Colchic flora (i.e. *Rhododendron ponticum* L.; i.e. Fischer in Baltzer, 1896) and sporadic tertiary relics detected through pollen analyses (Rossi, 2003). After the period characterised by interglacial conditions, a series of rapid climate oscillations is recorded. During these millennial scale fluctuations, vegetation assemblages alternate between conifers/steppic grasslands dominated intervals (that correspond to detritus-rich sediments) and broad-leaved forests dominated intervals (endogenic calcite rich sediments; Rossi, 2003).

The interglacial sequence was first indicated as belonging to the Riss/Würm interglacial, lately indicated as Eemian (i.e. Casati, 1968; Emmert Straubinger, 1991). This assumption was based on the recovery of only one moraine ridge above the lacustrine sequence (e.g. Baltzer, 1896). A direct dating of a tephra layer at 779 ± 13 ka B.P. correlated the varved sequence to MIS 19 (Pinti et al., 2001).

1.3. Overview of the articles

This Ph.D. thesis is based on five articles: I am the first author of three of them (Chapters 2, 5 and 6), while I am co-author of the other two (Chapters 3 and 4). The articles are presented in the thesis in chronological order.

The floating chronology of the Piànico record is composed of ca 15,500 varves (Chapter 4). The recent discovery of a tephra layer and its tephrochronological dating at 393 ± 12 ka BP allowed anchoring the Piànico interglacial sequence to MIS 11 (Chapters 3 and 6).
The detailed chronology of the upper 5,900 varves is presented in Chapter 4 together with the multi proxy data obtained from the varves. In particular, two periods of reduced calcite

DOI: 10.2312/GFZ.b103-07065

precipitation, indicative of cold climate, are highlighted: a 1000 years period within the interglacial and the last 480 years of the studied interval. In this 480 years interval, a rapid increase in frequency and thickness of detrital layers is observed (Chapter 2). The use of detrital layers as proxy for extreme runoff events is discussed in Chapter 2.

As the amount of endogenic calcite in the varves is very high (up to 98%; Moscariello et al., 2000; Chapter 4), isotope analyses on bulk carbonates were planned. The presence of detrital layers down to 0.03 mm thick and formed by Triassic dolomite coming from the catchment constituted, however, a problem; dolomite has different stable isotope values than endogenic calcite and, if included in isotope samples, dolomite will affect isotope values by adding heavier $\delta^{18}O$ values at the sequence (Chapter 5). Using mixed samples formed by dolomite and endogenic calcite it was possible, for the first time, to quantify the effect of dolomite on the isotope values of endogenic calcite (Chapter 5).

I solved the problem of dolomite presence in the sequence by developing a new sampling procedure (Chapter 5); the intervals to be sampled for isotope analyses were first selected at microscope using thin sections and marking the varves to be sampled, thus avoiding all the detrital layers. Only after applying this sampling methodology the isotope data could be used for palaeoclimate reconstruction (Chapter 6).

The 15,500 years sequence show short-term climate variability and, in particular, four negative $\delta^{18}O$ oscillations and a $\delta^{18}O$ drop at the very end of the studied period. All these oscillations are interpreted as cold periods (Chapter 6). The $\delta^{18}O$ drop at the end of the 15,5 ka period and the 780 years oscillation that takes place after 10,000 years of interglacial conditions coincide with periods of reduced calcite precipitation; the isotope data confirmed what already observed in the varves and support the interpretation of these phases as cold periods.

DOI: 10.2312/GFZ.b103-07065

2. Microfacies of detrital event layers deposited in Quaternary varved lake sediments of the Piànico-Sèllere Basin (Northern Italy)

Clara Mangili *, Achim Brauer *, Andrea Moscariello † and Rudolph Naumann ‡

* GeoForschungsZentrum (GFZ), Section 3.3 - Klimadynamik und Sedimente, Telegrafenberg, D-14473 Potsdam, Germany (E-mail: mangili@gfz-potsdam.de)
† Department of Geography, Godwin Institute of Quaternary Research, University of Cambridge, Downing Place, Cambridge CB2 3EN, United Kingdom
‡ GeoForschungsZentrum (GFZ), Section 4.2 - Anorganische und Isotopen-Geochemie, Telegrafenberg, D-14473 Potsdam, Germany

Published in Sedimentology 52, 927-943

Abstract - *A Quaternary interglacial lake sediment record from the Piànico-Sèllere Basin (Northern Italy) consists of biochemical calcite varves with intercalated detrital layers. At the end of the Piànico Interglacial, continuous varve formation was replaced by predominantly detrital sedimentation. However, 427 varve years before this shift, an abrupt increase in the frequency and thickness of detrital layers occurred. Microfacies analyses reveal a total of 152 detrital layers, ranging from 0.2 to 20.15 mm in thickness, deposited during the last 896 years of the Piànico Interglacial. Three microfacies types are distinguished: (1) graded layers, (2) non-graded silt layers, and (3) matrix-supported layers. The position of detrital layers within an individual varve provides additional information on the season in which they have been deposited. Microfacies analyses in combination with varve counting further enabled precise varve-to-varve correlation of the detrital layers for two sediment sections cropping out ca 130 m apart. The detailed intra-basin correlation allows the source regions of detrital layers to be inferred. Moreover, micro-erosion at sub-millimetre scale has been established. Of the described facies types, only the accumulation of summer and spring graded and non-graded silt layers abruptly increased before the end of interglacial varve formation whereas non-graded winter silt and matrix-supported layers are randomly distributed over the entire study period. Heavy rainfalls are assumed to have triggered spring and summer graded layers, so that the occurrence of these layers is thought to be a proxy for extreme precipitation events in the past.*

Keywords: Detrital layer, calcite varves, intra-basin correlation, Northern Italy

2.1. Introduction

Lakes act as traps for sediments transported by instantaneous mass movements and lake-floor sediments can thus provide a useful archive for reconstructing the nature, magnitude and frequency of event sedimentation in the past. The evaluation of such lacustrine records is important owing to the increasing interest of modern societies in predicting catastrophic events. However, a thorough understanding of the processes associated with each event is crucial. A range of different triggering mechanisms generating event beds in non-glacial lacustrine sequences are reported: (1) subaquatic slope failure due to either sediment instabilities (Ludlam, 1974; Hsü and Kelts, 1985), spontaneous liquefaction through seismic shocks from earthquakes (Rodríguez-Pascua *et al.*, 2000; Shiki *et al.*, 2000) or construction activity (Kelts and Hsü, 1980) and (2), extreme weather events in combination with geomorphological processes (e.g. Hsü & Kelts, 1985). However, the sedimentary processes associated with slope failure induced turbidites in lakes have seldom been observed in nature because the release and re-deposition of sediment is very rapid. The use of sediment traps to sample the flows has only been possible in the case of river-flood discharge events (Stumpf, 1916 in Lambert and Hsü, 1979; Lambert *et al.*, 1976; Hsü and Kelts, 1985). Such

DOI: 10.2312/GFZ.b103-07065

event deposits in lacustrine environments have been labelled as turbidites (Sturm and Matter, 1978) since sediment transport processes in turbulent flows are virtually the same as in the marine realm where the term turbidite was first introduced (Kuenen, 1950; 1951).

The term lacustrine turbidite is commonly used to describe a normally graded layer consisting of coarse to medium sand grains passing upwards to silt and clay. However, this study reports on a wide range of layers of detrital material washed into a lake by instantaneous events. These layers display a variety of internal structures and compositions. Therefore, in this study the generic term 'detrital (event) layer' will be used to describe laminae composed of allogenic material that can be microscopically distinctly distinguished from the autochthonous components of the sediments.

The aim of this study is to provide more detailed knowledge on the origin of detrital layers in lake sediments and their triggers. This includes the reconstruction of (i) sedimentary processes, (ii) the spatial distribution within the basin, and (iii) the timing (season) of deposition. Microfacies techniques are applied to achieve these goals. The Piànico-Sèllere lake deposits (Northern Italy) have been selected for two reasons: (1) their annual layering enables robust intra-basin correlation and precise determination of the timing of events, and (2) the detrital layers are of different composition to the autochthonous lacustrine sediments.

2.2. Site description

The Piànico-Sèllere Basin (45°48' N, 10°2' E; Province of Bergamo; Fig. 2.1) is located in the lower part of the Borlezza Valley (Orobic Prealps), a tributary valley of the Camonica Valley in Northern Italy. The Borlezza Valley is drained by a small river with a length of 27.3 km discharging into Lake Iseo (Bertuletti and Carollo, 1973). This river has incised a valley in to the sedimentary fill of the Piànico-Sèllere Basin revealing a series of outcrops of Quaternary lacustrine sediments (Moscariello *et al.*, 2000). The altitude of these exposures ranges between 280 m a.s.l. and 350 m a.s.l., but the lower boundary of the lacustrine deposits is not exposed so that the total thickness of the sediment infill remains unknown. The size of the palaeolake has been reconstructed to ca 3 km in length and 500-800 m in width (Casati, 1968; Figs 2.1 and 2.2a). The lake is assumed to have been rather deep as formation and preservation of varves clearly indicates anoxic conditions at the lake bottom. The steep slopes surrounding the palaeolake area reach more than 900 m a.s.l. (Fig. 2b).

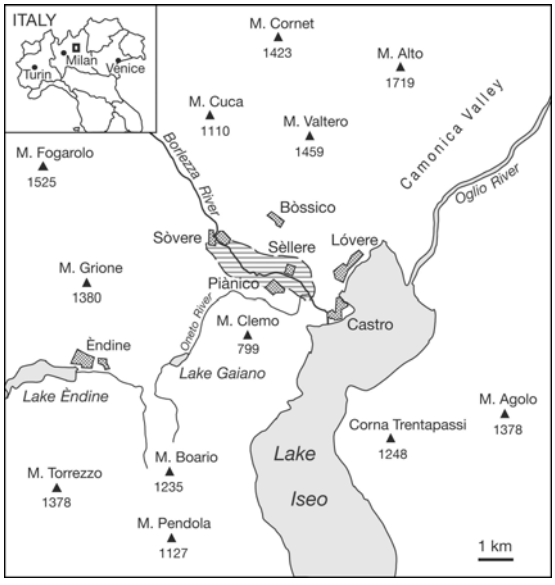

Fig. 2.1: Location of the Piànico-Sèllere Basin and reconstruction of the Piànico palaeolake (dashed area; modified after Casati, 1968).

DOI: 10.2312/GFZ.b103-07065

The current catchment area of the Borlezza River has been estimated as 146.3 km^2 (Bertuletti & Carollo, 1973). Separation of the lower section of the Borlezza Valley from the upper by a morphological barrier as suggested by Chardon (1969) would have reduced the palaeo-catchment to an area of less than 13 km^2 in the past (Moscariello *et al.*, 2000). The bedrock of the Piànico-Sèllere Basin consists mainly of Upper Triassic dolomitic rocks (Dolomia Principale) and of limestones of the Calcare di Zorzino Unit (Provincia di Bergamo, 2000).

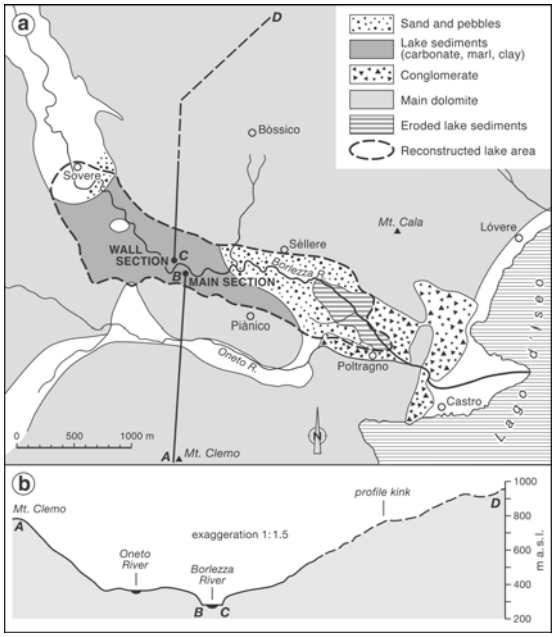

Fig. 2.2a: Distribution of the different sedimentation areas in the Piànico palaeolake during the early stages of lacustrine sedimentation (modified after Casati, 1968). A-B and C-D indicate the location of the cross section shown in Fig. 2.2b

2.3. Stratigraphy

The studied interval is part of a lacustrine sediment sequence outcropping in the Piànico-Sèllere Basin (Moscariello *et al.*, 2000). This lacustrine sequence has been deformed by overriding glaciers at its south-eastern and north-western margins. In the central part of the Piànico Basin the sequence shows a high degree of stratigraphical continuity and has been referred to as the Piànico Formation (Moscariello *et al*., 2000). The Piànico Formation has a total thickness of ca 48 m and includes four fine-grained laminated lithostratigraphical units termed (from base to top): the "Banco Torbiditico Basale" (BTB), the "Silt e Argille Basali" (SAB), the "Banco Varvato Carbonatico" (BVC) and the "Membro di La Palazzina" (MLP).

The focus of this study is on the uppermost part of the BVC unit which in total is about 9.6 m thick and laterally extends over ca 600 m and consists of deep-water lacustrine sediments. These deposits are made of biogeochemically precipitated calcite varves with intercalated detrital layers. Preliminary varve counts yielded a minimum duration of this period of sedimentation under interglacial conditions of ca 15,500 years. The top of the studied interval is at the boundary to the overlaying MLP unit which is ca 10.5 m thick and consists of predominantly detrital intervals intercalated with endogenic calcite.

Previously, the Piànico Formation has been thought to date from the last interglacial (Venzo, 1955; Lona and Venzo, 1956; Casati, 1968), mainly because its deposits are overlaid by only one till deposit. More recently, a distal tephra layer has been identified in the upper part of the varved sediments (BVC unit). Glass shards and biotite from this layer have been K-Ar dated revealing a weighted mean age of 779 ± 13 ka (Pinti *et al.*, 2001), thus suggesting an Early-Middle Pleistocene age for the Piànico Formation. This apparent contradiction between geomorphological evidence

DOI: 10.2312/GFZ.b103-07065

and radiometric dating requires further investigation. The interglacial period hereafter is referred to as the "Piànico Interglacial".

The boundary of the BVC with the overlying MLP unit is sharp and reflects a change in deposition from predominantly endogenic carbonate to clastic-detrital sedimentation. This reflects the transition from temperate interglacial to colder early glacial climate (Moscariello *et al.*, 2000). This study focuses on a ca 900 year time window preceding this major shift that lithologically reflects the final stage of the interglacial. Two clear marker layers bracket the studied section, the above mentioned tephra layer at the base and the BVC-MLP boundary on top (Fig. 2.3). The same stratigraphic interval has been studied in two outcrops located a distance of ca 130 m apart (Fig. 2.2a).

1. The Main Section (MS; Coordinates: UTM 32T NR 80547424, Tavoletta IGMI 34 III N.O. "Lovere") is the type section for the BVC unit (Moscariello *et al.*, 2000). The vertical extent of this N E trending outcrop is ca 20 m, while the lateral extent is ca 80 m.

2. The Wall Section (WS; Coordinates UTM 32T NR 80527420) is the type section for the lower part of the MLP unit (Moscariello *et al.*, 2000). The vertical extent of this S SW trending outcrop ranges between 10-14 m with a lateral extent of ca 70 m.

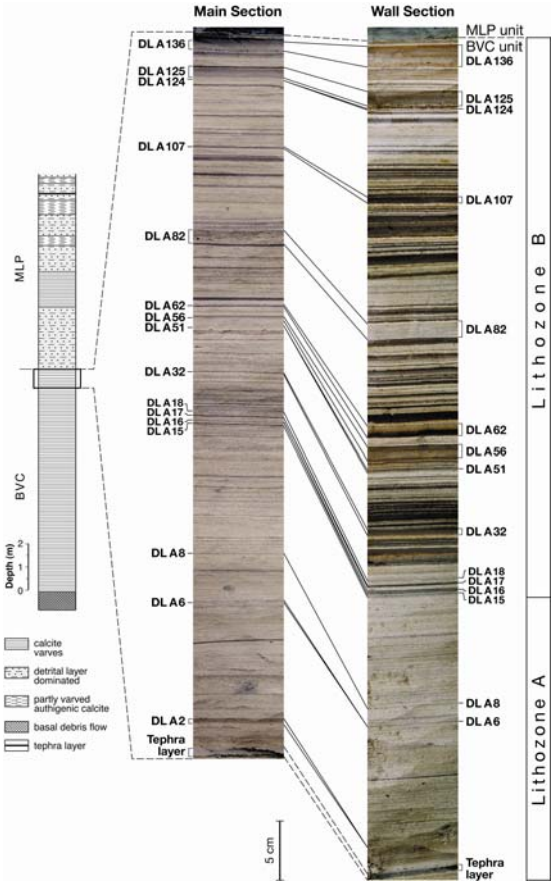

Fig. 2.3: Simplified stratigraphic log of the BVC and MLP units and lithology of the studied interval in the two studied sections. Detrital layers mentioned in the text are labelled. Upper limit of the studied section is the transition to the MLP unit, lower limit is the tephra layer.

2.4. Methods

Precise intra-basin correlations (Sturm and Matter, 1978; Drohmann and Negendank, 1993) are important to characterize lacustrine turbidites and their pathways within a lake. Generally, turbidite deposits show a pronounced lateral variability with maximum thickness close to the point where the density current entered the lake. Therefore the reconstruction of original inflow position and

DOI: 10.2312/GFZ.b103-07065

thus the source region can be inferred by mapping out the spatial distribution of sediment thicknesses. Robust intra-basin correlation has been demonstrated especially for annually laminated sediments, because an exact estimate of time intervals between individual detrital layers can be obtained from varve counts (Ludlam, 1974).
Since this study includes an analysis of very thin detrital layers, a microfacies approach is applied using techniques that were originally developed for varve analyses (Merkt, 1971; Zolitschka *et al.*, 1992; Brauer *et al.*, 1994; Ringberg and Erlström, 1999; Brauer, 2004). Microfacies analyses have also been demonstrated to be a valuable tool in glacial sedimentology for obtaining information that commonly is not provided by routine sedimentological techniques (van der Meer & Warren, 1997; Phillips and Auton, 2000; van der Meer *et al.*, 2003; Menzies and Taylor, 2003).

Continuous vertical profiles of sediment samples were collected from both study sites allowing preparation of overlapping large-format thin sections (120 x 35 mm) for microfacies analyses. For field sampling, special stainless steel boxes (33 x 5 cm) with removable side walls were designed. First, the outcrop was cleaned with a sharp knife until a smooth and vertical surface was obtained. Then a block of sediment the size of the steel box was carved out *in situ* to enable easy pushing of the box on to the sample without mechanically breaking the sediment. These samples were taken with at least 5 cm vertical overlap, ensuring that a marker layer allowing correlation was present in both samples. Due to the removable side walls of the steel boxes the samples could be easily extracted from the boxes in the laboratory without breaking the sediments. The samples were then slowly dried at room temperature to avoid quick shrinkage and cracking and then covered with a transparent epoxy resin (Araldite® 2020; Vantico, Basel, Switzerland). This procedure achieved impregnation with resin of the surface layer (1-2 mm) of the sediments. The samples were then cut in two halves with the fresh surface again carefully dried and impregnated. From one half, 10 cm thick samples with 4 cm overlap for final thin section preparation were cut out. The other half of the samples were kept for further analyses.

Overall, 19 thin sections were analysed with a petrographic microscope (Carl Zeiss Axiophot; Carl Zeiss, Germany). For measurement of varve and detrital layer thickness, 100x magnification was chosen. Thin-section images (Fig. 2.4) were obtained with a digital camera (Carl Zeiss Axiocam) and the software Carl Zeiss Axiovision 2.0.

A Detrital Layer Index (DLI) was introduced in order to better describe detrital layers in terms of intensity and possible source areas. This index has been defined as: $DLI = (DL_{WS}+DL_{MS}) * (DL_{WS}-DL_{MS})$, where DL_{WS} is the thickness of a detrital layer in the Wall Section and DL_{MS} the thickness of the same detrital layer in the Main Section. Thus the DLI is a function of both the layer thickness and the layer thickness difference between both sections. High DLI values generally reflect thick detrital layers with relatively large difference in thickness between both sites. In addition, the algebraic sign of the values indicates the more proximal location, *i.e.* that section where detrital layers are thicker (positive values indicate thicker layers in the WS).

X-Ray diffraction analyses were carried out on 12 individual detrital layers of different facies types using a 'Siemens Diffraktometer 5000' (Siemens, Karlsruhe, Germany). These layers were selected because they are thick enough (3.95 to 20.15 mm) to allow precise sub-sampling by scratching the samples with a razor blade. Quantitative mineral contents have been calculated for three samples using BGMN software from Seifert, Freiberg, Germany.

Grain-size analyses were carried out on the same 12 samples with a laser analyser (Malvern Laser Particle Sizer; Malvern Instruments, Malvern, UK). These layers were selected because they are thick enough (3.95 to 20.15 mm) to allow precise sub-sampling by scratching the samples with a razor blade. Sample pretreatment was (1) incubation at 90° C in 4.4% sodium pyrophosphate for approximately three hours, (2) centrifugation at 3500 rpm for 13 minutes, and (3) decantation of the supernatant. The samples were re-mobilised using a whirlmixer before sub-sampling for measurement.

DOI: 10.2312/GFZ.b103-07065

2.5. Results

The studied time interval is the uppermost part of the BVC unit. The boundaries of the studied sections are clearly defined by two distinct marker layers: at the bottom a 0.7 cm thick tephra layer and at the top a massive clay layer that marks the major change in depositional processes (Fig. 2.3). These marker layers are clearly visible in both outcrops. At macroscopic scale, the studied interval appears rather different in the two outcrops due to many thick brownish layers which are only visible in the Wall Section. At microscopic scale, it is proven that these differences are solely related to detrital layers microfacies whereas 99.2% of the varves is identified in both sections. This indicates an extremely quiet and regular seasonal deposition mode producing the same sub-millimetric layers within the lake in a distance of at least 130 m. This continuity of the varves is an additional proof that each of the outcrops can be considered as a representative climate archive.

In total, 285 detrital layers have been identified within the studied time interval. These detrital layers consist of discrete and continuous layers of predominantly terrigenous clastic material that distinctly differ from regular endogenic varve formation. The thickness of these layers ranges from about 0.02 mm to 20.15 mm. For this study, only layers thicker than 0.2 mm at least in one of the two sections have been selected for detailed analyses. This resulted in a total of 152 layers.

2.5.1. Microfacies analyses

Three distinct detrital layer microfacies are apparent: (1) graded layers (Fig. 2.4a, b), (2) non-graded silt layers (Fig. 2.4c, d) and (3) matrix-supported layers (Fig. 2.4e).

Graded layers

Graded layers are characterized by normal grading and sharp lower boundaries (Fig. 2.4a, b). They mostly consist of angular medium to coarse silt grains (Fig. 2.5). Some thicker graded layers also have discrete basal sub-layers of fine sand that sometimes exhibit flame structures at their base. Prevailing mineral phases are allochtonous carbonates with subordinated quartz, feldspars and clay minerals (Fig. 2.6). Thickness of graded layers ranges from 0.30 mm to 20.15 mm.

Non-graded silt layers

These layers occur as discrete layers with no obvious primary textural organisation (e.g. grading). They consist of detrital grains (Fig. 2.4c, d) with a dominance of medium to coarse silt particles (ca 25 – 63 µm). Isolated fine sand grains (up to ca 125 µm) were observed in only few cases. More commonly, small plant fragments are present, which are partly decomposed and formed nuclei for secondary pyrite growth. Prevailing mineral phases are carbonates, with subordinated quartz, feldspars and clay minerals. Detrital grains have typically irregular angular shapes and thus are easy to distinguish from the small isomorphic rhombohedral calcite crystals (1 – 20 µm) associated with endogenic carbonate precipitation. The maximum thickness of silt layers is 1.83 mm but the majority of non-graded silt layers are thinner than 0.60 mm.

Matrix-supported layers

These layers (Fig. 2.4e) consist of a mixture of isomorphic crystals of endogenic calcite forming the matrix and medium to coarse silt-sized detrital grains (25 – 63 µm). Occasionally, fragments of mollusc shells and of plant remains also occur. The top and base of these layers sometimes appear indistinct, partly because the matrix consists of the same isomorphic calcite crystals as the regular varves. Endogenic calcite and detrital carbonates (mainly dolomite) are the dominant mineral phases with subordinated quartz and feldspar (Fig. 2.6). The thickness of matrix-supported layers varies from 0.20 to 13.27 mm.

DOI: 10.2312/GFZ.b103-07065

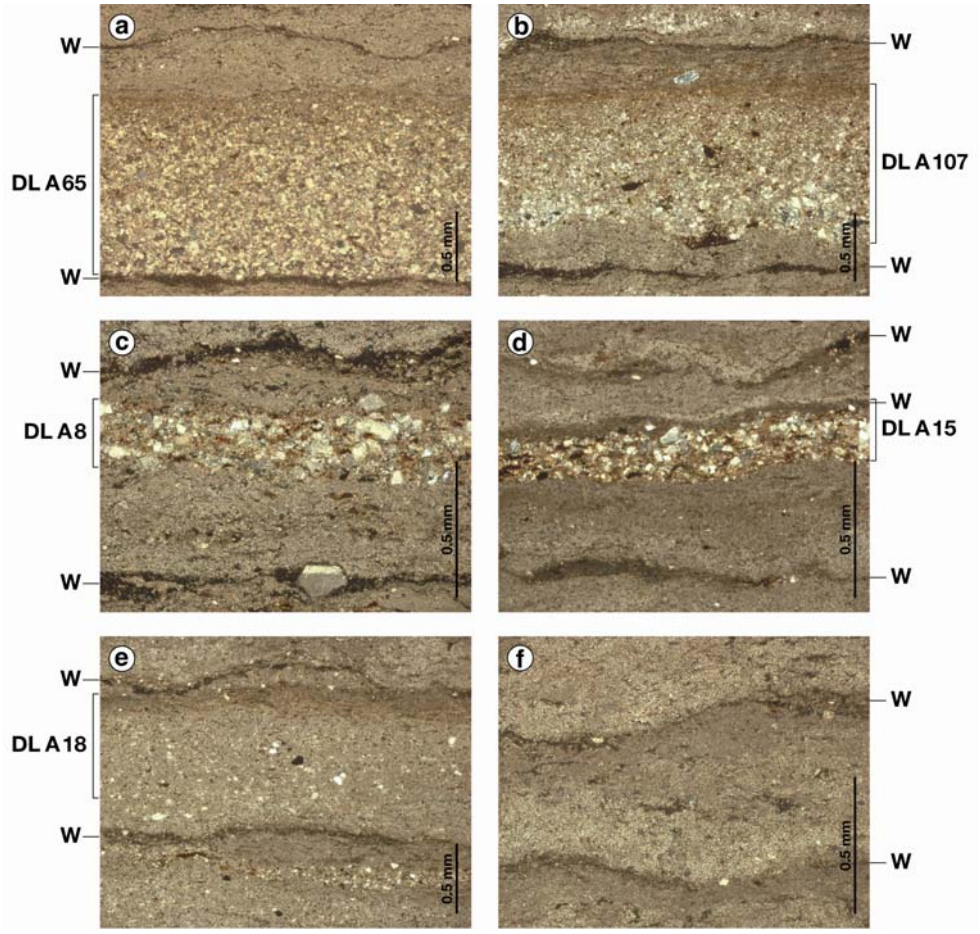

Fig. 2.4: Thin section images (crossed polarized light) of detrital layer microfacies types: (a) "graded" layer: normal graded layer (detrital layer settled before the precipitation of endogenic calcite; Wall Section, DL A65, 5x); (b) "graded" layer: normal graded layer (embedded in the calcite sub-layer of the varve; Main Section, DL A107, 5x); (c) "silt" layer: absence of grading within the detrital layer (detrital layer embedded in the calcite sub-layer of the varve; Main Section, DL A8, 10x); (d) "silt" layer: absence of grading within the detrital layer (detrital layer at the top of the calcite sub-layer; Main Section, DL A15, 10x); (e) non-graded matrix-supported layer. Note: boundaries with varves are not very distinct (Main Section, DL A18, 5x) and (f) typical biochemical calcite varve without any detrital layer (10x).

2.5.2. Mineralogy and grain size

Mineralogy and grain size analyses were carried out on 12 samples of the graded and matrix-supported microfacies types. The dominant mineral phases in all samples are dolomite and calcite whereas siliciclastic minerals (quartz, chlorite, muscovite) occur only in minor proportions. The main difference between graded and matrix-supported layers is the relative abundance of calcite and dolomite (Fig. 2.6). Dolomite dominates the graded layers (e.g. 86.59% ± 0.36% in DL A136) whereas the calcite content is much higher in the matrix-supported layers (e.g. 79.03% ± 0.81% in DL A82). The latter reflects the presence of isomorphic calcite as a matrix phase; this is rare to absent in the graded layers which are almost wholly composed of detrital grains.

DOI: 10.2312/GFZ.b103-07065

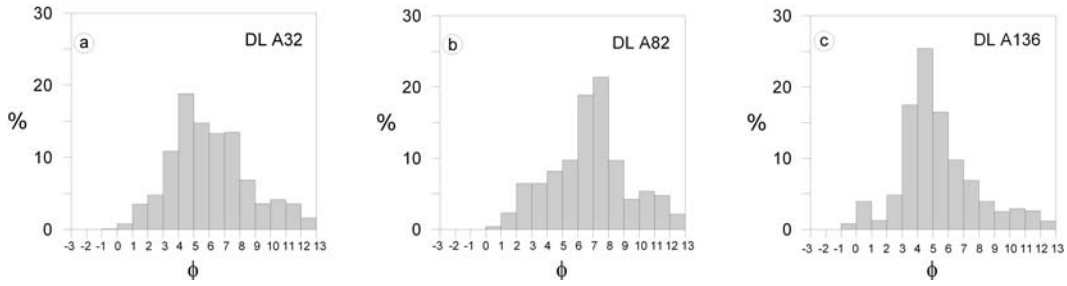

Fig. 2.5: Grain size distribution of three selected samples: (a) DL A32 (Summer graded detrital layer; Wall Section), (b) DL A82 (Matrix-supported detrital layer; Wall Section) and (c) DL A136 (Graded erosive detrital layer; Wall Section).

The observed mineralogical differences between graded and matrix-supported layers are also accompanied by distinct grain size distributions (Fig. 2.5). Grain sizes of 5.85–7.81 µm (7.5–7 Φ, Fig. 2.5b) for a typical matrix-supported layer are significantly smaller than that for graded layers (46.85–62.5 µm or 4.5–4 Φ). This is caused by the presence of endogenic calcite crystals precipitated from the lake water which are smaller in size than the detrital grains originating from the catchment of the lake. In addition, two microfacies sub-types of graded layers are also visible based on grain-size distribution: (i) graded layers with a distinct basal sand layer have a second minor peak between 0.75 mm and 1 mm (0.5–0 Φ; Fig. 2.5c) and, (ii) graded layers with a pronounced fine-grained cap show a bi-modal distribution with a second maximum besides coarse silt between 5.85 µm and 7.81 µm (7.5-7 Φ) suggesting the occurrence of endogenic calcite in the top of the layer (Fig. 2.5a).

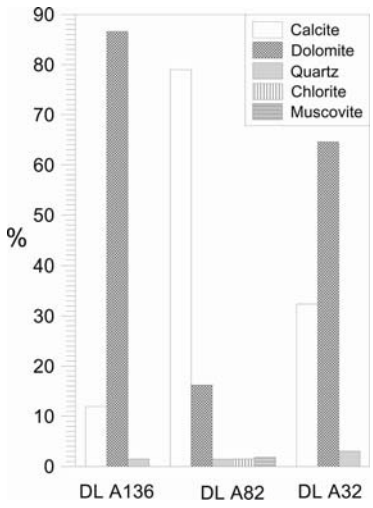

Fig. 2.6: Mineralogy of three selected samples [DL A32 (Summer graded detrital layer; Wall Section), DL A82 (Matrix-supported detrital layer; Wall Section) and DL A136 (Graded erosive detrital layer; Wall Section)].

2.5.3. Varve Chronology

The floating time scale in this study is based on varve counting in both sections; 893 varves were identified in the Wall Section and 892 varves in the Main Section (0.1% deviation). A comparison of the counting results in sub-intervals that are confined by prominent correlated detrital layers (Fig. 2.7) reveals that at seven positions, single varves are found only in one of the two sections (four cases in the Wall Section and three in the Main Section). This resulted in a total counting difference of one varve. No more than one individual varve was missing at any point in the studied section. The reason for the absence of a single varve might be either erosion or wedging out. In one case, erosion by a graded layer (DL A125) explains the loss of a varve in the Wall Section (Fig. 2.8). In both sections, varve years have been added at those positions to the chronology

DOI: 10.2312/GFZ.b103-07065

where 'missing varves' were identified. The resulting composite chronology is identical for both sections and comprises 896 varve years. The "t_0"-year for this floating time scale is defined as the varve in which the tephra is intercalated.

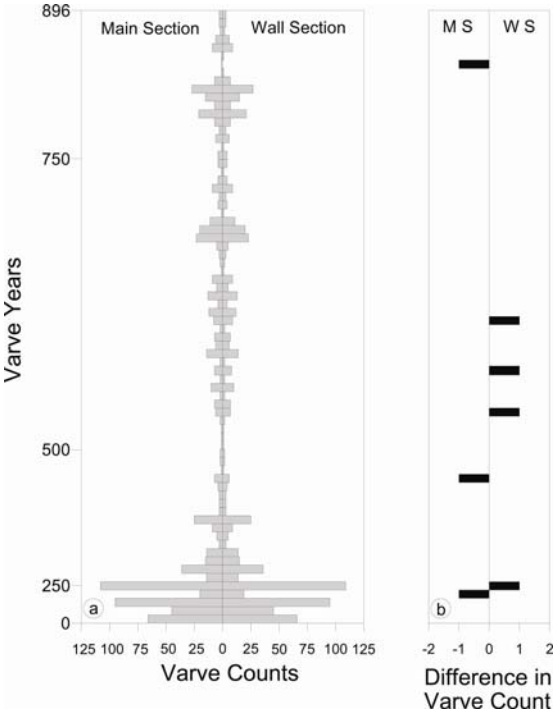

Fig. 2.7: a) Number of varves between successive detrital layers for the two studied sections. b) Positions where a varve distinguished in one section could not be traced to the other section.

2.5.4. Microstratigraphy

The Piànico varves are mainly composed of endogenic calcite (Fig. 2.4f) and this means they are easily distinguished from even extremely thin layers consisting of detrital carbonates. Detrital grains are non-isomorphic and angular and generally coarser (>20 μm), whereas the endogenic calcite is isomorphic and grain sizes are below 20 μm. Thus it has been possible to determine (1) the season of detrital layer deposition and (2) the number of such layers per year.

The compositional variation of the Piànico varves reflects biochemical calcite precipitation induced by algal blooms in spring and summer (light sublaminae) and organic matter influx in autumn/winter (dark sublaminae; Fig. 2.4f). The Piànico varves resemble Holocene varves from alpine lakes with calcite precipitation during lake productivity maxima in summer (i.e. Kelts & Hsü, 1978; Moscariello *et al.*, 1998). Using the succession of seasonal sublayers it is possible to determine even the season in which a detrital event layer was deposited. Spring layers are directly deposited on top of dark winter layers before the onset of calcite precipitation and thus before the productive period of the lake (Fig. 2.4a). Summer detrital layers are intercalated within the light sublaminae of endogenic calcite, i.e. calcite precipitation occurred before and after the detrital layer deposition (Fig. 2.4b, c). Autumn/winter layers occurred after the period of calcite formation either at the base or mixed within the dark sublaminae (Fig. 2.4d). A further differentiation between autumn and winter layers appears difficult due to the general thinness of the dark sublayer.

From the 152 studied layers, 88% of the graded layers and 80% of the non-graded silt layers occurred as summer layers (Fig. 2.4b, c) while 12% of the graded and 12% of the non-graded silt layers were deposited in spring. Within the winter sub-layer, only non-graded silt layers (8%) were found (Fig. 2.4d). Seasonal allocation was impossible for one of the thickest graded layers (DL

DOI: 10.2312/GFZ.b103-07065

A125, Fig. 2.3). This layer appears to be a spring layer but traces of basal erosion of endogenic calcite are evident at both studied sections so that summer deposition might also be possible. Matrix-supported layers are generally difficult to relate to a specific season since they contain reworked calcite that can be confused with a calcite sublayer of the same year.

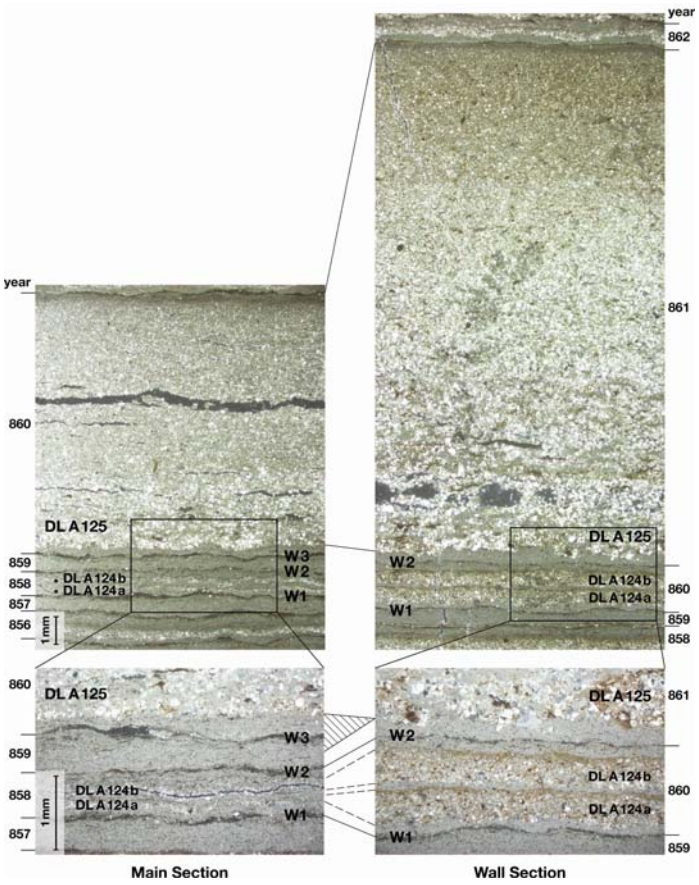

Fig. 2.8: Thin section images (crossed polarized light) of the same detrital layers (DL A124a, DL A124b and DL A125) in the Main and Wall Sections showing erosion at sub-millimetre scale in the Wall Section. Between the varve including two thin detrital layers (DL 124a and DL 124b) and the varve including the thick graded layer (DL A125), a complete varve without detrital matter is present in the Main Section (on the left). At the proximal site (Wall Section, on the right) the upper part of this varve including the dark winter layer has been eroded by the graded layer (DL A125).

Most of the studied detrital layers form the only detrital intercalation within an individual varve. Only in 14 cases have multiple (from 2 to 4) events per year been observed. However, this result slightly changes if layers below 0.2 mm in thickness are also considered. Then 40 varves contain two detrital events, four varves contain three and two varves have four detrital events (e.g. Figs 2.8 and 2.9).

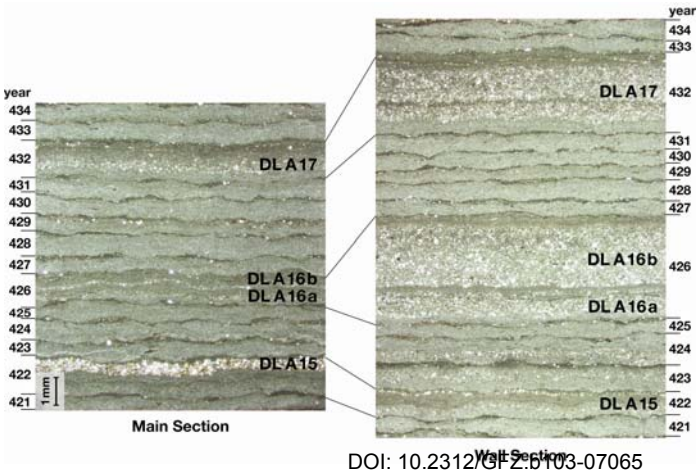

Fig. 2.9: Microscopic image of 14-year interval (crossed polarized light): DL A15 (winter silt layer) is thicker in the Main Section, whereas all detrital layers of other microfacies types are thicker at the Wall Section (on the right; 1.25x, crossed polarized light).

DOI: 10.2312/GFZ.b103-07065

2.5.5. Intra-basin Correlation

A precise correlation of the two exposures is based on varve counts in both sections (Figs 2.3 and 2.7) allowing the comparison of each individual detrital layer on a year-to-year basis (Fig. 2.10, Appendix 1). In this way, it was possible to detect detrital layers that occur only in one of the two sections: of 142 detrital layers in the Wall Section, 44 do not appear in the Main Section whereas of the 108 detrital layers in the Main Section, only 10 do not occur in the Wall Section (Figs 2.11, 2.12). In most of these cases, scattered detrital grains have been found at positions where detrital layers occur in the other section. The exclusive occurrence in only one of the two profiles appears to be related to layer thickness. All but four of the non-continuous layers are less than 1 mm thick (Appendix 1).

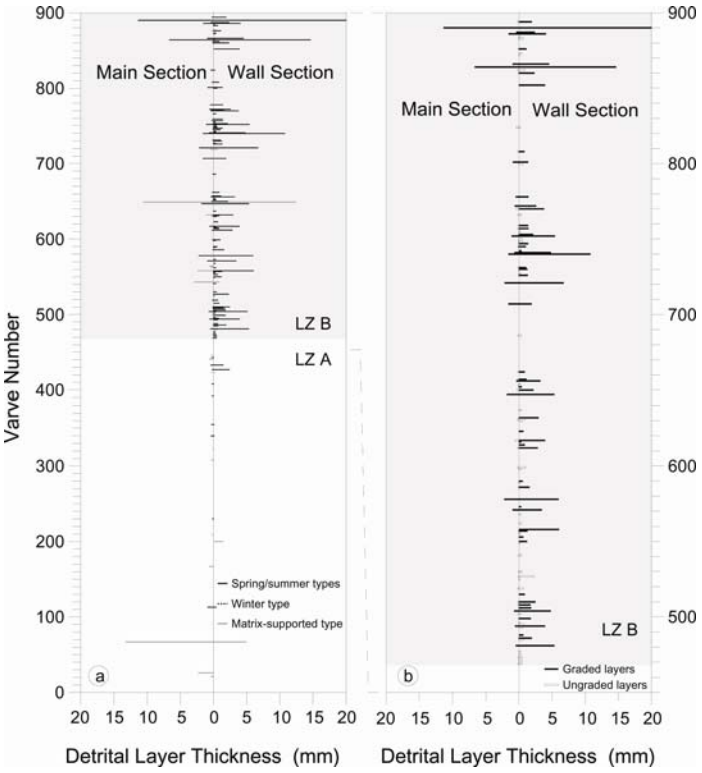

Fig. 2.10: a) Distribution, thickness and microfacies of the detrital layers thicker than 0.20 mm in the Main Section (left) and in the Wall Section (right). The shaded area marks lithozone B (LZ B) comprising the last 427 varves of the studied record. b) Distribution of graded and non-graded detrital layers. Note that only spring/summer detrital layers are plotted since only these microfacies types reflect the depositional changes.

The visible lithological difference between the two studied exposures (Fig. 2.3) is due to a more pronounced accumulation of terrigenous detrital layers in the Wall Section: the Wall Section has a cumulative detrital layer thickness of 23.97 cm, whereas the Main Section contains only 8.72 cm. In contrast, the cumulative sum of varve thickness is almost equal at both sites (WS: 44.66 cm; MS: 47.80 cm) confirming a uniform autochthonous lacustrine sedimentation at the two locations.

These differences in detrital layer deposition mainly occur in the upper lithozone (LZ B) which represents the younger 427 years of interglacial varve deposition. The boundary between LZ B and the lower LZ A in both sections is sharp and characterized by both a larger frequency of detrital layer deposition and higher thicknesses of these layers (Fig. 2.10). However, these changes do not apply to all microfacies and seasonal types. Whereas the frequency and thickness of non-graded spring and summer and graded spring layers increased, matrix-supported and winter silt layers are equally distributed over the entire time window and do not exhibit any significant change (Fig. 2.10). It is particularly remarkable that graded summer layers appear for the first time at the onset of LZ B (Appendix 1).

DOI: 10.2312/GFZ.b103-07065

Moreover, all the detrital layers of the microfacies types that characterize the rapid shift are proximal in the Wall Section (Fig. 2.13). Again this shift is most pronounced for graded layers. DLI values of these layers all exceed 0.8, indicating thick proximal layers in the Wall Section. Thus graded layers contribute most to the differences in the amount of detrital accumulation in LZ B between the sections. This is also expressed by the cumulative thickness of all graded layers in the Wall Section (17.72 cm) compared to the sum of their distal portions in the Main Section (4.43 cm).

A similar pattern of microfacies distribution is found for those detrital layers that appear only in one section. From 44 detrital layers only found in the Wall Section, 39 belong to the ´spring-summer´ types whereas all layers appearing only in the Main Section are winter silt or matrix-supported facies.

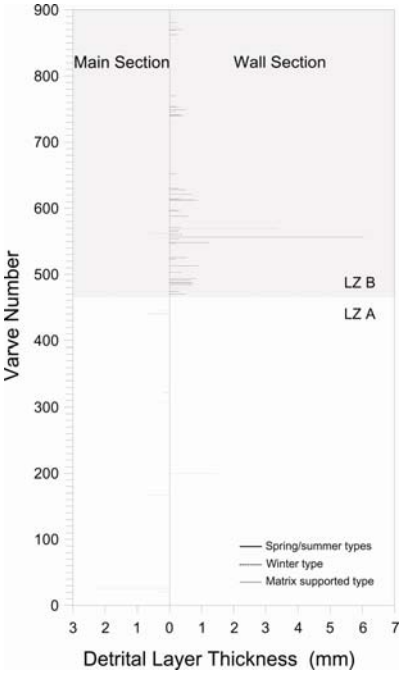

Fig. 2.11: Distribution, thickness and microfacies type of the detrital layers present only either in the Main Section (left) or in the Wall Section (right). The shaded area marks lithozone B (LZ B).

The occurrence of periods with an increased deposition particularly of spring and summer detrital layers in LZ B appears to be cyclic with a recurrence pattern of about 40-50 years. The mechanism behind this decadal-scale pattern remains unknown and requires further detailed time series analyses.

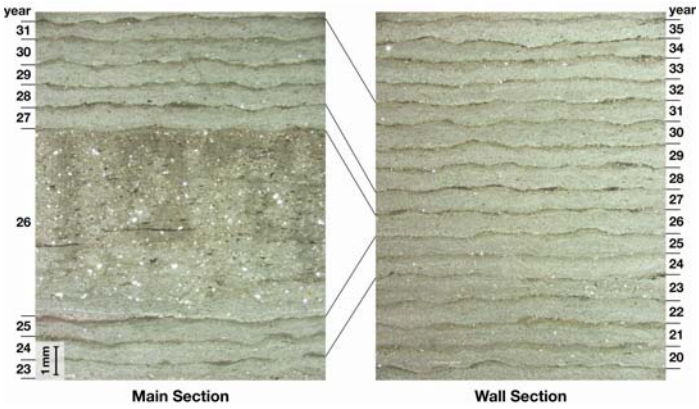

Fig. 2.12: Example of a matrix-supported layer (DL A2) present only in one section (MS). In the Wall Section no traces of this detrital layer are visible in the same stratigraphic interval (crossed polarized light).

DOI: 10.2312/GFZ.b103-07065

2.6. Interpretation and discussion

The most conspicuous change in detrital layer deposition in the Piànico palaeolake is the abrupt increase in layer frequency and thickness during the uppermost 427 years of interglacial varve formation (LZ B; Fig. 2.10). Such a sudden increase in detrital fluxes is an indication of intensified soil erosion processes that, in the first instance, could be related to a less dense vegetation cover. This is supported by an increase of non-arboreal species (NAP, mainly Poaceae and steppic plants; Rossi, 2003) at about the time when detrital layer deposition increased. However, whereas NAP percentages remain at high level during LZ B, the deposition pattern of detrital layers recurrently switches back for several decades to a low frequency mode (Fig. 2.10). This indicates that detrital fluxes into the lake were not a function of changes in the vegetation cover in the catchment. Other possible controlling mechanisms can be assessed by reconstructing sedimentary processes using microfacies variations which provide information on the seasonal occurrence and the spatial distribution of detrital layers:

(1) Graded layers are the thickest detrital layers in the studied sediments (Appendix 1, Figs. 2.10, 2.13) and most clearly reflect the abrupt change in detrital matter accumulation at the end of the Piànico Interglacial. These layers are assumed to have been deposited from turbidity currents and thus are regarded as lacustrine turbidites. Traces of erosion at the basal part of three graded layers (e.g. DL A125, Fig. 2.8) support the interpretation as deposits from hyperpycnal underflows, because deposition from overflows or interflows is related to low density currents that do not lead to turbidity currents (Sturm and Matter, 1978).

The most likely trigger for the graded layers is channelized streamflows from the hills at the northern lake shore (upslope at the Wall Section) following extreme precipitation events (Govi and Sorzana; 1980; Rapp and Nyberg, 1981; Rapp, 1985; Blikra and Nemec, 1998; 2000; Moscariello and Deganutti, 2000). The hill slopes at the northern shore (Fig. 2.2b) were prone to soil erosion and gully formation. Due to the proximity of the location of the Wall section to these northern shore slopes even thin detrital layers as reflection of minor events are recorded in this outcrop. Microstratigraphic evidence of 85% of the turbidites being deposited during summer let us assume that most of the erosional events took place after heavy summer rains.

Other possible triggering mechanisms for the graded layers like large river floods (Lambert *et al.*, 1976; Sturm and Matter, 1978; Hsü and Kelts, 1985; Moscariello *et al.*, 1998) or sub-aquatic continuations of sub-aerial mass-flows (Hsü and Kelts, 1985) are considered less likely. No major river entered the lake from the northern lake shore that has been clearly identified as a source area (Fig. 2.13) which excludes large river floods as a trigger. Transformation of large-scale debris flows (sediment gravity flows) can be ruled out because of the absence of larger quantities of reworked lake calcite and mudclasts from littoral environments that would be expected in such deposits.

(2) Non-graded silt layers might be considered either as weaker events resulting from low density currents operating as interflows or overflows (Sturm and Matter, 1978) or as extreme distal segments of underflows entering the lake at another point from the northern shoreline at greater distance from the Wall Section. The latter applies particularly to the 77% of the layers deposited in summer. In summertime, the lake was thermally-stratified and interflows and overflows would have been trapped in the thermocline (Sturm and Matter, 1978) whereas underflows were able to transport detrital material even through the thermocline down to the lake floor. Consequently, the releasing mechanisms for these layers could have been the same as for the graded layers. This is confirmed by the very similar pattern in seasonal occurrence and thickness distribution of both microfacies types (Fig. 2.13).

This does not apply, however, for those 8% of the non-graded silt layers that have been deposited within the winter layer. These layers always have low DLI values (Fig. 2.13), the frequency of their occurrence does not change, and they do not show a preferential thickness distribution between the two sections. Thus, different triggering process and/or source areas must be inferred.

DOI: 10.2312/GFZ.b103-07065

Perhaps the winter silt layers originated from interflows either from weak local surface runoff or from river discharge at a distant source (probably the narrow NW margin of the lake). This could be also an explanation for the generally low thickness of the winter silt layers. An alternative explanation for this observation would be a generally low influx of detrital matter from river discharge possibly due to a catchment smaller than today. However, these are only speculations that are not supported by further data.

(3) Matrix-supported layers reflect completely different sedimentary processes. Most of these layers (71%) appear in only one of the studied sections (Fig. 2.11), thus indicating that they have been preferentially released by local processes. The matrix of these layers is formed by endogenic calcite indicating reworked littoral sediments which suggest subaqueous slumping caused by local slope instabilities.

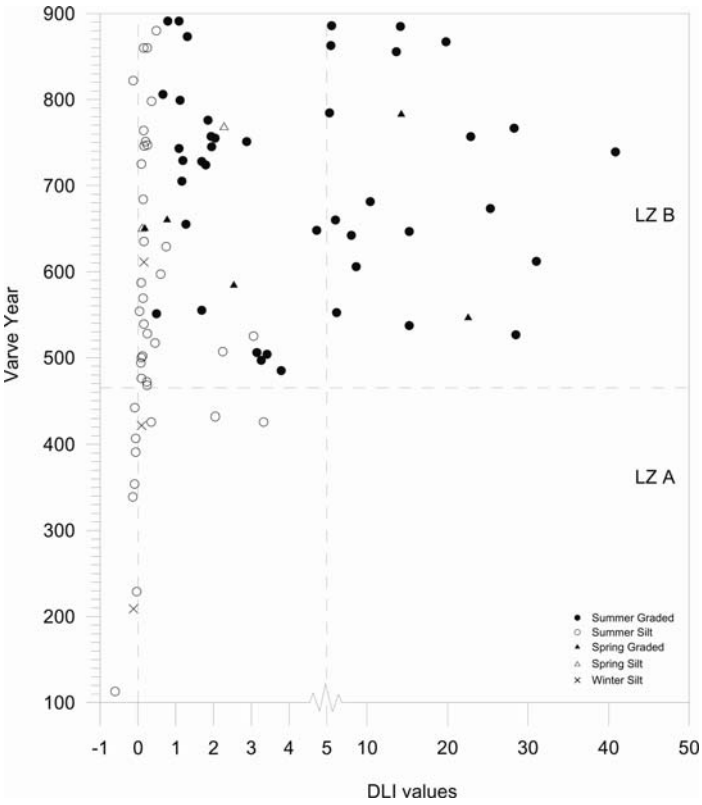

Fig. 2.13: (a) Distribution of the DLI values between -1 and 50 (a definition of DLI values is given is chapter 'Methods'). Three extreme values (DL A3: -151.09, DL A98: 113.93 and DL A136: 277.20) are not shown here because they are out of scale.

2.7. Conclusions

This study has demonstrated that successions of detrital 'event' layers in lake sediment records can provide long time series of extreme precipitation events in the past. Due to the varved nature of the autochthonous sediments from Piànico, it is possible to infer the season in which the deposition of an event layer took place. However, different types of detrital layers have been distinguished and apparently not all of them have been triggered by the same mechanisms.

The major shift in the pattern of detrital layer deposition about 430 years before the termination of interglacial calcite varve formation is expressed by an abrupt increase of graded layers as well as spring and summer silt layers, both deposited from turbidity currents. These turbidites were most likely released by channelized surface runoff from the northern lake margin mainly after heavy summer rains and to a minor degree after the spring snowmelt. In contrast, winter silt and matrix-supported layers are randomly distributed over the entire period and probably do not reflect any climatic signal.

DOI: 10.2312/GFZ.b103-07065

Hence, it is crucial to understand the sedimentary processes of detrital layers before such deposits can be used as indicators for changes in the nature of extreme weather conditions in the past. Microfacies analysis is essential to detect detrital layers even at sub-millimetric scale and determine the season of their deposition. This information provides a better understanding of the sedimentary processes and related triggering mechanisms associated with detrital layer deposition in lacustrine environments.

2.8. Acknowledgements

We thank Jaap J.M. van der Meer and Matti Saarnisto for their constructive reviews that helped to improve a previous version of the manuscript. We further acknowledge G. Arnold, D. Berger and M. Köhler (GFZ Potsdam) for preparing high quality thin sections, A. Hendrich (GFZ Potsdam) for drawing some of the figures, Chris Rolfe (University of Cambridge) for his assistance with grain size analyses and A. Aceti, F. Confortini, M. Gandossi and V. Valsecchi for their help in the field-work. CM is grateful to C. Smiraglia (Universitá di Milano) for his support during her diploma work.

DOI: 10.2312/GFZ.b103-07065

3. Tephrochronological dating of varved interglacial lake deposits from Piànico-Sèllere (Southern Alps, Italy) to around 400 ka

Achim Brauer[1)] *, Sabine Wulf[1)], Clara Mangili[1)], Andrea Moscariello[2)]

[1)] GeoForschungsZentrum (GFZ), Sektion 3.3 - Klimadynamik und Sedimente, Telegrafenberg, D-14473 Potsdam, Germany
[2)] Cambridge Quaternary, Department of Geography, University of Cambridge, Cambridge, U.K.

In press in Journal of Quaternary Science

Abstract - *The sediment record from the Piànico palaeolake in the southern Alps is continuously varved and spans more than 15,500 years, and represents a key archive for interglacial climate variability at seasonal resolution. The stratigraphic position of the Piànico Interglacial has been controversial in the past. The identification of two volcanic ash layers and their microscopic analysis provides distinct marker layers for tephrochronological dating of these interglacial deposits. In addition to micro-facies analyses reconstructing depositional processes of both tephra layers within the lake environment, their mineralogical and geochemical composition has been determined through major-element electron probe micro analysis on glass shards. Comparison with published tephra data traced the volcanic source regions of the Piànico tephras to the Campanian volcanic complex of Roccamonfina (Italy) and probably the Puy de Sancy volcano in the French Massif Central. Available dating of near-vent deposits from the Roccamonfina volcano provide a robust tephrochronological anchor point at around 400 ka for the Piànico Interglacial. These deposits correlate with marine oxygen isotope stage 11 and thus are younger than Early to Middle Pleistocene previously suggested by K/Ar dating and older than the last interglacial as inferred from macrofloral remains and the geological setting.*

Keywords: Tephrochronology; Micro-facies analyses; Varved lake sediments; Piànico Interglacial; Marine Oxygen Isotope Stage 11

3.1. Introduction

Varved lake sediments are unique terrestrial climatic archives providing seasonal to decadal proxy data (e.g. Brauer, 2004). Since knowledge of natural climate variability during warm interglacial conditions is becoming increasingly important, the search particularly for varved lake sediment records covering past interglacials has been intensified. However, in formerly glaciated regions like the Alps and northern Europe all such lake deposits are preserved as isolated records representing floating time intervals in the Pleistocene chronology. Absolute dating of these records is a crucial problem due to the lack of reliably applicable techniques for organic deposits beyond the range of radiocarbon dating. For regions with a comparable evolution of the vegetation, biostratigraphy has been successively used to establish relative stratigraphies for floating interglacial records (e.g. Turner, 1998). Correlation especially of floating lake records older than the last interglacial with the marine oxygen isotope stratigraphy, however, often remained controversial. A prominent example is the debate about the correlation of the Holsteinian Interglacial in northern Germany with either OIS 7 (Linke, 1993), OIS 9 (Zagwijn, 1996; Geyh and Müller, 2005) or OIS 11 (Beaulieu and Reille, 1995). On the long-term perspective an unequivocal correlation of high-resolution lake records with marine sequences will be crucial for an impartial evaluation of the ocean-atmosphere interactions that control the climate system.

One alternative dating approach for floating interglacial lake records is bound to the occurrence of volcanic ash layers and their detection in lake sediment records. Even if most direct Ar/Ar dating of tephra layers in lake sediments is extremely difficult due to the distal, *i.e*. very fine-grained, character of these tephras, they have been demonstrated to be extremely valuable for establishing robust chronostratigraphical frameworks through tephrochronology (Wastegård and Rasmussen, 2001; Wulf *et al*. 2004; Wastegård *et al*. 2005). This approach is based on precise correlation of

DOI: 10.2312/GFZ.b103-07065

distal tephra layers based on their geochemical and mineralogical characteristics with proximal tephras near the eruption centre that have been radiometrically dated.

A key sediment archive for interglacial climate variability at decadal, annual and seasonal resolution has been reported from Piànico-Sèllere, Italy (Moscariello *et al*. 2000). In the Piànico palaeolake an unique continuous succession of >15,500 calcite varves has accumulated. The interglacial origin of these varves has been confirmed by palynology (Rossi, 2003) but the stratigraphic position of the Piànico Interglacial remained controversial (Moscariello *et al*. 2000; Pinti *et al*. 2001). Here we present a revised chronostratigraphy for this interglacial based on a tephrochronological approach.

3.2. The Piànico stratigraphy – a history of controversy

Since the finely laminated lacustrine deposits from Piànico-Sèllere were first described almost 150 years ago, their chronostratigraphic position has been controversial. The original interpretation of these sediments as being deposited during glacial times because of their stratigraphic position between two tills (Stoppani, 1880), was soon revised when remains of interglacial flora and fauna were found (e.g. Corti, 1895; Sordelli, 1896). The stratigraphical position was further refined to the last interglacial (Riss/Würm) because only one till occurred on top of the lacustrine sequence (Penck and Brückner, 1909). Apparently, this was supported by faunal remains (Casati, 1968) and pollen data (Lona, 1952) as well as plant macro remains (Emmert-Straubinger, 1991). Recent palynostratigraphic work, however, showed that a precise stratigraphic classification is not possible on the base of the vegetational evolution (Moscariello *et al*. 2000) since no well-dated regional palynological reference profiles are available. Thus the only chance to date the Piànico sediments appeared to be through radiometric methods. Since radiocarbon dating (Orombelli, 1974) as well as attempts with U-Th and OSL did not yield satisfactory results, the only available date was obtained from K-Ar dating of a distal tephra layer. The resulting age of 779 ± 13 ka suggested an early Middle Pleistocene age of the Piànico interglacial sediments (Pinti *et al*. 2001).

3.3. Methods

3.3.1. Thin section and SEM analyses

Overlapping series of large-scale thin sections (120 x 35 mm) for micro-facies analyses have been prepared from the Piànico sequence (Mangili *et al.* 2005). Two of these thin sections contained the tephra layers which are the focus of this study. Sediment blocks of 33 cm length were cut out from the outcrop as described in detail by Mangili *et al.* (2005) and then carefully dried at room temperature in the laboratory before coverage with a transparent epoxy resin (Araldite 2020). This procedure warranted complete impregnation with resin of the surface layer of the sediment block (1-2 mm). After a drying period of two days for the epoxy, smaller blocks with the format of the thin sections were cut out and again carefully dried and impregnated. From these smaller blocks the final thin sections were prepared with a thickness of ~20 µm. Analyses were carried out with a petrographic microscope (Carl Zeiss Axiophot). Images of the thin sections were obtained with a Carl Zeiss Axiocam digital camera and processed with Carl Zeiss Axiovision 2.0 software. Samples for SEM analyses (Carl Zeiss NTS Digital Scanning Microscope DSM 962) were washed in distilled water and treated with 30% H_2O_2 in order to remove organic coatings.

3.3.2. Tephrochronological methods

The assemblage and chemical composition of tephra components (vitrics, phenocrysts, lithics) were determined on polished thin sections, which also provided information about the original structure of tephra layers and grain size distribution of their components. In addition, a bulk sample of one tephra (T32) has been taken and washed in 30% H_2O_2 in order to remove the

DOI: 10.2312/GFZ.b103-07065

organic matter and surface coatings. The silt-sand fraction was dried, sieved with a 63 µm fine mesh polyester sieve, and the coarser fraction was selected for thin section analyses.
Major-element electron probe micro analyses (EPMA) on single glass shards were carried out using a Cameca SX-100 electron probe (WDS) with an accelerating voltage of 15 kV and a beam current of 20 nA. Because of the known loss of sodium from volcanic glass during EPMA (Nielsen and Sigurdsson, 1981), large beam sizes of 15 µm and 20 µm diameters were chosen depending on the size of the glass particles. Peak counting times were 20 s for each element, apart from 10 s for Na. Instrumental calibration used interlaboratory natural mineral and glass reference materials (Lipari obsidian; Hunt and Hill, 1996).

3.4. Site and sediments

The Piànico-Sèllere Basin is located in the Orobic Prealps within the Borlezza Valley, a tributary of present Lake Iseo (Fig. 3.1). The elongated Piànico palaeolake has been reconstructed as being around 3 km long and 500 to 800 m wide (Casati, 1968; Fig. 3.1). The lake is assumed to have originally been between 50 and 100 m deep (Moscariello *et al*. 2000). The Borlezza River cut a deeply incised valley in the sedimentary infilling of the Piànico-Sèllere Basin revealing a series of outcrops (Fig. 3.1) at altitudes between 280 m and 350 m a.s.l. (Carta Tecnica Regionale (CTU), Regione Lombardia, Elemento 078133 - Sovere Scale 1:5000).

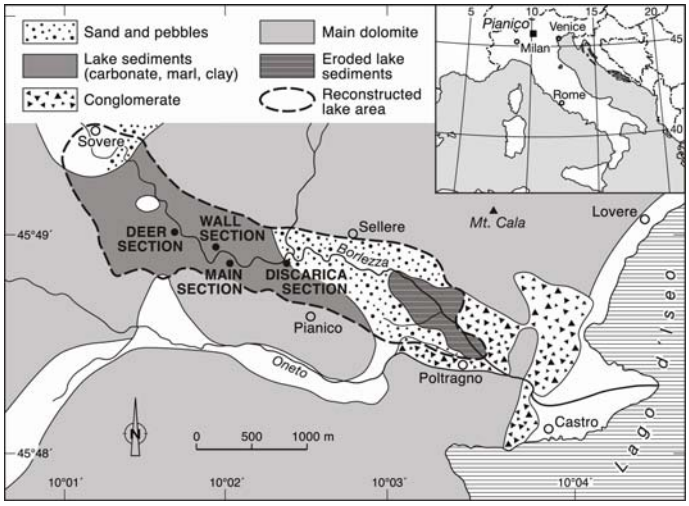

Fig. 3.1: Location of the Piànico palaeolake and reconstruction of its former extent (after Casati, 1968). Main geological units indicated by different hatchings with alluvium covering blank areas. Outcrops mentioned in the text marked by black dots (for more details on the outcrop positions see Moscariello *et al*., 2000).

The sequence is about 48 m thick and includes four fine-grained laminated lithostratigraphical units that have been described in detail by Moscariello *et al*. (2000). The tephra layers described in this study are included in the upper two units, the MLP ('Membro di La Palazzina'; Fig. 3.2) and BVC ('Banco Varvato Carbonatico'; Fig. 3.2). Due to the difference in elevation and downward gradient of the Borlezza Valley, the MLP and BVC units (thickness ca 21 m) are not accessible as one single outcrop. The top of the MLP is only accessible in the upper part of the valley (Deer Section, Fig. 3.1,), while downstream the BVC/MLP transition including the lower part of the MLP (Wall Section, Fig. 3.1) and the BVC (Main Section, Fig. 3.1) are best exposed. Therefore, a composite profile has been established from these three outcrops (Fig. 3.2). Lithological correlation between the overlapping parts of these outcrops is well defined and supported by detailed microstratigraphical studies based on a varve-to-varve analysis (Mangili *et al*. 2005).

The BVC unit is predominantly composed of biogeochemically precipitated calcite varves, which indicates that these sediments were deposited under warm interglacial climatic conditions. Preliminary varve counts yielded a minimum duration of 15,500 ± 620 varve years for this interglacial. The lithological transition to the overlaying MLP unit is sharp and reflects threshold

DOI: 10.2312/GFZ.b103-07065

effects of regional glacial processes. The MLP unit itself exhibits an intercalation of six intervals of mainly detrital sediments (16 – 267·5 cm thick) and five intervals of endogenic calcite sediments (10 – 154 cm thick). Thickness of both allogenic and endogenic dominated sediment sections generally decreases towards the top of the profile (Fig. 3.2). Only the lowermost section of endogenic calcite is continuously varved and of the same micro-facies type as those in the BVC unit. Endogenic calcite intervals reflect biologically productive phases in the lake favoured by rather warm interstadial climatic conditions. This is confirmed by pollen analyses indicating a dominance of mesothermophilous taxa in these sediments (Rossi, 2003). In contrast, predominantly detrital deposits indicate low biological productivity with surface runoff processes from the catchment dominating the sediment accumulation.

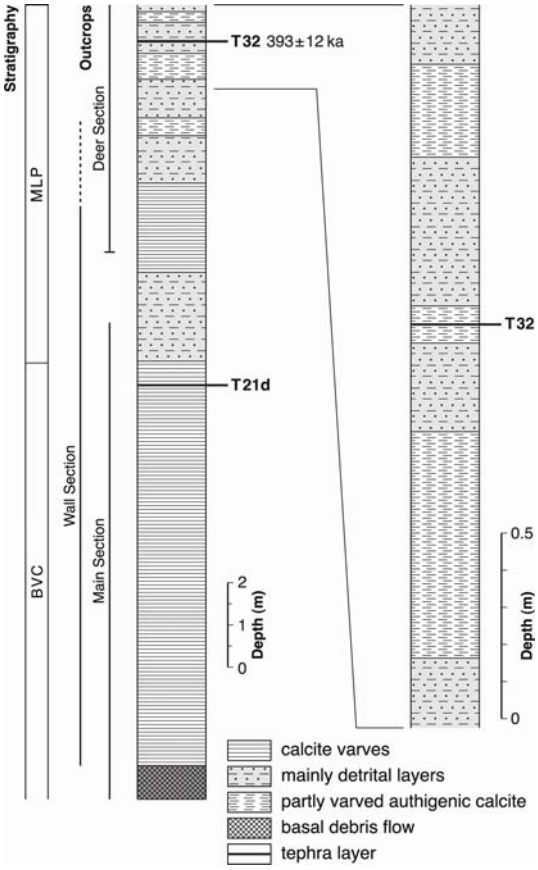

Fig. 3.2: Generalized lithological log for the upper part of the Piànico sediment sequence including the BVC (Banco Varvato Carbonatico) and MLP (Membro di La Palazzina) units. The uppermost 2 m have in the right column been expanded in order to show the exact position of tephra T32 in a 10 cm thick section of endogenic calcite. Note: the black lines marking the tephra layers are not at scale (both tephra layers are 7-8 mm thick).

3.5. Stratigraphical position of tephra layers

In addition to an earlier detected tephra (labelled as T21d) which was dated by Pinti *et al*. (2001), a second volcanic ash layer (T32) has now been identified by microscopic analyses. Both tephra layers are deposited in endogenic calcite-dominated intervals (Figs 3.2-3.4). Tephra T21d occurs in the BVC unit, 56 cm below the boundary with the MLP unit. Its microstratigraphical position within the calcite layer of a single varve (Fig. 3.3a-c) indicates that this eruption occurred during the summer season when the lake was biologically productive. The deposition of a fine-grained ash layer almost without disturbance of the thin calcite layer indicates a rather large distance to the volcanic source. Only post-depositional micro-diapirism appeared at some positions where tephra material penetrated a few mm into the later accumulated calcite varves (Fig. 3.3d). Varve counting revealed that tephra T21d was deposited about 900 years before the end of the BVC unit (Mangili *et al*. 2005). Tephra T32 occurs in superposition 8·1 m above tephra T21d, in the upper part of the MLP unit. Lithologically, this tephra appears within a thin (10 cm) non-varved endogenic calcite section indicating a short period of interstadial climate conditions. The time between the two

DOI: 10.2312/GFZ.b103-07065

volcanic eruptions can be assessed by a combination of varve counting and estimation of sedimentation rates based on micro-facies analyses. In addition to the 896 varves between tephra T21d and the BVC/MLP boundary, another 1,120 varves have been counted in the only varved calcite section of the MLP (Fig. 3.2). If sedimentation rates in the other, non-varved endogenic calcite intervals are assumed to be similar, then a total of approximately 4,500 years can be estimated for all the periods of endogenic calcite formation. More difficult and thus of larger uncertainty, is estimating the time represented by detrital dominated sedimentation. In addition to ~500 varves intercalated in the lowermost section of detrital sediments of the MLP unit, a total of ca 2,500 detrital layers has been counted. If each of these layers represented one year, an approximate time of 3,000 years can be estimated. However, interpreting detrital layers as annual events might lead to an over-estimate as multiple layers can be deposited in one year. On the other hand, it has been proven that especially thick detrital layers have caused erosion in the sediment sequence (Mangili *et al*. 2005), which in turn would result in underestimating this time interval. Both sources of error cannot be satisfactory quantified. Since they will tend to cancel each other out, they have been ignored. On this basis, the total time between both tephra layers is estimated to be around 7,500 years.

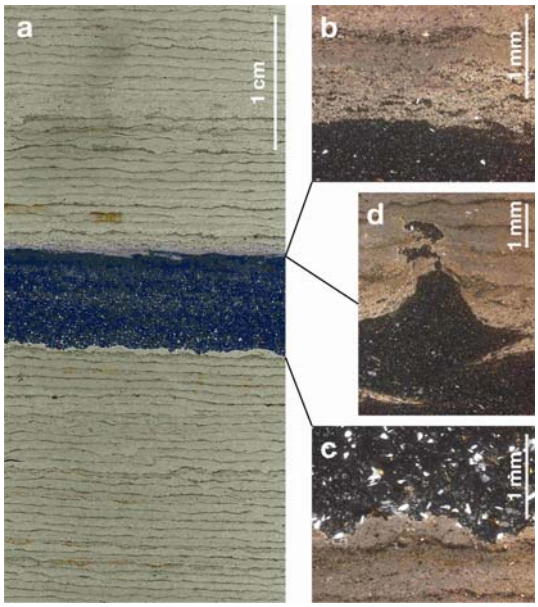

Fig. 3.3: Thin section images of T21d tephra taken with polarized light. (a) Overview showing the dark, optically isotope glass layer deposited within the calcite varves, each roughly 0.7 mm thick (b) the fine-grained top of the ash layer with transition to the autumn/winter sub-layer, (c) the coarser grained basal layer with (light) feldspar grains, (d) micro diapirism at top of ash layer that can occasionally be observed.

3.6. Description of tephra layers

3.6.1. Tephra T32

This tephra appears as an eight mm thick dark brown layer with a thin blackish top (Fig. 3.4). It is composed of a 2 mm-thick coarser basal layer of sand to silt-sized angular particles with a maximum diameter of 150 µm. In the upper part of the layer, only few coarse grains are scattered within a dark fine-grained matrix. The main juvenile phases are colourless low vesicular pumice fragments (Fig. 3.5a) and brown blocky glass shards occurring in different states of alteration. Most of them contain abundant leucite and apatite microcrystals. Lithic components are rare and comprise altered tuffs and fragments of lava. The mineral assemblage is made up, in decreasing order, of clinopyroxene, plagioclase, sanidine, biotite, leucite phenocrysts and rare olivine xenocrysts. Two types of clinopyroxenes can be distinguished according to their chemical composition (Tab. 3.1): a dark green homogeneous pleochroic augite (salite) containing inclusions of brown glass, apatite and titanomagnetite, and a light-greenish to colourless diopside (Fig. 3.6). Plagioclase typically contains inclusions of brown glass and augite crystals, whereas sanidine is

DOI: 10.2312/GFZ.b103-07065

nearly free of inclusions. Leucite phenocrysts are euhedral showing radial inclusion patterns. Olivine xenocrysts are strongly altered and often rimmed by dark-brown microcrystalline material.

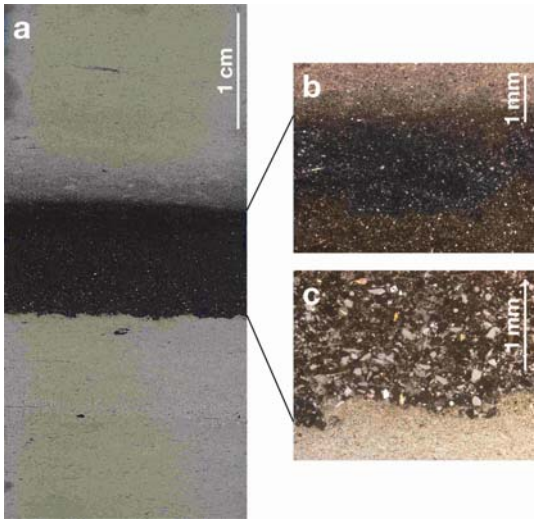

Fig. 3.4: Thin section images of T32 tephra taken with polarized light. (a) Overview showing the dark, optically isotrope glass layer deposited within homogeneous endogenic calcite, (b) the fine-grained black top of the ash layer, (c) the coarser grained basal layer with (light) feldspar grains.

	cpx1 Diopside	cpx2 Diopside	cpx3 Salite	cpx4 Salite	cpx5 Salite	cpx6 Salite	cpx7 Salite	cpx8 Salite	cpx9 Salite
SiO_2	52.26	51.37	49.16	48.39	44.91	43.98	43.53	43.30	41.49
TiO_2	0.44	0.60	1.08	1.00	1.64	2.01	1.72	2.15	2.42
Al_2O_3	2.13	3.31	4.95	5.56	8.32	8.68	7.29	9.51	10.01
Cr_2O_3	0.14	0.20	0.08	0.01	0.02	0.01	0.03	0.00	0.00
FeO^{tot}	3.47	4.19	5.56	7.50	10.02	11.35	16.50	9.82	14.73
FeO	1.30	2.51	2.58	4.53	5.63	7.31	12.82	3.86	9.28
Fe_2O_3	2.42	1.88	3.33	3.31	4.89	4.49	4.10	6.63	6.07
MnO	0.08	0.06	0.10	0.16	0.22	0.32	0.82	0.21	0.48
MgO	16.75	15.67	14.49	13.07	10.44	9.31	6.31	10.66	7.04
CaO	24.60	24.43	24.36	24.05	24.04	23.69	22.68	24.00	23.16
Na_2O	0.11	0.15	0.17	0.22	0.39	0.63	1.10	0.34	0.62
Total	100.24	100.18	100.31	100.32	100.50	100.44	100.41	100.66	100.58
Wo	0.459	0.461	0.452	0.451	0.442	0.442	0.432	0.426	0.424
En	0.509	0.489	0.486	0.449	0.414	0.383	0.272	0.449	0.320
Fs	0.031	0.049	0.062	0.100	0.144	0.176	0.295	0.125	0.257

Tab. 3.1: Selected microprobe analyses of clinopyroxene crystals from T32 tephra. Oxides in wt %. FeO and Fe_2O_3 calculated by stochiometric criteria after Droop (1987). Wo ($CaSiO_3$); En ($MgSiO_3$); Fs ($FeSiO_3$).

According to the total alkali silica (TAS) diagram (Le Bas *et al*. 1986), the chemical composition of volcanic glasses of tephra T32 is inhomogeneous, ranging from phonolitic to phonotephritic (based on anhydrous normalized data). The distribution of major elements shows a broad spectrum (Tab. 3.2) indicating a complex magma mixing system and/or different states of alteration particularly in terms of the alkali content. The latter is interpreted to be related to the analcimization of leucite, which can cause significant increases in the Na/K ratio of volcanic glass (e.g. Gupta and Fyfe, 1975).

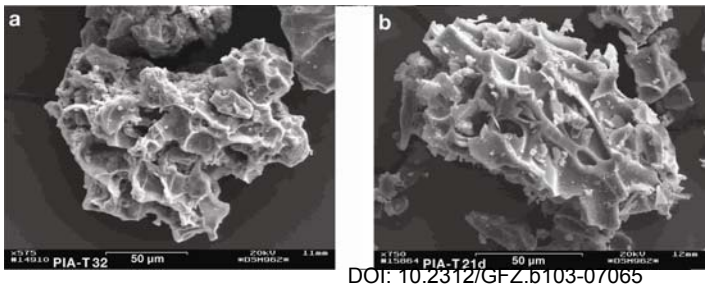

Fig. 3.5: SEM images of (a) leucite-bearing pumice fragment from tephra T32 and (b) micro-pumice fragment from tephra T21d: scale bars 50 µm.

DOI: 10.2312/GFZ.b103-07065

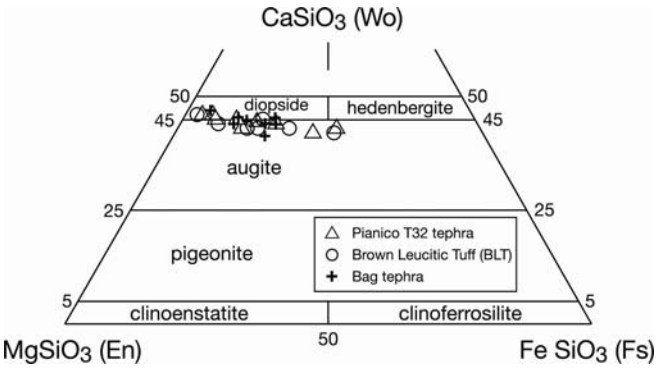

Fig. 3.6: Composition of clinopyroxenes of T32 tephra, the Brown Leucitic Tuff (Luhr and Giannetti, 1987) and 'Bag' tephra (Pouclet *et al.* 1999) after Morimoto *et al.* (1988).

	T32, type a (n = 24)			T32, type b (n = 3)			T32, type c (n = 3)		
wt %	ARD	(SD)	AWFD	ARD	(SD)	AWFD	ARD	(SD)	AWFD
SiO_2	52.42	(1.77)	53.61	47.92	(1.35)	49.22	46.07	(1.19)	47.29
TiO_2	0.56	(0.13)	0.58	0.83	(0.12)	0.86	1.09	(0.06)	1.12
Al_2O_3	20.95	(1.09)	21.42	18.03	(0.44)	18.52	15.77	(0.09)	16.19
FeO	4.62	(0.84)	4.73	7.68	(0.38)	7.90	8.87	(0.54)	9.11
MnO	0.21	(0.04)	0.22	0.23	(0.04)	0.24	0.22	(0.05)	0.18
MgO	0.87	(0.50)	0.90	2.75	(0.17)	2.83	4.39	(0.27)	4.51
CaO	5.25	(1.13)	5.38	8.83	(0.07)	9.07	11.07	(0.81)	11.36
Na_2O	6.39	(1.29)	6.52	5.49	(0.78)	5.63	4.15	(0.55)	4.25
K_2O	6.32	(1.24)	6.48	5.00	(0.62)	5.14	5.05	(1.07)	5.20
P_2O_5	0.18	(0.13)	0.18	0.58	(0.10)	0.60	0.73	(0.22)	0.76
Total	97.78		100.00	97.34		100.00	97.40		100.00

Tab. 3.2: Mean electron microprobe data from single glass shards in T32 tephra. Types a - c indicate different glass populations; n = number of glass shards, ARD = averaged raw data, SD = 1σ standard deviation, AWFD = averaged water-free data (normalized to 100 wt %).

3.6.2. Tephra T21d

Tephra T21d is a 7-8 mm thick slightly pinkish vitric ash layer (Fig. 3.3a) comprising predominantly silt-sized glass shards with only few larger shards, which reach at maximum a size of 140 µm. These shards are colourless and highly vesicular pumice fragments (Fig. 3.5b). The scarce mineral assemblage is made up of alkali-feldspar, plagioclase, biotite, zircon, apatite and sphene phenocrysts. Major-element chemical data of glass shards (Table 3.3) defines tephra T21d as alkaline rhyolitic to trachytic belonging to the shoshonite series. Low total oxide values of <95 wt % indicate high water contents suggesting incipient hydration/alteration processes although these glasses may also contain higher amounts of primary magmatic water.

	single glass shards, EPMA (n = 12)			glass fraction, ICP-MS *
wt %	ARD	(SD)	AWFD	ARD
SiO_2	67.78	(0.29)	71.16	65.27
TiO_2	0.37	(0.02)	0.39	0.30
Al_2O_3	15.39	(0.09)	16.16	15.47
FeO	1.72	(0.06)	1.80	1.75
MnO	0.12	(0.02)	0.12	0.09
MgO	0.22	(0.01)	0.23	0.21
CaO	1.00	(0.09)	1.05	1.13
Na_2O	3.76	(0.19)	3.95	4.37
K_2O	4.86	(0.10)	5.10	5.75
P_2O_5	0.03	(0.02)	0.03	<d.l.
Total	95.25	-	100.00	94.34

Tab. 3.3: Mean value and 1σ standard deviation (SD) of major element chemistry obtained by Electron microprobe-analysis (EPMA) of single glass shards from T21d tephra (this study) compared with published ICP-MS data obtained on the glass fraction of the same tephra (*Pinti *et al.* 2001). ARD = averaged raw data, SD = 1σ Standard Deviation, AWFD = averaged water-free data (normalized to 100 wt %), n = number of glass shards; < d.l. = below detection limit.

DOI: 10.2312/GFZ.b103-07065

3.7. Sources of the tephra layers

Defining the volcanic sources of these tephras necessitates a careful inspection of published petrological data from all the explosive volcanoes whose ejected tephras could have reached the Pànico lake. During the Quaternary, numerous highly-explosive volcanic fields were active in central and southern Europe: the Massif Central in France; the Eifel in Germany; central and southern Italy; the Hellenic Arc; the eastern Carpathians; central Anatolia (Fig. 3.7). The calc-alkaline volcanoes east of Pànico from the Hellenic Arc, eastern Carpathians and central Anatolia can be excluded as possible sources for tephras T32 and T21d because of differing glass chemistry and the predominant dispersal of fallout products to the east.

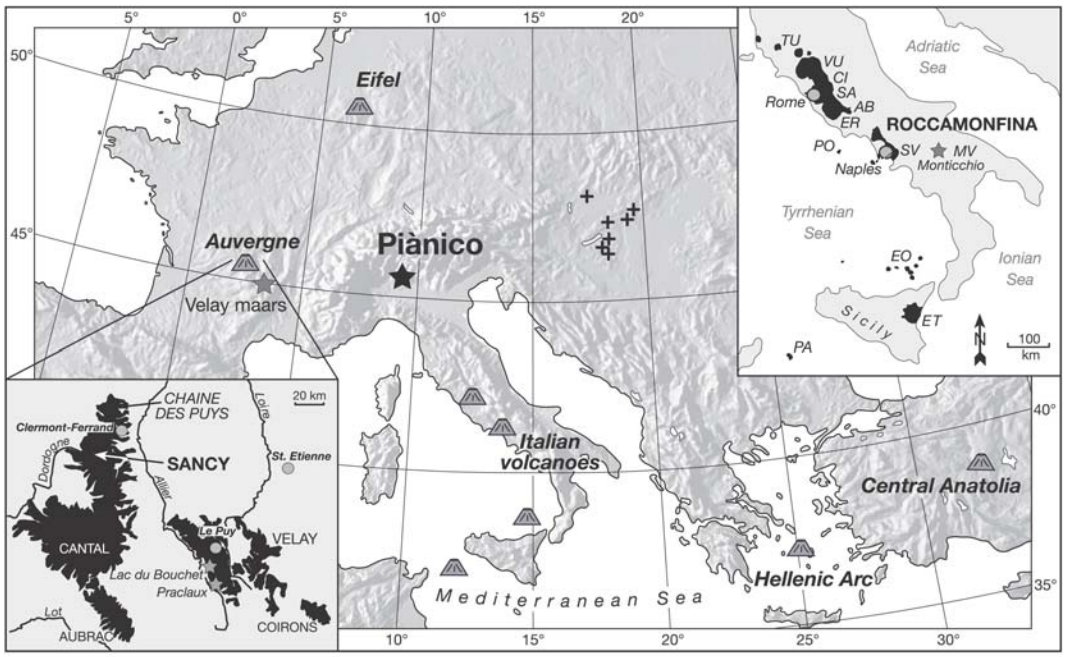

Fig. 3.7: Location of the Pànico palaeolake and main volcanic provinces mentioned in the text. Black crosses indicate 'Bag' tephra sites in the Danube valley. Within the enlarged map of the Auvergne the Velay lake sediment records Lac du Bouchet and Praclaux are indicated with grey stars. Italian volcanoes on the enlarged map: TU = Monte Amiata, Tuscany; VU = Vulsini Hills; CI = Cimini District; SA = Sabatini Volcanic District; AB = Alban Hills; ER = Ernici Volcanic Field; PO = Ponza Island; SV = Vesuvius; MV = Monte Vulture; EO = Eolian Islands; PA = Pantelleria; ET = Etna.

3.7.1. Tephra T32

The phono-tephritic composition of tephra T32 suggests an origin from Italian volcanoes or the Eifel volcanic field rather than from Massif Central stratovolcanoes, which produced fallout with mainly trachytic to rhyolitic composition (e.g. Monts Dore, Sancy, Chaîne des Puys). In the eastern Eifel volcanic field the Rieden volcanic complex was active between 450 and 350 ka BP, but related tephra is only sparsely exposed and mainly distributed to the east (Windheuser and Brunnacker, 1978). In Italy, leucite bearing phonolitic to phonotephritic volcanic rocks are described from the Roman Comagmatic Province in central Italy (Sabatini Hills, Monte Vulture, Roccamonfina) and the Island of Vulcano (Eolian Arc, southern Italy). While volcanic activity on the Island of Vulcano is restricted to the last 120 ka, the volcanoes of the Roman Comagmatic Province erupted large volumes of tephra during the last 740 ka. However, due to the differing major element composition of related volcanic products these volcanoes can be excluded as possible sources for the tephra T32 (Fig. 3.8): pyroclastics from the Sabatini volcanic complex are generally ultrapotassic in composition and additionally bear sedimentary rock fragments (De Rita *et al*. 1993); The Monte Vulture volcanic complex includes phonolitic to tephritic pyroclastics, which are also similar in major-element chemistry but differ from T32 in the prevailing content of the feldspathoid, hauyn and sedimentary rock fragments. In addition, ash falls from Monte Vulture

DOI: 10.2312/GFZ.b103-07065

tend to be distributed eastwards as indicated by their occurrence in sediments of the Venosa Basin (Raynal *et al*. 1998).

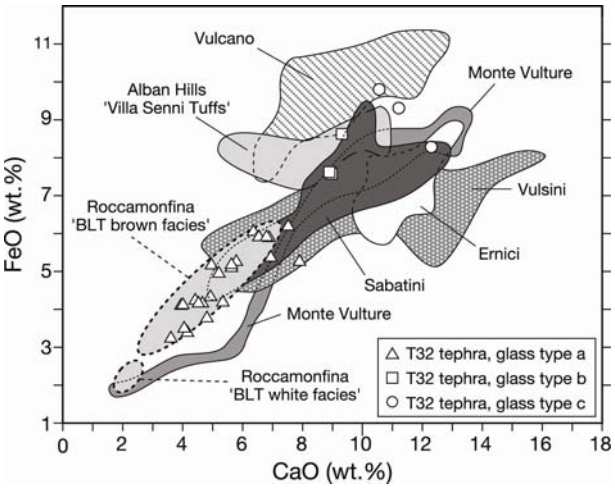

Fig. 3.8: Weight percentage diagram for the three T32 tephra glass types and published data: Vulcano (De Astis *et al*. 1997); Alban Hills (Freda *et al.* 1997); Roccamonfina (Luhr and Giannetti, 1987); Monte Vulture (De Fino *et al.* 1982; Raynal *et al*. 1998); Vulsini (Palladino and Agosta, 1997; Nappi *et al*. 1998); Ernici (Civetta *et al*. 1981); Sabatini (Conticelli *et al*. 1997).

According to the petrological composition, the volcanic complex of Roccamonfina provides the most likely source for tephra T32. Roccamonfina is a Pleistocene stratovolcano located 50 km NNW of Naples in the Campanian region (41°32'N, 13°98'E). Its history of activities is divided into three distinct stages (Giannetti, 2001): the leucite-rich high-potassium series (HKS) of stage I (546 to 374 ka), the leucite-poor to leucite-free low-potassium series (LKS) of stage II (317 to 96 ka) and the HKS-LKS rocks of an intermediate state, between 374 to 323 ka. The intermediate series comprise a complex succession of latitic to basaltic lava flows and trachytic pyroclastic fall and flow deposits (e.g. 'White Trachytic Tuff'; Giannetti and Luhr, 1983), whereas pyroclastic materials and laves from stage I activity are leucite tephritic to phonolitic in composition. One of the major pyroclastic eruptions near the end of stage I produced the 'Brown Leucitic Tuff' (BLT), dated by $^{40}Ar/^{39}Ar$ laser on sanidine crystals at 393 ± 12 ka (Giannetti, 2001). The BLT is a compositionally zoned pyroclastic flow deposit made up of three facies, which primarily differ in colour of pumices (white, brown, orange), lithic content and chemical composition (Luhr and Giannetti, 1987). Pumices from the BLT range from leucite trachytes in the lowermost white facies to phonolitic leucite-tephrites in the brown and orange facies covering a broad spectrum of High-K Series magma. In mafic BLT pumices (>5.6 wt % CaO), Na_2O is enriched relatively to K_2O reflecting strong analcimization of abundant groundmass leucites in these pumices. All BLT units contain <10% phenocryst volumes of green augite (salite), plagioclase, sanidine, biotite, titanomagnetite, leucite/analcime, apatite, pyrrhotite, xenocrysts of colourless diopside and olivine. The BLT flow deposits directly overlie a phonolitic pumice and ash-fall succession with a comparable composition, which may represent an early Plinian phase of the BLT eruption (Luhr and Giannetti, 1987).

Due to the very similar mineralogical and chemical composition of tephra T32 (Tabs 3.1, 3.2, 3.4; Figs 3.6, 3.8) with the BLT Plinian eruption of Roccamonfina it is assumed that tephra T32 represents a distal facies of the BLT eruption dated 393 ± 12 ka. This implies a widespread distribution of the BLT fallout products at least 600 km to the NNW, indicating southerly winds during the eruption. This may be confirmed by a possible correlation with the 'Bag' tephra found in Quaternary loess deposits along the river Danube in Hungary and Slovakia (Pouclet *et al*. 1999) which has a similar geochemical composition as tephra T32 (Figs 3.6 and 3.7; Table 3.4). Thus distal deposits of the BLT might become a key time marker for comparing terrestrial palaeoclimate records over a wide area in southern and central Europe.

DOI: 10.2312/GFZ.b103-07065

	T32, type a (n = 24)	T32, type b (n = 3)	T32, type c (n = 3)
BLT brown facies[a]	0.69 – 0.89	0.75 – 0.82	0.66 – 0.88
‚Bag' tephra, type 1a[b]	0.59	0.78	0.89
‚Bag' tephra, type 1b[b]	0.65	0.89	0.87
‚Bag' tephra, type 2[b]	0.81	0.78	0.69

[a]Luhr and Giannetti (1987), XRF whole rock data.
[b]Pouclet *et al.* (1999), EMPA data.

Tab. 3.4: Similarity coefficients of major elements of T32 tephra populations, the BLT brown facies and 'Bag' tephra types (after Borchardt et al. 1972). Major elements include the values of oxides SiO_2, TiO_2, Al_2O_3, FeO, MgO, CaO, Na_2O and K_2O.

3.7.2. Tephra T21d

Quaternary volcanoes producing alkaline rhyo-trachytic tephra are generally known from the Auvergne (Chaîne des Puys, Monts Dore), central Italy, the Eolian Islands and the Island of Pantelleria in southern Italy. Regarding the Italian volcanoes, the Islands of Salina (Eolian Arc), Ventotene and Santo Stefano (Eastern Pontine archipelago) as well as Monte Amiata (southern Tuscany) and Vico (Roman Province) have produced pyroclastics within the considered time span, but erupted trachytes are either under-saturated in silica or strongly enriched in potassium (Cioni *et al*. 1987; Ferrari *et al*. 1996; Perrotta *et al*. 1996; Bellucci *et al.* 1999; Fig. 3.9). The volcano of Pantelleria in the Straight of Sicily has produced large volumes of ignimbrites during the last 324 ka (e.g. Green Tuff, Ante-Green Tuffs; Civetta *et al*. 1984), which were widely distributed in the Tyrrhenian Sea (Paterne *et al*. 1988) and the Italian peninsula (e.g. in the Monticchio maar lake; Wulf *et al*. 2004). However, these pyroclastics are Na-alkaline in composition, richer in iron (Figs 3.9, 3.10) and feature a unique phenocryst assemblage. The major-element chemistry of Vulcano pyroclastics (Eolian Arc) matches well with the chemical composition of the T21d tephra (Fig. 3.9), but this volcano was active only during the last 120 ka (De Astis *et al*. 1997). The volcanic activity of the nearby Island of Lipari (Eolian Arc) was restricted to the last 42 ka and has only erupted rhyolites, which are over-saturated in silica (Crisci *et al*., 1991). Volcanism on the Island of Ponza (Western Pontine archipelago) occurred between 4.4 and 0.93 Ma and was characterized by the emplacement of older rhyolitic hyaloclastites and younger sub-aerial trachytic pyroclastic deposits (Bellucci *et al*. 1999), which have a different chemical composition than the T21d tephra (Fig. 3.9).

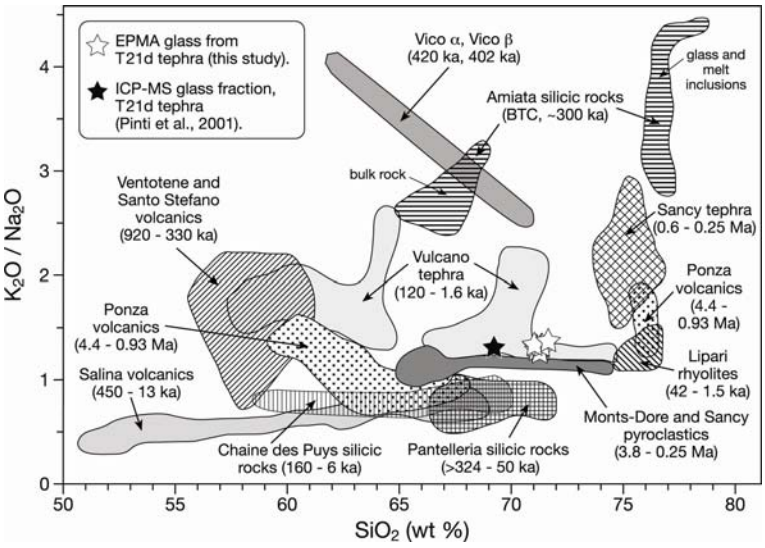

Fig. 3.9: Weight percentage diagram for T21d tephra and discussed volcanic sources. Data from: Amiata (Ferrari *et al*. 1996); Vico (Cioni *et al*. 1987); Ponza, Ventotene, Santo Stefano (Perrotta *et al*. 1996; Bellucci *et al*. 1999); Vulcano (De Astis *et al*. 1997); Salina (Keller, 1980); Lipari (Crisci *et al*. 1991); Pantelleria (Civetta *et al*. 1984; 1998); Monts Dore, Sancy (Briot, 1990; Briot *et al*. 1991; Roger, 2000); Chaine des Puys (Boivin *et al*. 1994; Vernet *et al*. 1998).

DOI: 10.2312/GFZ.b103-07065

In the Auvergne (Massif Central, France), numerous volcanoes with rhyolitic-trachytic composition were active during the Quaternary: the Western fault-scarp of the Limagne (160 to 70 ka) and the Chaîne des Puys (70 to 6 ka) in the north as well as the Guery (3.8 to 1.0 Ma) and Puy de Sancy stratovolcanoes (1000 to 250 ka) in the Monts Dore massif to the south (Fig. 3.7). The northern volcanoes produced tephras which are minor rhyolitic in composition and distributed only locally (Vernet *et al.* 1998*)*. Highly-explosive eruptions of the Monts Dore volcanoes, in turn, emitted tephras of trachytic and rhyolitic composition, which are widespread in the east and southeast (Pastre and Cantagrel, 2001). In particular, the Sancy volcano was active within the considered time span, producing several pumice flow and ash fall deposits at 900 to 700 ka, 580 ka and 450 to 250 ka (Pastre and Cantagrel, 2001). During its final phase of activity, two tephra events occurred:

(1) The Plinian 'Queureuilh' eruption produced a basal pumice fallout deposit and a succession of ash beds and pumice fall and flow units. A relative age estimate of this formation is given by the underlying shoshonitic Puy de L'Angle lava flow dated at 290 ± 30 ka (Cantagrel and Baubron, 1983).

(2) The 'Rivaux' eruption emitted a small-volume pumice flow and several fall out units of ash and pumice. The age of this tephra formation is constrained by its intercalation between a 470 ± 200 ka shoshonitic lava flow and the 320 ± 30 ka 'nuées ardentes' from the Puy de Cliergue (Cantagrel in Lavina, 1985).

The 'Queureuilh' and 'Rivaux' tephras are both rhyo-trachytic in composition and characterized by a mineral assemblage of feldspar, biotite, green clinopyroxene, sphene, apatite and zircon (Pastre and Cantagrel, 2001) resembling that of the Pànico T21d tephra. The comparison of EPMA major-element data of glass components shows higher CaO and FeO values for the 'Queureuilh' tephra than for the T21d tephra, whereas the 'Rivaux' tephra matches well the chemical composition of the Pànico tephra (Fig. 3.10). Accordingly, we suggest the Pànico T21d tephra correlates with the 'Rivaux' tephra from the Sancy volcano (320 ± 30 to 470 ± 200 ka). This implies a widespread distribution of 'Rivaux' fallout products at least 550 km to the east, indicating westerly wind direction during the eruption.

In contrast to these results, Pinti *et al*. (2003) concluded that the T21d tephra originated from an unspecified source in the southern Tyrrhenian Sea. However, they only considered volcanic eruptions around the time of their obtained K/Ar age (779 ± 13 ka) leading them to rule out younger volcanic events as possible sources.

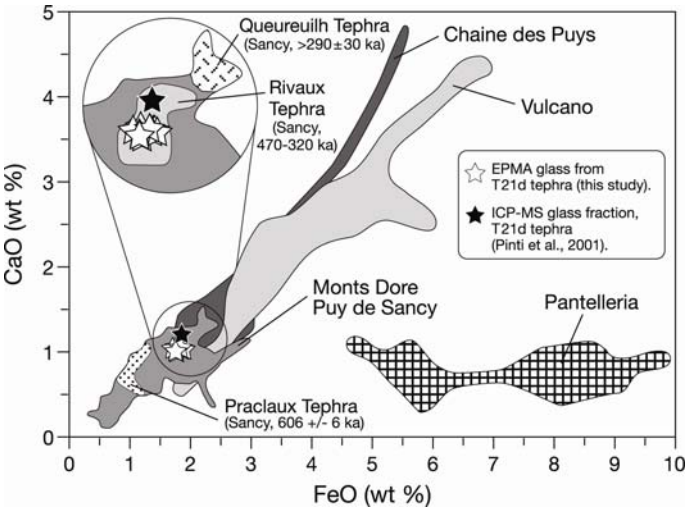

Fig. 3.10: Weight percentage diagram for T21d tephra and data from Monts Dore and Puy de Sancy volcanics (Roger, 2000; Pastre and Cantagrel, 2001).

3.8. Discussion

On the basis of the identification of the Brown Leucitic Tuff in the lake deposits, an age of about 400 ka is inferred for the Pànico interglacial record. This implies correlation with marine oxygen

DOI: 10.2312/GFZ.b103-07065

isotopic stage (OIS) 11, which, however, contradicts the K/Ar age of 779±13 ka obtained for the T21d ash layer (Pinti *et al*. 2001). Two potential causes for this discrepancy are conceivable. These are either a major hiatus in the sediment record between the two tephra layers, or, problems with the K/Ar dating.

A hiatus of more than 300 ka between both ash layers is very unlikely. Only two processes could have caused such a long interruption of lacustrine deposition, either complete drainage of the lake or post-sedimentary erosion by an overriding glacier. Environmental processes of such extent should have left traces in the sedimentary record. If the lake had completely dried out, one would expect soil horizons or at least root systems to develop, which do not occur. In contrast, the lacustrine facies is continuous at least over 20 m from the base of the BVC until the top of the present profile including the 8·1 m interval between both tephra layers. This continuity of sedimentation is further confirmed by the continuous pollen succession (Rossi, 2003). Problems in connecting the three outcrops (Main Section, Wall Section, Deer Section, see Figs 3.1 and 3.2) can be also excluded because of the robust correlation in thin sections down to an annual level (varve micro-facies). From this we conclude that the K/Ar date of 779 ± 13 ka for the T21d tephra must be too old.

In addition to general problems with K/Ar dating of young volcanic deposits (Richards and Smart, 1991) dating of the Piànico tephra is particularly difficult because it is a very fine-grained distal ash layer. Grain sizes of the glass shards with potassium concentrations <5% are only between 40-80 µm in seven of eight dated samples (Pinti *et al*., 2001). Only one sample contained somewhat coarser, but still rather fine glass shards of 80-125 µm. Consequently, the total surface area of dated grains was large which makes the sample more sensitive to water-rock interactions (Kraml, 1997). A well-known example for an over-estimation of a distal tephra layer is the Praclaux tephra in the lake record from Praclaux in the French Massif Central. Palynological interpretation reveals that the sediment interval in which this tephra layer occurs clearly correlates with OIS 11 (Reille *et al*. 2000). In contrast, radiometric dates suggest a 200 ka older age although even laser $^{40}Ar/^{39}Ar$ dating was applied on single sanidine crystals (Roger, 2000). In this case the radiometric date was regarded as 'disturbing' and rejected Reille *et al*. (2000). In contrast, Pinti *et al*. (2001) tried to confirm their K/Ar dates for the T21d tephra through palaeomagnetic analysis. They found one sample showing a reversed polarity, but their conclusion placing the Brunhes/Matuyama boundary within the Piànico interglacial sediments is not convincing. Firstly, the only sample showing reversed polarity is taken 5 m below the BVC unit that is the varved interglacial sediment unit on top of which the T21d tephra occurs. The sample has been taken from the SAB unit, and between the SAB and BVC distinct unconformities occur with the probability of even major gaps in the sediment sequence. Secondly, the sample originates from a clearly distorted outcrop (Discarica Section, Fig. 3.2).

Apart from the indications that the published K/Ar age of ~780 ka is too old it would have been desirable to confirm our dating of ~400 ka for the Piànico interglacial sediments by independent means. However, an attempt with U/Th dating failed because the carbonate succession of Piànico does not represent a closed system (M. Stein, pers. comm.). Also relative biostratigraphic dating did not reveal a clear result although a detailed pollen diagramme has been established (Rossi, 2003). The vegetation succession in the nearest long and continuous pollen records from Bouchet/Praclaux (Reille *et al.* 2000; de Beaulieu *et al*. 2001*)* and Ioannina/Tenaghi Philippon (Tzedakis *et al*. 1997) which include the interglacial at ~400 ka differs too much from the southern Alps to allow an unambiguous correlation. Nevertheless, the abundance of exotic pollen taxa might be an indicator for the stratigraphical position of the interglacial. The only sporadic occurrence of *Pterocarya* and *Tsuga* in the Piànico sediments (Martinetto and Ravazzi, 2002; Rossi, 2003) is more similar to the Praclaux interglacial (correlating with OIS 11; Reille et al. 2000), where also small amounts of *Pterocarya* have been found, than to early Middle Pleistocene interglacial sediments from Italy such as Leffe (>880 ka BP; Ravazzi *et al*. 2005) and Cesi (>600-

DOI: 10.2312/GFZ.b103-07065

700 ka BP; Bertini, 2000), which have a different floristic composition and contain higher abundances of exotic taxa.

If the correlation of both the Praclaux and Piànico interglacials to OIS 11 is correct, one might expect the 'Rivaux' ash to appear not only at Piànico (about 550 km to the east of the Sancy volcano; Fig. 3.7) but also in the sediments from Praclaux (about 100 km to the southeast of the Puy de Sancy). However, the chemistry of glass shards from the only ash layer reported so far within the Praclaux interglacial is to a certain degree different (Roger, 2000). Si concentrations are 3-5 % higher, whereas Na concentrations are 1-2% lower. Nevertheless, it is interesting to note that radiometric dating of both the Praclaux and Piànico T21d tephras have produced ages 200-300 ka older than the assumed age of ~400 ka as derived from biostratigraphy and tephrochronology, respectively. Further investigations on the distal tephra layers in Piànico and Praclaux records as well as the proximal near vent deposits are needed to establish this ash layer as a distinct marker layer to compare unequivocally two key interglacial lake sediment records.

3.9. Conclusions

- Two volcanic ash layers have been detected by microscopic analysis within the interglacial lake sediment record from Piànico in the southern Alps. These tephra layers occur during the final phase of the interglacial and a period of interstadial conditions within a time span of ~7500 varve years. The chemical composition of volcanic glasses from the older tephra is alkaline rhyo-trachytic, whereas the younger ash layer is phonolitic to phonotephritic.
- Tephrochronological correlation of the younger tephra with the Brown Leucitic Tuff from the Roccamonfina volcano is unambiguous and dates the Piànico interglacial sediments to ~400 ka, which makes it contemporaneous with OIS 11. Since this interglacial is regarded as good analogue for the present interglacial (Loutre, 2003), the varved sediments of Piànico are a key archive for natural interglacial climate dynamics at seasonal to decadal resolution.
- The older tephra in the Piànico record probably originates from the 'Rivaux' eruption of the Puy de Sancy volcano in the Auvergne. Even if this correlation requires further proof by studies of near vent deposits, it is the first indication for long distance transport of volcanic ash from the Massif Central over hundred kilometres to northern Italy. This ash layer has a high potential for establishing a distinct marker horizon for correlating terrestrial interglacial lake records in France and Italy.
- Absolute dating is still a major problem in Quaternary stratigraphy and terrestrial palaeoclimate studies dealing with floating records of past interglacial sediments. It has been demonstrated that radiometric dating of tephra layers in lake sediments alone can for various reason be misleading. Typical problems in dating such distal tephra layers are insufficient grain size and a lack of feldspar. However, tephrochronology has great potential to fill this gap by correlating these fine-grained tephra layers with near-vent deposits that are more reliably dated by radiometric techniques.

3.10. Acknowledgements

We would like to thank Helga Kemnitz for support with the SEM analysis, Michael Köhler for preparing high quality thin sections and Andreas Hendrich for his help with designing the figures. We are also grateful to Anna Paganoni, Federico Confortini and Matteo Malzanni (Museo di Scienze Naturali di Bergamo) for their help with our field work. Comments from D.A.G. Nowell and an anonymous reviewer greatly improved the manuscript.

DOI: 10.2312/GFZ.b103-07065

4. Palaeoclimatic implications from micro-facies data of a 5900 varve time series from the Piànico interglacial sediment record, Southern Alps

Achim Brauer[a,*], Clara Mangili[a], Andrea Moscariello[b], Annette Witt[c]

[a] *GeoForschungsZentrum Potsdam, Sektion 3.3 Klimadynamik und Sedimente, D-14473 Potsdam, Germany*

[b] *Cambridge Quaternary, Department of Geography, University of Cambridge, Cambridge, U.K.*
[c] *King's College London, Department of Geography, Environmental Monitoring and Modelling Group, London, U.K.*

Submitted to Palaeogeography, Palaeoclimatology, Palaeoecology

Abstract - *Varve micro-facies analyses have been carried out on a 405 cm thick annually laminated sediment sequence from the Piànico palaeolake in the Southern Alps. This varve counted interval represents the uppermost 5900 years of a ca 400 kyrs old interglacial lacustrine deposit with a minimum length of 16 000 varve years. Intercalated in the varve succession are: (i) detrital layers, (ii) debris flows (slump deposits), and (iii) micritic calcite layers. The annual couplets are composed of a dominant light summer layer of biochemically precipitated calcite and a thin dark winter layer consisting of organic and minerogenic detritus. Microscopic correlation of individual couplets in two outcrops 130 m apart demonstrated basin-wide continuity of varve deposition. Summer layers have been found to be composed of up to four sub-layers differing in grain size, most likely reflecting discrete pulses of calcite precipitation. Two long periods of pronounced decreases in varve thickness occur within the interglacial (1100 varve years) and during the decline of full interglacial conditions (480 varve years) suggesting colder climatic conditions. The decreases in varve thickness are further accompanied by changes in the pattern of summer sub-layering. The first cold interval reflects an exceptionally long intra-interglacial climatic fluctuation indicating a mode of climatic variability different from the present interglacial. Wavelet analyses of seasonal layer thickness data revealed that periodic variations of solar activity (88-yr and 208-yr cycles) and probably of thermohaline circulation (512-yr cycle) impact on varve formation at certain intervals of the studied time window.*

Keywords: interglacial, calcite varves, varve micro-facies, varve chronology, wavelet analyses

4.1. Introduction

Annually laminated lake sediments are considered as valuable archives of past environmental and climatic changes because they provide an essential of palaeoclimatic records: precise chronologies. Apart from the widespread use of varves as chronological tool, however, the palaeoclimatic information inherent in the composition and structure of seasonal layers (i.e. varve micro-facies) is only rarely evaluated (Brauer, 2004). In case of varves applied as climate proxy, mainly thickness variations have been facilitated although this parameter integrates various sedimentation processes that are controlled by different climatic and environmental factors at different periods of the year (Brauer et al., 1999). More detailed information on changes in seasonality (Lücke and Brauer, 2004) and on the nature of decadal-scale oscillations (Prasad et al., 2006) has been obtained from varve micro-facies underlining the large potential of varves as climatic indicator for changes in seasonality.

Soon after the first discovery of annual laminations in proglacial environments and their definition as varves (de Geer, 1912), seasonally formed calcite laminations have been reported in carbonatic lake settings that formed under warm climate in the Holocene (Nipkow, 1920). Since that time numerous studies demonstrated that temperature and biological productivity are the main controlling factors for calcite precipitation in modern environments (e.g. Minder, 1922; Brunskill,

DOI: 10.2312/GFZ.b103-07065

1969; Koschel et al., 1983; Gruber et al., 2000). Based on this knowledge it was possible to interpret Holocene and Lateglacial calcite varve records in terms of past climate changes (e.g. Ludlam, 1969; Geyh et al., 1971; Lotter, 1989; Goslar et al., 2000).

One problem of using Holocene climate records for tracing natural climate variability, however, are human activities on local to global scale that not only might have a direct impact on climate evolution, but certainly also affect sediment deposition in lakes. Since human impact might have started even rather early in the Holocene (Ruddiman, 2003), it is important to gather additional information from high resolution sediment records from past interglacials that reflect exclusively natural climate variability. However, as with Holocene records, varves in the few reported annually laminated interglacial records (Müller, 1965, 1974; Moscariello et al., 2000; Nitychoruk et al., 2005) were used only for chronological issues, *i.e.* the estimation of interglacial lengths. Thus, the potential of varve micro-facies data for tracing seasonal to decadal-scale climatic variability is not exploited yet. A first attempt has been presented by Mangili et al. (2005) who discuss seasonal occurrences and frequencies of detrital layers within the varved record of the Piànico interglacial record based on micro-facies analyses. This study focuses on varve micro-facies and thus is considered a further step towards a better palaeoclimatic interpretation of the Piànico interglacial record.

4.2. Site and sediments

The sediments of the Piànico Formation formed near the north-western margin of the present Lake Iseo in the southern alpine foothills (Fig. 4.1). Today, lacustrine sediment sequences of the Piànico palaeolake outcrop on both sides of the steep valley incised by the Borlezza stream, a tributary of Lake Iseo (45°48'N, 10°2'E). For this work a 405 cm thick interval has been investigated in detail in two outcrops, labelled Main Section and Wall Section (Fig. 4.1).

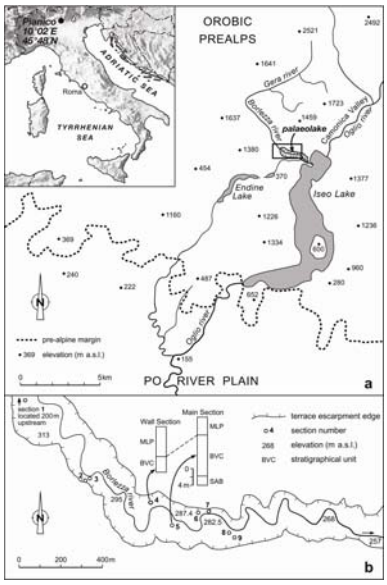

Fig. 4.1: (a) Location of the Piànico palaeolake at the southern margin of the Alps within the Borlezza valley. (b) Borlezza valley with the locations where lacustrine sediments are outcropping (sections) including schematic profiles of the two studied sections (Main Section and Wall Section). The stratigraphical units are: MLP (La Palazzina Member, predominantly clastic-detrital with endogenic calcite intercalations); BVC (carbonate varved bed, continuous calcite varve formation); SAB (basal silt and clay).

The palaeolake was about 3–4 km long and about 700–800 m wide (Casati, 1968; Fig. 4.1). The depth of the palaeolake might be roughly calculated from the difference of the reconstructed lake level (about 380 m a.s.l., Penck and Brückner, 1909) and the elevation of the present lacustrine

DOI: 10.2312/GFZ.b103-07065

outcrops (281–329 m a.s.l., Moscariello et al., 2000). Assuming that no major vertical movements have taken place in the basin, the lake was about 50 - 100 m deep.

The deposits from the Piànico-Sèllere basin are known since more than 150 years and a detailed summary of previous work is given by Moscariello et al. (2000). A major issue of controversy in the past was the stratigraphical position of the interglacial sediments (Brauer et al., 2006). Recently, a distal volcanic ash layer found in the sediments has been correlated with the the Brown Leucitic Tuff (BLT) originating from the Roccamonfina volcano in southern Italy (Brauer et al., 2006). This eruption is well-dated by Ar/Ar methods to 393±12 ka (Giannetti, 2001) thus correlating the Piànico interglacial record with marine isotope stage 11.

4.3. Methods

For micro-facies analyses and measurements of seasonal layer thickness optical techniques have been applied. A continuous series of 62 overlapping large-format thin sections (120 x 35 mm) has been investigated with a petrographic microscope (Carl Zeiss Axiophot) at various magnifications and optical conditions (plain parallel light and polarized light). Thickness measurements were always made at 100x magnification. Thin-section images were obtained with a digital camera (Carl Zeiss Axiocam). In addition, 23 selected samples have been studied with a Scanning Electron Microscope (SEM, Zeiss NTS DSM 962).

Thin section preparation techniques had to be adjusted to the special requirements of hard and compact outcrop sediments for which the method developed for soft sediments from modern lakes (Brauer et al., 1994; Lotter and Lemcke, 1999) was not applicable. Samples have been taken from the outcrops in especially designed stainless steel boxes (33 x 5 cm) with removable side walls. These enabled to remove the sediment blocks in the laboratory without mechanically breaking them. The outcrops were cleaned with a sharp knife until a smooth and vertical surface was obtained before a block of sediment with the size of the steel box was carved out in situ so that the steel box could be pushed on the sample. The sample block was then carefully cut out without breaking the sediment. These sample blocks were taken with a minimum of 5 cm overlap. It was assured that at least two distinct marker layers appeared within the overlapping part.

In the laboratory the sediment blocks were removed from the steel boxes and placed into larger aluminium boxes in which they were carefully dried 1-2 days at room temperature to avoid quick shrinkage and cracking. The dry surfaces then were covered with a transparent epoxy resin to obtain a surface impregnation of 1-2 mm. The coverage with resin further stabilized the sediment blocks so that three ca 2 cm thick slices could be cut off with a belt saw. The freshly cut surfaces of these slices were again impregnated with resin. From one of these slices ca 10 cm long and 1.5 cm wide sub-samples have been cut out with an overlap of at least 2 cm each. These sub-samples have been used for preparation of thin sections following standard procedures. Identification of either single marker layers or a characteristic succession of varves within the overlapping interval enabled to link all thin sections to a continuous time series through microscopic varve-to-varve correlation.

Wavelet analysis has been applied to search for periodic variations in varve thickness data. This data analysis technique is appropriate to identify occurrence intervals and related amplitudes of periodic components of non-stationary time series (Torrence and Compo, 1998). A standard example of a non-stationary time series is a super-position of several periodic signals, each of them with temporarily varying amplitude. This appears to be an appropriate model for the series of varve thicknesses from the considered sediment. Due to the large observational interval of almost 6000 years, varying environmental and climate boundary conditions should have caused temporal

DOI: 10.2312/GFZ.b103-07065

variations of the susceptibility of varve formation to periodic forcing mechanisms making a time-continuous response unlikely. In addition, paleoclimate proxy data must be treated appropriately: uneven time sampling or gaps along the time axes cause standard approaches to fail. However, the wavelet analysis algorithm proposed by Foster (1996), that is designed for investigating unevenly spaced data, has shown to be suitable for the analysis of such time series (Witt and Schumann, 2005).

4.4. Results

4.4.1. The studied sediment interval

The Piànico Formation has a total thickness of ca 48 m and is subdivided into four main lithostratigraphical units (Moscariello et al., 2000). This study focuses on the uppermost 405 cm of the continuously varved section labelled as BVC (carbonate varved bed; Fig. 4.2). The transition to the overlying MLP unit (La Palazzina Member), which is characterized by an intercalation of clastic-detrital lamination and partly varved endogenic calcite intervals, is marked by a sharp boundary. Micro-facies changes at this boundary reflect major changes in climatically-driven environmental processes (Mangili et al., 2005). The contact of the varved BVC unit to the underlying silt and clay unit is marked by a thick debris flow deposit that includes slumped varve intervals (basal slump, Fig. 4.2). The total thickness of the BVC (including the basal slump) is ca 11.50 m and slightly varies between different outcrops. For this study continuous micro-facies and seasonal layer thickness data are obtained for the uppermost 5900 calcite varves from a total of approximately 16 000 (counted with 10x magnification lense in the outcrop) in the BVC. Intercalated in the studied varve series are three types of non-annual layers reflecting different depositional processes: (i) slump deposits, (ii) detrital layers, and, (iii) dense micritic calcite layers which also will be briefly described.

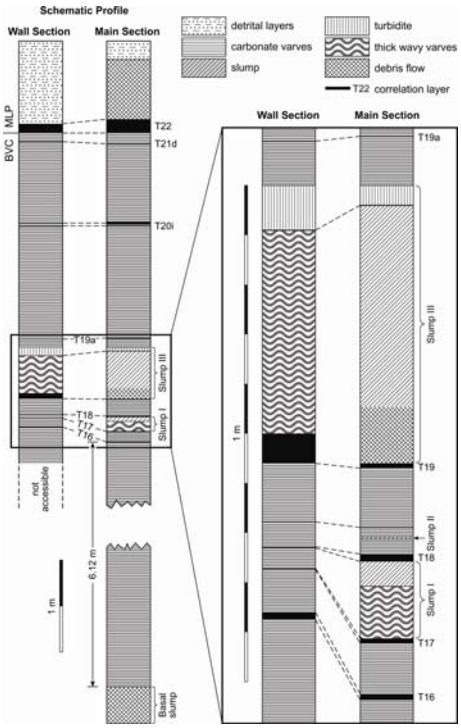

Fig. 4.2: Schematic composite profile from the two studied outcrops termed Main Section and Wall Section. The slumped part in the Wall Section has been bridged by the corresponding part in the Wall Section using well defined correlation layers (T16, T17, T19a). Note: on the right side the correlation for the interval including the slump succession is enlarged to show more details of the correlation.

DOI: 10.2312/GFZ.b103-07065

4.4.2. Calcite varve micro-facies

The regular and finely laminated sediments of the BVC unit consist of couplets of predominant light and subordinate dark layers (Fig. 4.3). Light layers consist of euhedral calcite crystals of up to 15 µm in size, comparable to observations in Holocene sediments from Lake Zürich in Switzerland (Kelts and Hsü, 1978) and Schleinsee in southern Germany (Geyh et al., 1971).

The common crystal habits are blocky polyhedric and simple rhombic forms (Fig. 4.4a) which are characteristic for low-Mg calcite in freshwater environments (Folk, 1974). The blocky polyhedric crystals usually have some rough crystal faces indicating obstructed surface growth (Koschel, 1997). Dissolution features are generally absent, except for a section of thinner varves where crystals with rounded edges have been found (Fig. 4.4b). Within the calcite layers few dispersed diatom frustules with dissolution features occur. The commonly thin dark sub-layers are composed of amorphous organic matter and plant remains (leaves, seeds) and abundant fragments of diatom frustules. Occasionally, few angular-shaped quartz and dolomite grains up to 60 µm diameter (coarse silt) are scattered within the fine-grained (<2 µm) matrix (Fig. 4.3b). These isolated detrital grains are assumed to be wind-transported. Some thicker dark layers contain higher amounts of clastic and organic detritus. The transition from calcite layers to the overlaying organic-detrital layers is mostly diffuse, whereas the boundary between the dark layer and the following calcite layer is sharp (Fig. 4.3c) reflecting a break in sediment accumulation. This seasonal layer succession is predominantly controlled by the annual cycle of calcite precipitation in spring and summer resulting in light layer deposition proving the Piànico couplets as true varves. This interpretation is confirmed by the similar seasonal deposition pattern in Holocene varves described in Swiss lakes (e.g. Kelts and Hsü, 1978; Lotter, 1989).

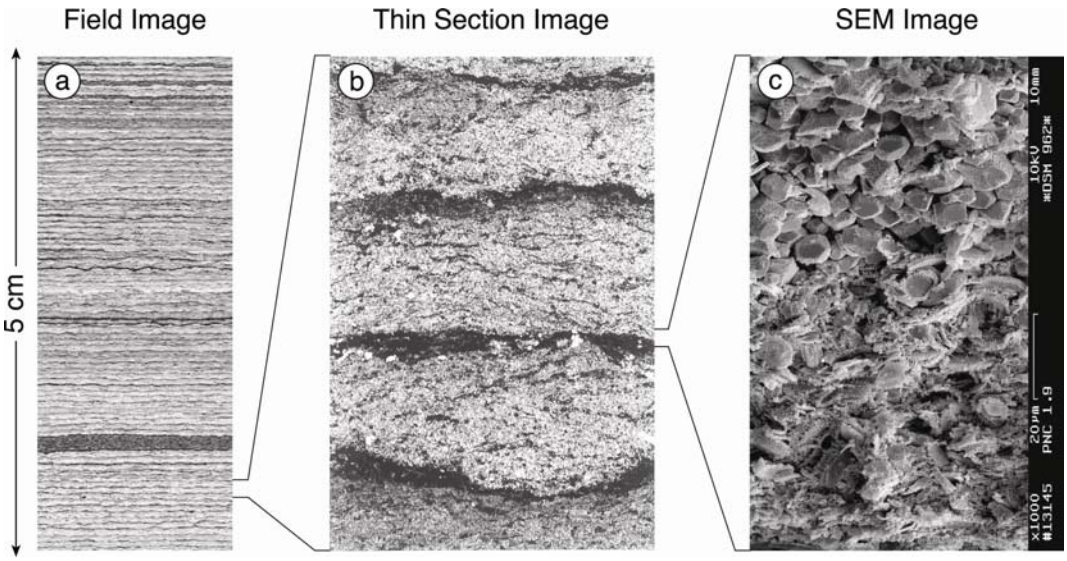

Fig. 4.3: Scanned section of a polished sample of the varved succession in original size (a), zoom of three varves photographed from a thin section with white summer and dark winter layers (b), SEM-image of the boundary between a winter and a summer layer (c).

DOI: 10.2312/GFZ.b103-07065

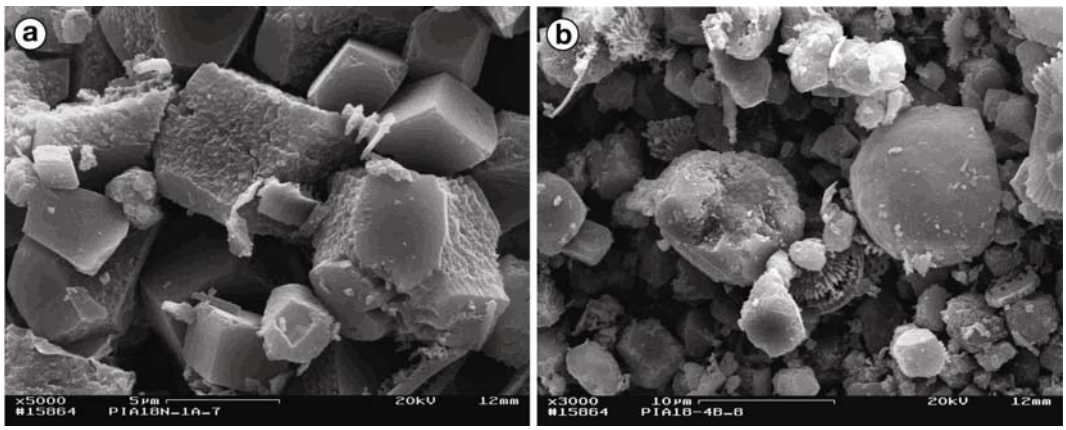

Fig. 4.4: SEM-images from two summer calcite layers exhibiting variations in calcite crystal morphologies: (a) Image from an average thick varve before the interval of reduced calcite layer thickness (varve no. 5325) showing simple rhombic forms and blocky polyhedra with rough crystal faces. (b) Image from a summer layer of the early part of the interval with reduced varve thickness (varve no. 5180) comprising calcite crystals with distinct dissolution features.

Most of the summer calcite layers in the studied interval (67.1%, Tab. 4.1) show a further distinct subdivision in a lower sub-layer of coarser calcite crystals and an upper layer of finer crystals (Fig. 4.5c, d) that has been also observed in calcite varves from other lakes (Geyh et al., 1971; Kelts and Hsü, 1978). The coarse crystals are about 7-15 µm, whereas the finer crystals do not exceed 7 µm in size. The relatively sharp boundary between sub-layers of different crystal sizes (Fig. 4.5c, d) suggests a succession of two production pulses rather than deposition due to different settling velocities. However, not all summer layers show this two-fold structure but exhibit more complex patterns of sub-layering which so far have not been described from calcite varves. Some calcite layers (5.7%) consist of two coarse – fine cycles summing up to four sub-layers (Tab. 4.1). For 7.6% of the summer layers a clear three-partition has been observed. Most of these layers start with a sub-layer of small crystals followed by a coarse-grained and another fine-grained sub-layer (Fig. 4.5b). This is a further proof that the sub-layering is not caused by different settling velocities but by a succession of distinct pulses of calcite precipitation. Only 11.1% of the calcite layers in the studied interval do not show any sub-layering. Almost all (97.6%) of these layers are formed by fine crystals (Tab. 4.1, Fig. 4.5a).

Number of Sub-layers	Subdivision Pattern (crystal sizes)	Number of Varves	% of all Varves
1	fine[#1]	657	11.1
2	coarse – fine	3958	67.1
3	fine – coarse – fine[#2]	448	7.6
4	coarse – fine – coarse – fine	339	5.7
	unidentified	500	8.5

[#1] pattern of 97.6% of these layers, 2.4% are formed by coarse calcite crystals
[#2] pattern of 91.3% of these layers, 8.7% show a coarse-fine-coarse pattern

Tab. 4.1: Number and succession of summer calcite sub-layers

DOI: 10.2312/GFZ.b103-07065

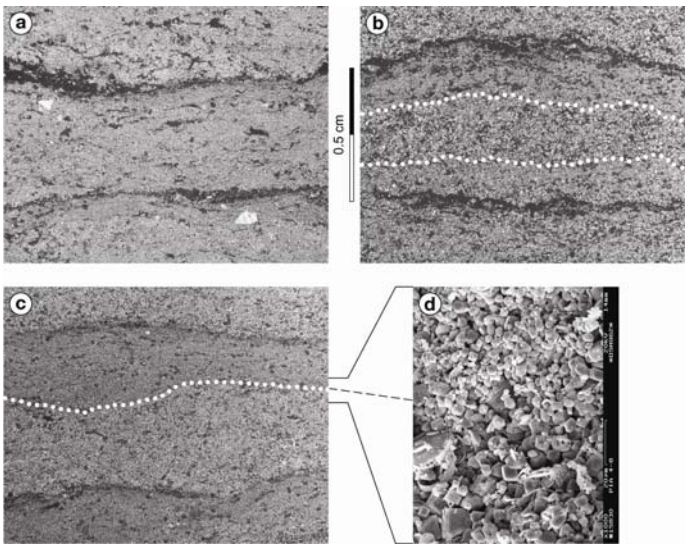

Fig. 4.5: Thin section images of different calcite sub-layer micro-facies based on sizes of calcite crystals: (a) one sub-layer, (b) three sub-layers showing a fine-coarse-fine succession, (c) two sub-layers, fine above coarser grained, (d) SEM zoom out of transition between coarse and small crystal sub-layers.

4.4.3. Varve and seasonal layer thickness

Thickness measurements of light and dark layers have been obtained for all varves (Fig. 4.6) except for 350 couplets that were deformed by post-depositional processes. The floating varve series ends with the youngest varve (varve no. 1) deposited on top of the BVC unit just before the shift to the detrital dominated sediments of the MLP unit. Total varve thickness of the measured series varies between 0.14 and 1.1 mm with an average of 0.56 mm. An interval of approximately 1100 thinner varves appears in the lower part of the studied section between varve numbers 4150 and 5250 (Fig. 4.6). A clear trend of decreasing varve thickness is further observed for the uppermost ca 480 varves.

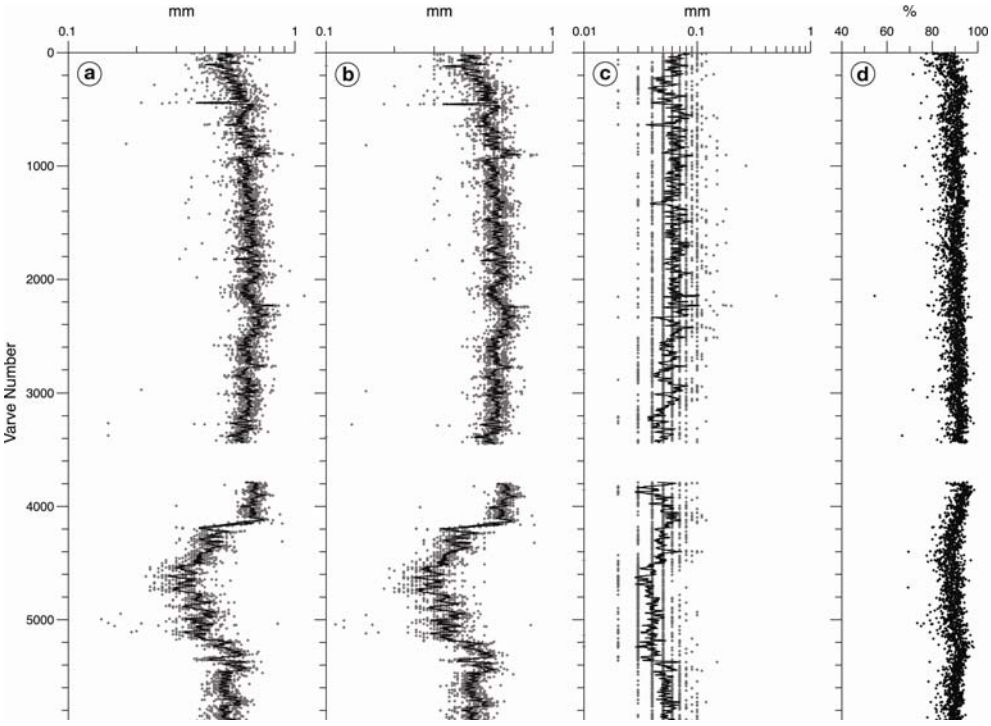

Fig. 4.6: Varve and sub-layer thickness variations (a) total varve, (b) summer sub-layer, (c) winter sub-layer thickness, (d) % of summer layer from the total varve thickness. Note: the '1' varve marks the boundary between the BVC and MLP units.

DOI: 10.2312/GFZ.b103-07065

In general, summer calcite layers are 5-10 times thicker than detrital winter layers (Fig. 4.6 a, b). This is clearly expressed in Fig. 6d showing the portion of calcite layer in percent of the total layer thickness. In more than 99% of all varves the calcite layer constitutes >80% of the total varve thickness. This is in good agreement with observations in recent Fayetteville Green Lake where 90% of the mass of annual sedimentation occurred through calcite precipitation in summer (Brunskill, 1969). Thus variations in total varve thickness are mainly controlled by variations in calcite layer thickness (Fig. 4.6). This general pattern is in agreement with observations from Lake Soppensee with variable sedimentation rates of calcite and rather constant sedimentation rates of organic carbon (Gruber et al., 2000).

Wavelet analysis was carried out over the entire observational epoch for period lengths between 10 and 1000 years. Timings and frequencies are identified whose related amplitudes are significantly larger than the red noise background signal. The results are presented separately for the series of summer and winter layer thicknesses (Fig. 4.7). We have focussed on period lengths that have maximum amplitudes over a time interval of at least three times the length of that period. The related pattern in the wavelet amplitude map is a horizontal light stripe (Fig. 4.7). Three cycles of 88, 208, and 512 years and their multiples appear over certain time intervals (Tab. 4.2; Fig 4.7). The multiples of the original cycles are related to amplitude modulations. For instance, a fourfold cycle length is generated if a high-amplitude oscillation is followed by three ones with small amplitudes. It may happen that the multiples of a cycle are found, but not the cycle itself. This is a side effect of the wavelet method itself: for each period, data in a window with a length of 10 times that period are analyzed. Consequently, larger cycles are related to longer windows. If the studied periodic oscillation is superposed by other oscillations or by noise, it can be identified only if a sufficiently long data series is considered. Since the number of analyzed data points is proportional to the period, the original periodic signal may be covered by the remaining signal components, but the amplitude modulated multiples can be detected. Further, if a cycle over a certain period is identified, but none of its multiples, then this cycle is of almost constant amplitude. Two of the detected periodicities are related to solar activity variations, the well-known Gleissberg cycle (88 yr) and the 208 yr cycle (Gleissberg, 1944; Stuiver and Braziunas, 1993; Damon and Peristykh, 2000), whereas the 512-yr cycle may have an origin in ocean thermohaline circulation (Damon and Peristykh, 2000). None of the shorter decadal periodicities related to solar activity like, for instance, the 11-yr sunspot cycle has been found.

Periodicity	Summer layers (varve numbers)	Winter layers (varve numbers)
88-yr (Gleissberg)	4000-5600*	1-900
178-yr (2-fold)	400-1200	
356-yr (4-fold)		2500-5900
712-yr (8-fold)		3800-5900
208-yr	2700-4200 5000-5900	500-3900
416-yr (2-fold)	1800-5800	
832-yr (4-fold)	1-3200	
512-yr	1-2500	1-1300 2500-4000

* With two short-term interruptions

Tab. 4.2: Periodicities detected in summer and winter layer thickness data by wavelet analysis (see also Fig. 4.7)

DOI: 10.2312/GFZ.b103-07065

In general, more cycles and more periods in which periodicities appear have been found in the summer layer data. In the calcite layer series the 88-yr cycle and its twofold multiples preferably appear in the lower part of the record, in particular around the period of decreased varve thickness (Fig. 4.7c). In the winter layer record the Gleissberg cycle is restricted to the upper part (Fig. 4.7d) as well as its fourfold and eightfold multiples. A similar pattern is observed for the 208-yr cycle with the exception that multiples also appear in the younger part of the series. The 512-yr cycle occurs more frequently in the winter layer data but not at all in the lowermost 2000 varves.

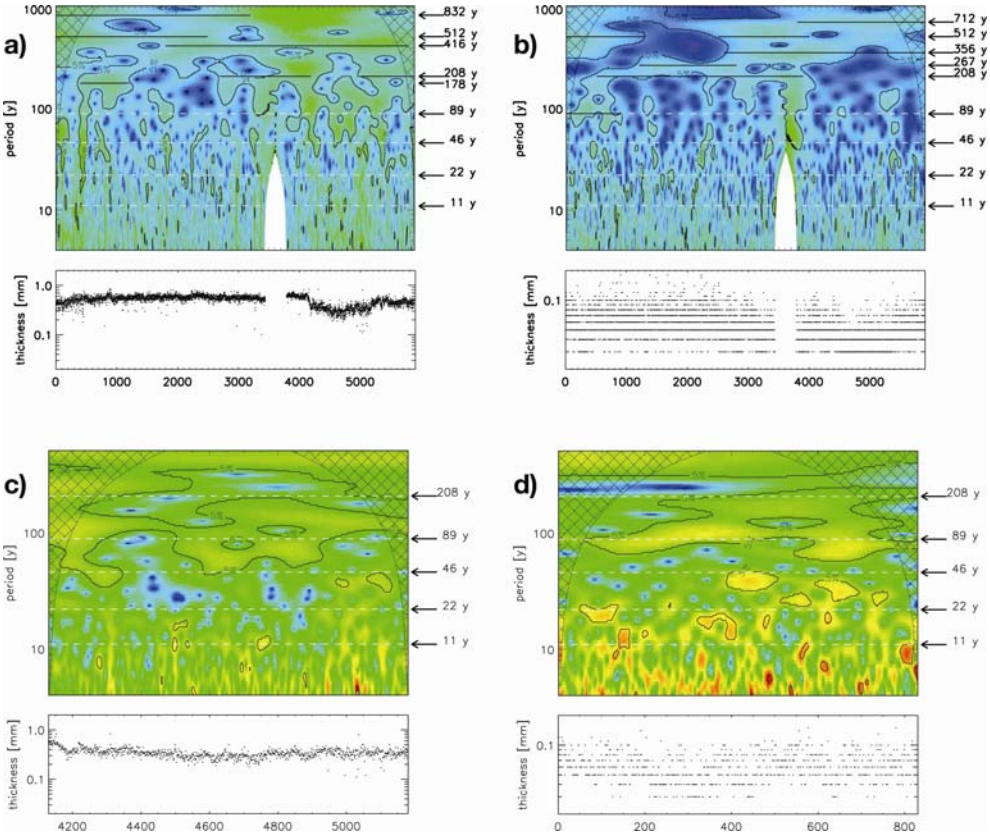

Fig. 4.7: Wavelet amplitudes maps for (a) total summer layer data, (b) total winter layer data, (c) selected interval of summer layer data from varve no. 4130–5180, (d) selected interval of winter layer data from varve no. 1-830. Depending on varve number and period length, wavelet amplitudes are colour coded from black (very low amplitudes) over grey to light grey (highest amplitudes). White areas along the bottom are related to the gap in thickness data from varve no. 3473-3787, where wavelet amplitudes cannot be estimated reliably. Cross hatched regions indicate the cone of influence, where wavelet analysis is affected by edge effects. Contoured areas indicate time intervals and period length that are significantly different from the red noise background (an error probability of 5 % is assumed).

4.4.4. Slump deposits

Slump deposits are a rare facies within the 16 000 year time series. The thickest slump (>2m) occurs at the base of the BVC (basal slump, Fig. 4.2) and has been found in all inspected outcrops (Fig. 4.1). The lower part of this slump deposit consists of detrital material from the catchment including large dolomite boulders up to decimetre size indicating a high energy event. In the upper part reworked shallow water sediments as inferred from the occurrence of littoral mollusc species like *Tanousia sp.* (Esu, pers. comm.) and lumps of intensively folded varve interval suggest

DOI: 10.2312/GFZ.b103-07065

significant erosion caused by this event. Thus a major hiatus at this position in the sediment profile is likely.

After deposition of the basal slump no slumping occurred for ca 11 500 varve years until a series of three slumps (labelled as slump I – III, Fig. 4.2) was deposited within 250 varve years. The first two of these slumps (I and II) only locally appear in the Main Section (MS). Slump I is ca 20 cm thick and comprised of a basal clay layer, which probably acted as a sliding plane, followed by a section of thicker, extremely undulating varves, an interval of strongly folded varves and a detrital layer on top (Fig. 4.2). Both the basal an the top layer of slump I can be correlated with their distal expressions in the Wall Section (WS), 130 m to the NW from the MS (Fig. 4.2). In between, 62 varves are preserved without any disturbances. Above slump I, 46 varves uniformly formed at both observation sites (MS and WS) proving calm sedimentation. The following slump II is the thinnest of the three events and wedges out already within the 80 m that the MS outcrop extends laterally. At the sampling position near the western margin of the outcrop, this slump appears as an only 2 cm thick layer of completely disintegrated varve structures, while in the middle of the outcrop the slump is up to 11 cm thick. Micro-stratigraphic correlation with the WS proves that slump II has eroded only one varve in parts of the MS sequence (Fig. 4.8a).

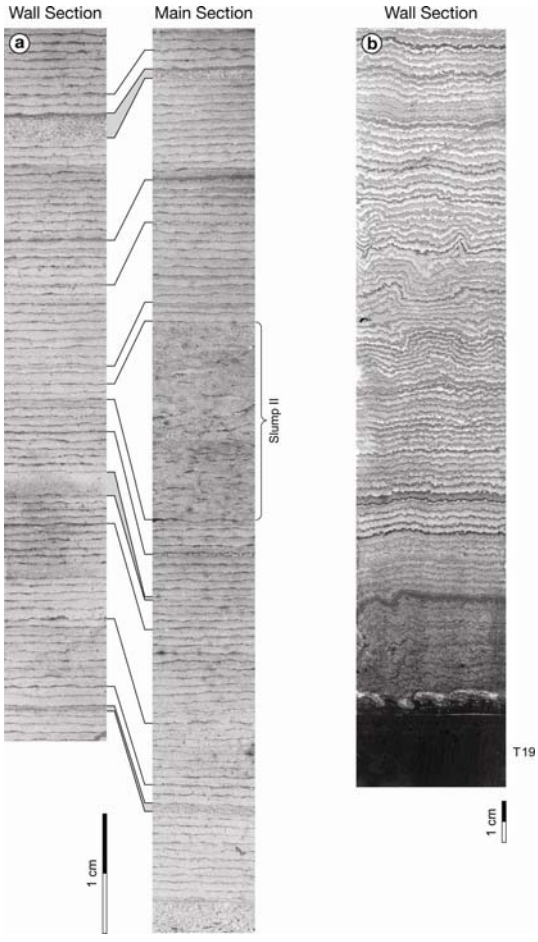

Fig. 4.8: (a) Varve-to-varve correlation between the Wall Section and Main Section demonstrating marginal Slump II deposits only in the Main Section. (b) Basal part of the interval of thick wavy varves in the Wall Section (see also Fig. 4.2) that correspond to Slump III deposits in the Main Section. Note: black, clay-rich layer at the base is correlation layer T 19.

198 varve years after the occurrence of slump II, the thickest of the mid-interglacial slump deposits accumulated. Slump III appears in the MS as a ca 60 cm thick deposit including lumps of folded varve intervals and large dolomite boulders from the catchment indicating a catastrophic debris flow. The top of slump III is formed by a graded layer. The corresponding facies in the WS

DOI: 10.2312/GFZ.b103-07065

does not contain any coarse debris but appears as a distinct interval of 350 extremely undulating and two times thicker than average varves intercalated between a basal clay layer and an upper graded layer (Figs. 4.2, 4.8b). From this distal facies in the WS outcrop it is inferred that slump III, as the ones before, originated from the southern lake shore closer to the MS outcrop. Interestingly, in the interval of strongly undulating varves no folding or even complete disintegration of the layering appears (Fig. 4.8b). This implies partial liquefaction, *i.e.* temporary suspension of sediment grains in pore fluid induced as a result of vibrations or rapid pore pressure increases (Ringrose, 1989), rather than accumulation of reworked sediments. Similar structures have been related to palaeoseismic events (Ringrose, 1989; Mörner, 1996) but might have also been triggered by the strong and sudden lateral compression caused by the injection of the mass flow at the MS location.

4.4.5. Detrital layers

Detrital layers have been deposited after short-term pulses of surface runoff and thus reflect extreme precipitation and snow-melt events (Mangili et al., 2005). Micro-facies studies and varve-to-varve correlation between the MS and WS outcrops demonstrated a clear proximal-distal pattern within the basin that enabled tracing the source of these event layers (Mangili et al., 2005). In the studied section of 5900 varves a total of 657 detrital layers have been accumulated in 615 varves (in some varves more than one detrital layer occur). Thickness values of these layers range from sub-millimetre scale to 30.6 mm. However, all except seven detrital layers are <1 cm thick. In some cases thicker detrital layers can cause erosion at sub-millimetre scale (Mangili et al., 2005) as, for instance, shown for the detrital layer labelled as ‘T20i’ which cut off and deformed 2-3 varves (Fig. 4.9).

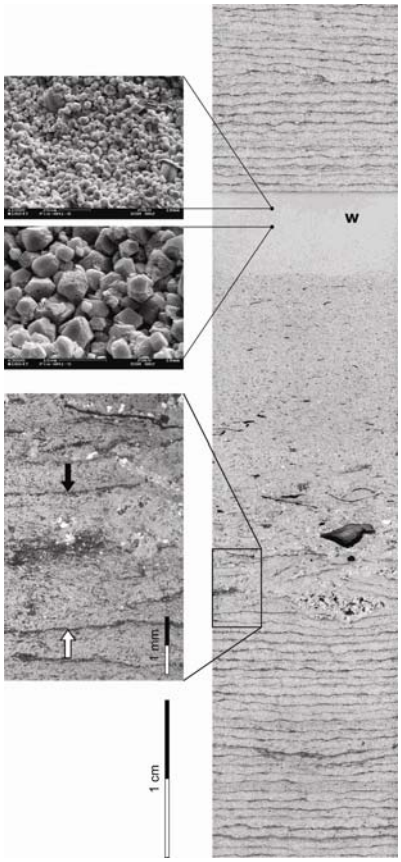

Fig. 4.9: Scanned thin section (cross-polarized light) showing the deposit of detrital layer labelled as T 20i with a thickness of 27.3 mm. Zoom-out from the coarse basal part of the deposit exhibiting reworking of varves. The varve indicated by the black arrow is turned by 180° and thus in upside-down position due to reworking by the turbidite (see inverse grading of calcite sub-layers). For comparison the varve below the base of the detrital layer with calcite sub-layers in normal position (fine above coarse). The entire layer shows a grading and the top is formed by a layer of micritic calcite (‘w’).

DOI: 10.2312/GFZ.b103-07065

4.4.6. Micritic calcite layers

Rare features in the BVC are very fine-grained and compact white layers. Only 19 of these layers with thicknesses between 0.2 and 14 mm have been deposited within the entire sequence of about 16 000 varves. The formation of micritic layers seems to be related to deposition of thick detrital layers since 17 of these layers formed on top of detrital layers (Fig. 4.9). Despite their apparent relation to detrital layers these layers are formed by euhedral calcite crystals of very homogeneous and fine grain-sizes <5µm (Fig. 4.9). This suggests their formation due to massive calcite precipitation events described as 'whitings' (Kelts and Hsü, 1978; Thompson et al., 1997). The occurrence of small diatom frustules in the micritic calcite layer on top of T20i (Fig. 4.9) indicates that such calcite precipitation events occurred during the biologically productive phase of the lake in spring/summer. Probably, pronounced calcite precipitation was favoured by pulses of enhanced nutrient and calcium ion influx through major detrital layers.

4.5. Palaeoclimatic implications

Calcite precipitation in hardwater lakes commonly takes place in the epilimnion from late spring to midsummer (e.g. Minder, 1922; Brunskill, 1969; Kelts and Hsü, 1978; Koschel et al., 1983) when the ionic activity product of calcium and carbonate ions (Ca^{2+}) (CO_3^{2-}) exceeds the equilibrium constant resulting in saturation or supersaturation with respect to calcite (Kelts and Hsü, 1978). Calcium ions are derived from surface runoff and groundwater flow and commonly abundant in carbonatic lake settings. Carbonate ions can originate from bacterial reduction of organic matter and/or from the atmosphere through exchange processes on the water surface. Supersaturation with respect to calcite in modern lakes has been found to be controlled by an increasing pH that in turn results from decreasing CO_2 concentrations in the epilimnion (Kelts and Hsü, 1978). In principle, two mechanisms can trigger a reduction in CO_2: (1) consumption by photosynthesizing plants during phases of algal growth, and (2) increasing water temperatures. Temperature increase has an additional direct effect on calcite precipitation since the solubility of calcite is temperature dependent. Thus even the warming of cold deep water in the epilimnion after spring turnover is sufficient to lead to supersaturation with respect to calcite (Brunskill, 1969). Since biological productivity is controlled by both temperature and nutrient supply, it is not possible to reliably quantify the temperature effect on the amount of calcite precipitation. It has to be further considered that the Piànico varves formed under purely natural conditions and thus have no modern analogue. Therefore, calibrations of recent biochemical varves which formed only as a consequence of anthropogenic eutrophication with climate variables (Lotter and Birks, 1997) are not applicable.

The most striking features in the varve thickness record are two periods of up to 50% thinner calcite layers: the 1100-varve period in the lower part of the studied interval and the uppermost 480 varves (Fig. 4.6). The traces of calcite dissolution observed in these intervals (Fig. 4.4) probably are a consequence of the lowered accumulation rate (Ohlendorf and Sturm, 2001). These intervals of reduced calcite precipitation are thought to reflect periods with lower summer temperatures even if a decrease in nutrient supply might also have contributed to the decrese in calcite precipitation. A cooling is further supported by vegetation changes (Moscariello et al., 2000; Rossi, 2003) and oxygen isotopes of the calcite (Mangili et al., submitted). This intra-interglacial cold interval is particularly intriguing because of its long duration of about 1100 years. None of the known Holocene climatic fluctuations has a comparable duration suggesting a different type of climate variability during the Piànico interglacial. The decline in summer calcite precipitation in the upper 480 years marks the transition towards the even more pronounced

DOI: 10.2312/GFZ.b103-07065

lithological shift leading to an almost complete cessation of calcite varve formation. This major change towards predominantly detrital sedimentation marks the boundary between the BVC and MLP units. Corresponding vegetation changes at this transition have been interpreted as a shift from interglacial to interstadial conditions (Rossi, 2003).

Moreover, it is interesting to note that the intervals of reduced varve thickness exhibit significant changes in the subdividsion of summer layers. The portion of varves with a pronounced three-partition of calcite layers increases from 2-4% in periods with average varve thickness to more than 23% in the 1100-varve interval and to 13.8% in the 480 upper varves (Tab. 4.1). This increase in number of varves with three summer sub-layers is particularly surprising since the total calcite layer thickness is lower during this interval. Although this indicates that the number of calcite precipitation pulses is linked to climate change, it is difficult to decipher this in more detail because of the lack of modern analogues for such differentiated sub-layer pattern. Probably, changes in seasonality are involved since a delayed warming in spring might cause an immediate exceeding of critical supersaturation leading to rapid crystallization of small calcite crystals (Folk, 1974) during the first pulse of calcite precipitation. This is in agreement with the observation that the first of the three calcite sub-layers consist of small-sized crystals. The effect of rapid supersaturation might have been enhanced by wave activity during storms resulting in increased aeration of the surface waters and further release of excess CO_2 (Minder, 1922).

In addition to the demonstrated large amplitude changes in varve thickness also secular variations have been detected by wavelet analyses. The occurrence of the 88-yr Gleissberg cycle and the 208-yr cycle strongly indicates that the same solar variations modulated the climate during the Piànico interglacial as known from Holocene records (Brauer et al., 1994; Stuiver and Braziunas, 1993; Vos et al., 1997). Interestingly, these cycles do not occur continuously throughout the entire time series but disappear in certain intervals. The reason for this remains unknown. Excluding inherent changes in the sun and thus assuming constancy of the periodic solar variations two alternative explanations remain. Either the climate system is capable to amplify the small-scale changes in solar irradiation only in certain modes, or sedimentation (*i.e.* varve formation) is susceptible to record such variations only under certain boundary conditions. The preferential appearance of solar periodicities around the interval of low summer layer thickness suggests a possible link to the climate system. Finally, it has to be noted that none of the decadal-scale solar periodicities as the 11-yr cycle which have been reported, for instance, from thickness variations in biochemical calcite varves from Lake Soppensee (Livingstone and Hajdas, 2001), has been found in the Piànico data. This might suggest that the much smaller Lake Soppensee (800 x 400 m) might be more susceptible to record smaller cycles than the large Piànico lake was.

4.6. Conclusions

Calcite varve formation was the dominant process in the interglacial Piànico palaeolake about 400 ka ago. Intra-basin correlations on a varve-to-varve base demonstrated that annual layer deposition was uniform within the basin and thus is a representative measure for climate and environmental change. Two periods of major decrease predominantly of summer layers are observed: (1) a ca 1100-year period that commenced about 10 000 years after the onset of the interglacial and, (2) the 480-year transition period at the end of the varve time series. These intervals indicate periods of decreased summer temperatures and particularly the long intra-interglacial cool period suggests mechanisms of the climate system which are unknown from the present interglacial. Changes in the subdivision pattern of summer calcite layers during this cold period indicate that summer warming might have been delayed. Moreover, secular variations of solar activity (88, 208-yr

DOI: 10.2312/GFZ.b103-07065

cycles) and probably thermohaline circulation (512-yr cycles) had an impact on the varve formation process during the Piànico interglacial.

These first results demonstrate that the varved sediments of Piànico are a key archive for deciphering interglacial climate variability under natural conditions. Further work including micro-facies, oxygen isotope and geochemical analyses is ongoing aiming a better mechanistic understanding of natural interglacial climate variability.

4.7. Acknowledgements

We would like to thank the Bergamo Natural Science Museum for providing accommodation during field work and to Monica Gandossi and Verushka Valsecchi for their help in the field. Andreas Hendrich helped with drawing the figures. We are grateful to Daniela Esu (University ‘La Sapienza’, Rome) who identified mollusc shells. Comments by Jaap J.M. van der Meer and an anonymous reviewer were helpful to improve an earlier version of this manuscript. A.W. was financially supported by the European Commission's project No. 12975 (NEST) “Extreme Events – Causes and Consequences (E2-C2)”.

DOI: 10.2312/GFZ.b103-07065

5. Effects of detrital carbonate on the interpretation of stable oxygen and carbon isotopes from the interglacial lake record of Piànico

Clara Mangili[a,*], Achim Brauer[a], Birgit Plessen[a], Peter Dulski[a],
Andrea Moscariello[b], Rudolf Naumann[c]

[a]*GeoForschungsZentrum (GFZ), Section 3.3 - Klimadynamik und Sedimente, Telegrafenberg, D-14473 Potsdam, Germany*
[b]*Cambridge Quaternary, Department of Geography, University of Cambridge, Downing Street, Cambridge CB2 3EN, United Kingdom*
[c]*GeoForschungsZentrum (GFZ), Section 4.2 - Anorganische und Isotopen-Geochemie, Telegrafenberg, D-14473 Potsdam, Germany*

To be submitted to Quaternary Science Reviews

Abstract*- The interglacial lake deposit of Piànico (400 ka BP, Southern Alps) contains a long series of annual laminations. The summer layer of these varves is composed of biochemically precipitated calcite that constitutes up to 98% of the total varve thickness from a 9 350 varve year interval of the Piànico sequence. Within the varve sequence, detrital layers mainly composed of dolomite are intercalated. These layers reflect surface runoff events and thus the mineralogical signature of the catchment. Microscopic inspection in thin sections allows detecting detrital layers at sub-millimetric scale, providing an ideal tool for precise selection of different sets of samples in order to evaluate the effect of varying amounts of dolomite on stable isotope data. For this study, three different types of samples have been selected: (a) endogenic calcite varves (five varves per sample), (b) individual detrital layers and (c) 'mixed' samples of five calcite varves including 1 - 4 detrital layers.*

The $\delta^{18}O$ results show that detrital layers are up to 5.7‰ heavier than neighbouring endogenic calcite samples. The deviation towards more positive $\delta^{18}O$ values of mixed samples is less strong and apparently depends on the amount of detrital contamination. We were able, for the first time, to assess that isotope values of samples including at least 5% of dolomite will show deviation towards more positive $\delta^{18}O$. This quantification has also been confirmed by XRD analyses. Moreover, presence or absence of samples containing detrital dolomite also influences covariance of $\delta^{13}C$ and $\delta^{18}O$. Covariance is high ($r = 0.76$; $n = 393$) when the correlation coefficient is calculated on the base of all samples, but absent ($r = –0.43$; $n = 293$) when samples containing detrital material have been removed from calculation.

Keywords: oxygen isotopes, bulk carbonates, covariance, calcite varves, detrital layers

5.1. Introduction

Stable oxygen and carbon isotopic analyses are a valuable tool to obtain information on past climatic and environmental changes. Stable isotope data in lake records are mainly derived from ostracodes (e.g. von Grafenstein et al., 1994; von Grafenstein et al., 1999; Frogley et al., 2001; Lawson et al., 2004) and bulk carbonates (Siegenthaler and Eicher, 1986; Dean and Stuiver, 1993; Leng et al., 1999; Schwander et al., 2000; von Grafenstein et al., 2000; Anderson and Leng, 2004). Since table isotope data from ostracodes, bivalve molluscs and bulk carbonate have been demonstrated to be in good agreement (von Grafenstein et al., 2000), each of these carbonate sources is a potential palaeoclimate proxy. This is valid for the bulk carbonates of Gerzensee as they are dominated by summer produced *Chara* incrustations. This indicates that bulk carbonates can be used as palaeoclimate proxy if their content is dominated, for example, by endogenic calcite precipitated in the lake during spring and summer. The main problem of bulk carbonate analyses, however, is contamination of endogenic calcite with detrital carbonates. Runoff processes transport detrital carbonates which carry the isotopic signal of catchment rocks into the lake, biasing the climatic information of biochemically precipitated calcite. Different analytical techniques are applied to minimize contamination with allochthonous material. (1) Separation of

DOI: 10.2312/GFZ.b103-07065

grain sizes based on the assumption that the size of endogenic crystals is distinctively smaller than the grain sizes of detrital carbonate. However, there is no agreement on the grain size limit that separates the two components and different boundaries are suggested as the limit for endogenic component: <4 µm (Hilfinger IV et al., 2001), <63 µm (Kirby et al., 2002), <80 µm (Roberts et al., 2001). Direct measurements of endogenic calcite crystal sizes show variations: between 2-30 µm in Lake Zurich (Kelts and Hsü, 1978) and >10µm for calcite crystals in Baldeggersee (Teranes et al., 1999). In sediment-traps of Lake Neuchâtel, the bulk carbonate fractions <2 µm and >60 µm include high percentages of detritus (Filippi et al., 1998). (2) Separation between detrital dolomite and endogenic calcite during dissolution for isotope analyses. This method uses the different reaction times of dolomite and calcite on digestion in phosphoric acid at 25° C (Degens and Epstein, 1964; Epstein et al., 1964). However, it is demonstrated that the resulting isotope values are a function of the grain size of the analysed samples (Clayton et al., 1968), so that collection times for CO_2 produced by calcite must be different for each grain size fraction (Walters et al., 1972). (3) Smoothing of the resulting curves in order to eliminate data biased by detrital carbonate (Kuc et al., 1998). This approach assumes that outliers are generally caused by detrital carbonate contamination.

Although it is commonly agreed that varying amounts of detrital carbonates can affect stable isotopes in bulk samples, the order of magnitude of this effect remains to a large extent unknown. This study for the first time tries to quantify this effect by gathering detailed sedimentological and mineralogical data from lake sediment samples to evaluate stable isotope data.

5.2. Study site and sediments

Deposits of the Piànico palaeolake are outcropping in the Borlezza Valley (45° 48' N, 10° 2' E; Fig. 5.1), a northestern tributary to recent Lake Iseo, northern Italy. The Piànico palaeolake was ca 3 km long, 500-800 m wide (Casati, 1968) and its topmost deposits are outcropping at an altitude of ca 350 m a.s.l.. The presence of varves indicates meromictic deep water conditions. The catchment of the palaeolake forming the lower part of the Borlezza Valley (Fig. 5.2) is constituted mainly by Upper Triassic dolomitic rocks (Dolomia Principale) and subordinated by limestones belonging to the Calcare di Zorzino Unit (Provincia di Bergamo, 2000).

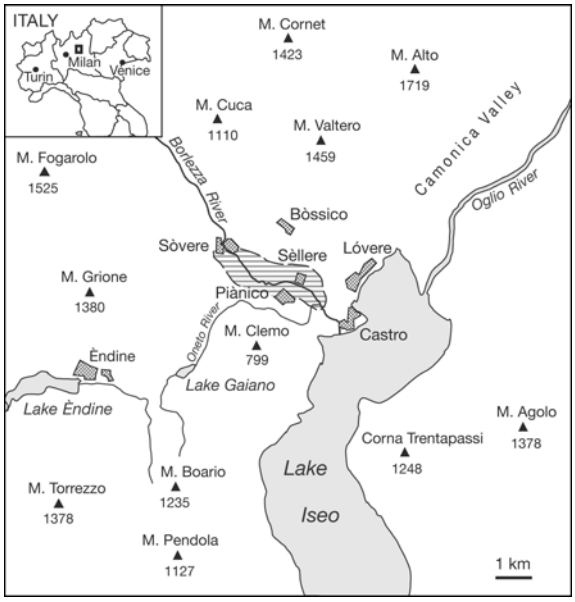

Fig. 5.1: Location of the Piànico-Sèllere Basin and reconstructed extension of the palaeolake (dashed area; modified after Casati, 1968).

In the northeastern part of the palaeolake basin, long sequences of lacustrine sediments, known as the Piànico Formation, are outcropping (Fig. 5.2; Moscariello et al., 2000). The Piànico Formation is 48 m thick and has been subdivided into four units of partly finely laminated sediments: in this

DOI: 10.2312/GFZ.b103-07065

paper only the unit labelled as BVC (Banco Varvato Carbonatico; Fig. 5.3) is considered. The BVC represents a long period of ~15 500 years of interglacial climate as revealed by the continuous formation of calcite varves (Brauer et al., submitted) and vegetation reconstructions (Moscariello et al., 2000; Rossi, 2003). The interglacial sequence has been dated by means of tephrochronological correlation at ca 400 ka BP (Brauer et al., in press).

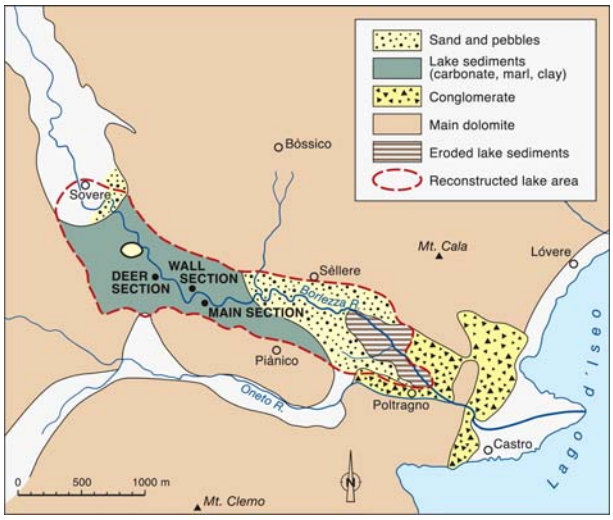

Fig. 5.2: Distribution of the Pleistocene sediments in the basin of the Piànico palaeolake during the early stages of lacustrine sedimentation (modified after Casati, 1968). Some of the outcropping sections are indicated. Sampling for this study has been carried out at the Main Section.

The varves of the BVC unit are composed of two laminae: a spring-summer light lamina composed of biochemically precipitated calcite with crystal sizes of 2-15 µm and an autumn-winter dark lamina composed by organic matter, diatom frustules and few scattered detrital grains (Fig. 5.4; Brauer et al., submitted). Summer layers consist up to 98% of calcite and constitute 69-98% of the total varve thickness. Intercalated detrital layers reflect short surface runoff events that were likely induced by extreme precipitation events (Fig. 5.4; Mangili et al., 2005). At the Main Section, one major debris flow containing large dolomite boulders of several cm in diameter interrupts the sequence in the upper half of the BVC unit (Fig. 5.3).

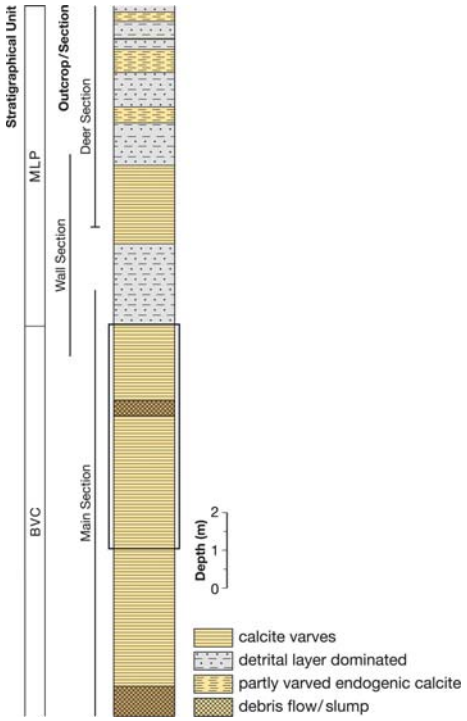

Fig. 5.3: Simplified composite lithological and stratigraphical log of the BVC and MLP units. The MLP unit exhibits a succession of five intervals of predominantly endogenic calcite sediments intercalated with six intervals of detrital sediments, the lower of which marks the end of the BVC unit. The black rectangle indicates the studied interval from 825 – 1418 cm depth. Zero-point of the depth scale is at the top of the sequence.

DOI: 10.2312/GFZ.b103-07065

5.3. Methods

This study focused on a 9 350 varve year interval in the upper 593 cm of the BVC unit (825 – 1418 cm depth in the composite profile depth as defined by Brauer et al., submitted). The samples were taken in the Main Section (Fig. 5.2). First, the outcrop was cleaned with a sharp knife until a smooth and vertical surface was obtained. From this surface, 5-10 cm thick sediment blocks (33 x 5 cm) were carved out in situ with at least 5 cm overlap and then carefully removed from the outcrop in stainless boxes equipped with removable side walls without breaking the sediment. The sample blocks were taken out from the boxes in the lab and dried at room temperature for ca 24 hours before covering with a transparent epoxy resin (Araldite® 2020). Impregnation of the surface layer (1-2 mm) of the samples was then obtained (Mangili et al., 2005). In this way, the sample blocks were sufficiently stable to be cut into 3-4 slices. One of these slices was used for thin section preparation and a second one for parallel isotope sub-sampling. Thereby isotope sub-sample intervals could be precisely selected on the base of microscopic information.

5.3.1. Sub-sampling for isotope analyses

In total, 393 samples were carefully scratched from a fresh cut surface of the sediment block with a sharp scalpel. On the basis of micro-facies and mineralogical composition three different types of samples were selected through thin section examination (Figs 5.4 and 5.5):

(1) 'Endogenic calcite' samples were 3-4 mm thick and included exactly five varves without any detrital layer (293 samples). More than 80% of each sample was constituted by calcite which biochemically precipitated in the epilimnion during spring and summer month. The thin winter layers (<20% of a single varve) are mainly composed of siliciclastic material and by diatom opal. Sporadically, only in the winter layers, some scattered detrital quartz and dolomite grains, which cannot be removed, might have occurred;

(2) 'Detrital' samples were taken from thick, discrete detrital layers usually dominated by dolomite originating from the catchment (23 samples). Detrital layers can include a certain amount of endogenic calcite that was reworked by erosion from littoral sediments and incorporated in the detrital layers. Typical grains forming detrital layers were angular and often larger in size than endogenic calcite crystals. The thickness of sampled detrital layers varied between 0.2 and 17.5 mm;

(3) 'Mixed' samples comprised five varves each like endogenic calcite samples but additionally included one to four intercalated thin (0.04-4.42 mm thick) detrital layers (73 samples).

In addition, four individual dolomite boulders were collected from the major debris flow deposit within the BVC unit (Fig. 5.3). These samples were analysed in order to obtain information about the isotopic signature of pure detrital material that was transported to the studied site. These rubbles were 1-9 cm in diameter and grinded to fine powder for the analyses.

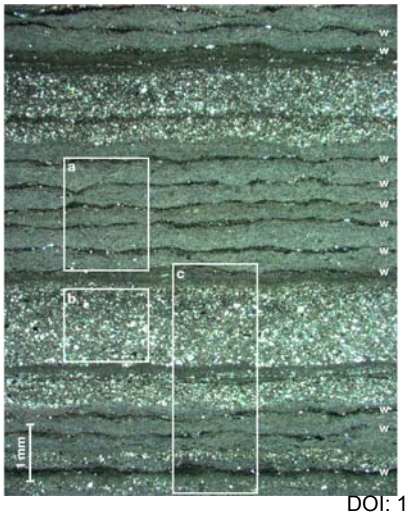

Fig. 5.4: Thin section image of varves and detrital layers (crossed polarised light). Winter layers (w) are marked on the picture. The different types of samples analysed in this study are shown: a. Endogenic calcite sample integrating 5 varves; b. Detrital samples taken from individual detrital layers; c. Mixed sample integrating 5 varves and additionally 1 – 4 detrital layers.

DOI: 10.2312/GFZ.b103-07065

5.3.2. Isotope analyses

The stable-isotope composition of the sediments was analysed in continuous flow mode with a Finnigan GasBench II connected with a DELTAplusXL mass spectrometer. From each sample, 0.25 ± 0.05 mg were loaded into 10 ml Labco Exeteiner® vials and used for a duplicate measurement. After automatically flushing with He, the samples were reacted in phosphoric acid (100%, density 1.93) at 75° C for 60 minutes in a Finnigan Gas Bench preparation system. Supplemental information on the analysis procedure is given in Spötl and Vennemann (2003). Isotope compositions of the sediments were given relative to the VPDB standard in the conventional δ-notation and were calibrated against three international reference standards (NBS 19, CO1, CO8) and an internal reference standard. The standard deviation (1 sigma) calculated on the 12 reference samples of each run is 0.06‰ for $\delta^{13}C$ and 0.08‰ for $\delta^{18}O$.

Isotope analyses of dolomite rock material were carried out with the same reaction time and the same procedure used for endogenic calcite to allow comparison of the data; the isotopic data for dolomite were not corrected for the temperature dependent fractionation between dolomite and CO_2.

5.3.3. XRD analyses

XRD analyses were carried out to study the geochemical composition of 12 selected isotope sample and to compare these results with the observations from thin section analyses.

X-ray diffraction analyses were performed using a 'Siemens Diffraktometer 5000' (Siemens, Karlsruhe, Germany). Three samples for each facies types (endogenic calcite, mixed layers, detrital layers and bedrock) were analysed. Quantitative mineral contents were calculated using BGMN software (Seifert, Freiberg, Germany).

5.3.4. µ-XRF analyses

The µ-XRF analyses were performed with an EDAX Eagle III XL Spectrometer. The machine is equipped with a X-Ray Tube and uses capillary optics to focus X-rays onto a sample. The X-ray fluorescence emitted from the sample as a result of the X-ray excitation is captured by the Si (Li) detector, processed and translated into elemental information which is displayed on the computer.

The dwell time used to analyse the samples from Pianico was 60 s, the spot size 54 µm, the tube voltage 40 kV, the tube current 200 µA, the time constant 17 µs and the step size 40 µm. The measurements were performed under vacuum directly on sediment blocks. For this study, three stratigraphic intervals were analysed (Fig. 5.5): one endogenic calcite sample (17-2D; Fig. 5.5a), one mixed sample (17-5; Fig. 5.5b) and one detrital layer (17-9; Fig. 5.5c). Ca, Si and Mg curves are plotted for each sample.

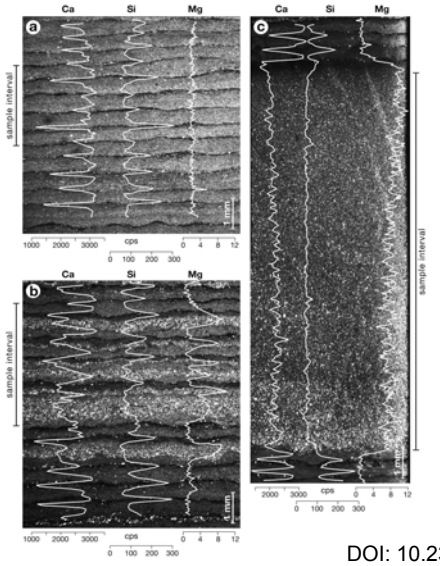

Fig. 5.5: Ca, Si and Mg counts per second (cps) from µ-XRF scanning of different types of isotope samples. 5a. Endogenic calcite sample (sample 17-2 D). 5b. Mixed sample that include 5 varves with detrital layers in (sample 17-5). 5c. Detrital layer (sample 17-9). The bars at the sides of the pictures indicate the sampled stratigraphic interval.

DOI: 10.2312/GFZ.b103-07065

5.3.5. Quantification of the 'detrital bias' of 'mixed' samples

In order to quantify the bias in $\delta^{18}O$ and $\delta^{13}C$ caused by detrital matter in mixed samples, the deviation (D) of the isotope value of a mixed sample from the mean isotope value of two neighbouring endogenic calcite samples was calculated (Fig. 5.6) as

$$D = \delta_{ms} - (\delta_{ecp} + \delta_{ecf})/2$$

with D being the deviation between (i) $\delta(^{18}O$ or $^{13}C)$ value of a mixed sample (δ_{ms}) and (ii) the mean of $\delta(^{18}O$ or $^{13}C)$ values of the endogenic calcite samples that precede (δ_{ecp}) and follow (δ_{ecf}) the mixed sample. If D> (<) 0, the mixed sample had heavier (lighter) $\delta^{18}O$ or $\delta^{13}C$ values than the mean of the endogenic calcite samples. The distance between a mixed sample and the two endogenic neighbour samples used to calculate D-values is maximum 80 years.

The isotopic bias was related to the amount of detrital contribution to each mixed sample described as percent detrital layer thickness of the total sample thickness. This was considered a sufficiently good approximation of the content in dolomite from the catchment although detrital layer thickness was not linearly related to dolomite content because such layers may have also contained different amounts of endogenic calcite which was reworked from littoral deposits.

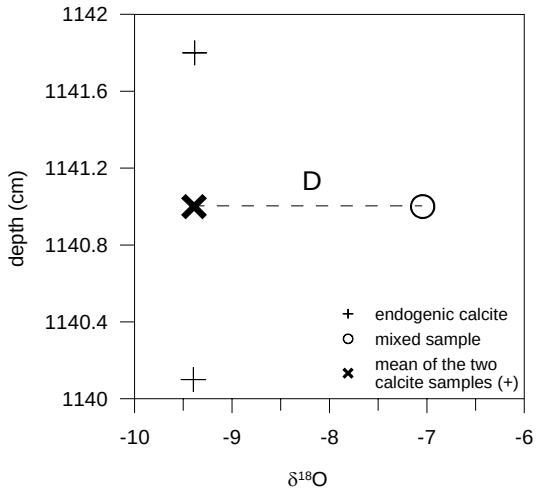

Fig. 5.6: Calculation of Deviation (D). The difference between the $\delta^{18}O$ of a mixed sample and the mean $\delta^{18}O$ of two neighbouring endogenic calcite samples is defined as isotopic deviation (D). The same procedure is used to calculate D for $\delta^{13}C$ values.

5.4. Results

5.4.1. Isotopes

The $\delta^{18}O$ values of all 393 samples varied between –10.06‰ and –2.47‰ (Fig. 5.7a) while $\delta^{13}C$ values ranged from –7.24‰ to +1.16‰ (Fig. 5.7b) resulting in amplitudes of 7.59‰ ($\delta^{18}O$) and 8.4‰ ($\delta^{13}C$). Endogenic calcite samples revealed clearly lighter $\delta^{18}O$ (between –10.06‰ and –8.01‰) and $\delta^{13}C$ values (between –7.24‰ and –5.51‰) than those taken from discrete detrital layers with $\delta^{18}O$ between –8.07‰ and –4.35‰ and $\delta^{13}C$ from –6.13‰ to –0.40‰. The latter were closer to those values obtained from the bedrock dolomite samples ($\delta^{18}O$: –6.66‰ - –2.47‰; $\delta^{13}C$: –0.77‰ - +1.16‰). Mixed samples revealed intermediate isotope signatures between both end-members represented by endogenic calcite and bedrock samples. 'Mixed' $\delta^{18}O$ values ranged from –9.83‰ to –6.33‰ while $\delta^{13}C$ varied between –7.05‰ and –2.24‰. The percentage of detrital layers in mixed samples varied from ~0.7% to 58% of the total sample thickness (Fig. 5.8a, c). For samples with less than 5% detrital layers, D varied between –0.29‰ and +0.62‰ (Figs 5.8a, b). 13 of these samples were within the analytical error of isotope measurements, but 14 samples were 0.09‰ to 0.62‰ heavier than expected. Only three samples showed slightly lighter D values. Samples containing 5% to 20% detrital layers revealed 0.1‰-1‰ heavier $\delta^{18}O$ values than their endogenic neighbour samples (Fig. 5.8a). Samples with more than 20% of detrital layers showed D values up to 3.51‰ enriched than the neighbours. In a similar way, detrital material in mixed

DOI: 10.2312/GFZ.b103-07065

samples affected also $\delta^{13}C$ values (Fig. 5.8c). D values of up to 4.15‰ more positive values were recorded for mixed samples.

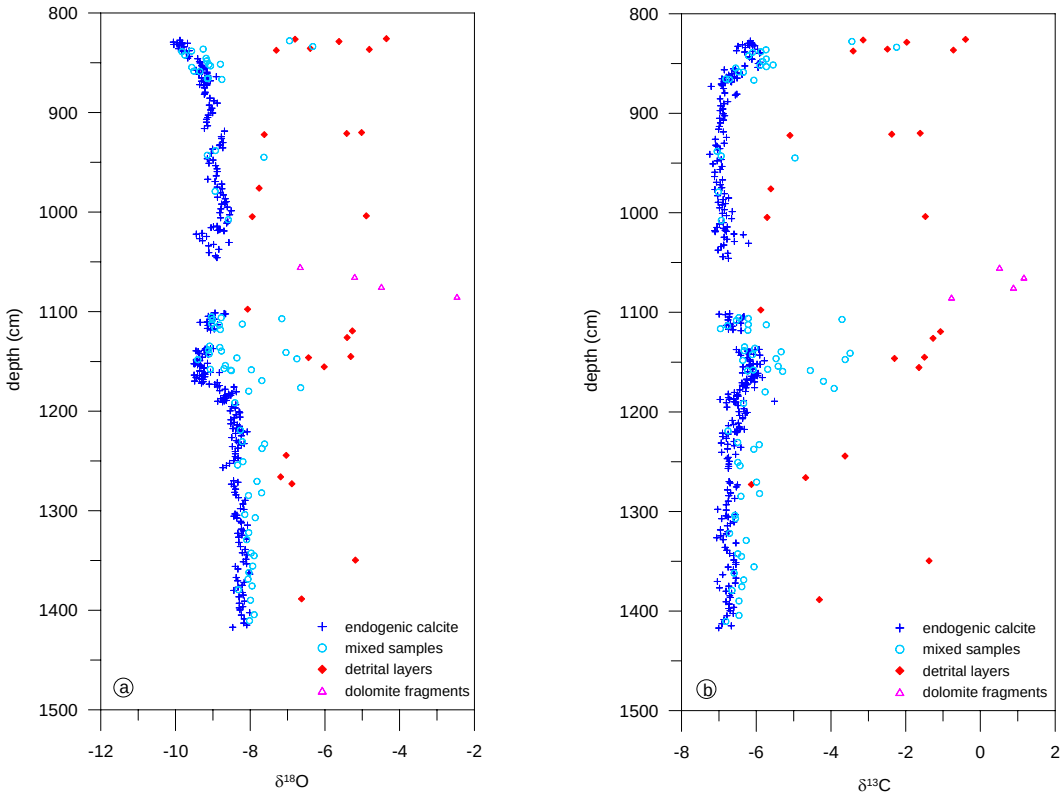

Fig. 5.7: $\delta^{18}O$ (a) and $\delta^{13}C$ (b) records for the studied interval comprising 9 350 calcite varves. Different sample sets are indicated by different symbols.

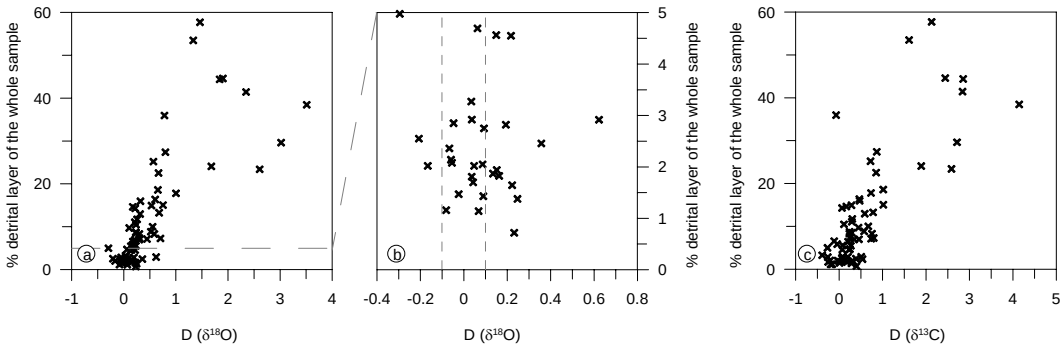

Fig. 5.8: a. $\delta^{18}O$ D plotted against the percentage of detrital layers in mixed samples (% of the total sample thickness, see text). Negative values indicate that the $\delta^{18}O$ of a mixed sample is lighter than the mean of the two neighbouring samples. b. Enlargement of the $\delta^{18}O$ D values below 5%. The vertical dashed lines indicate the analytical error of isotope measurements. c. $\delta^{13}C$ D plotted against the percentage of detrital layers in a mixed sample (% of the total sample thickness). Negative values indicate that the mixed sample has a $\delta^{13}C$ value lighter than the mean of the neighbouring samples.

In addition, the presence of samples containing detrital material had also an influence on the calculation of covariance. Including the entire set of samples in the calculation revealed a strong covariance between $\delta^{13}C$ and $\delta^{18}O$ (correlation coefficient r=0.76; n=393; Fig. 5.9). However, if

DOI: 10.2312/GFZ.b103-07065

samples comprising detrital matter are excluded, covariance disappeared and a weak anticorrelation (r = –0.43; n = 293; Fig. 5.9) was obtained.

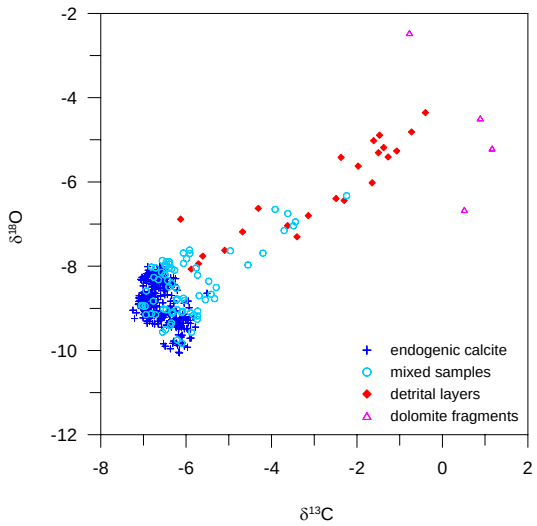

Fig. 5.9: Covariance between $\delta^{18}O$ and $\delta^{13}C$. Different sample sets are indicated by different symbols.

5.4.2. Identification and quantification of detrital material in the samples (µ-XRF and XRD analyses)

The annual signal is nicely shown in µ-XRF data of the varve succession (Fig. 5.5). Ca peaks reflect endogenic calcite which forms the summer layers; Si peaks reflect biogenic opal from diatom debris washed in during winter. Peaks in Mg correspond to detrital grains (isolated peaks) and/or detrital layers. As a result of higher concentration of calcite, count rates of Ca (cps) are much higher for Ca than for Si and Mg.

XRD analyses of 12 samples show dominance of calcite and dolomite (Tab. 5.1). The three bedrock samples (Tab. 5.1) are constituted by 99-100% dolomite. Detrital layers have a mixed composition; their dolomite content ranges between 26 and 83%. Calcite in these samples has been reworked and included in the detrital layers during deposition. For mixed samples, the dolomite content ranges between 3 and 35%. For endogenic calcite samples, the dolomite content does not exceed 3.5%. Quartz is almost always present in the samples, with higher amount (2-5%) in detrital and mixed layers. Minor components such as illite and pyrite are sometimes present in detrital and mixed samples. The $\delta^{18}O$ isotope values of these 12 samples range between –2.47‰ and –9.20‰, while $\delta^{13}C$ between +1.16‰ and –7.16‰.

Sample	Calcite (%)	Dolomite (%)	Quartz (%)	Gypsum (%)	Illite (%)	Pyrite (%)	$\delta^{13}C$	$\delta^{18}O$	category
D5	0.94 ± 0.24	99.06 ± 0.24					-0.77	-2.47	bedrock
D2		100					1.16	-5.20	bedrock
D1		100					0.51	-6.66	bedrock
17-9	24.29 ± 0.63	70.46 ± 0.93	2.3 ± 0.29		2.54 ± 0.99	0.41 ± 0.14	-1.50	-5.31	detrital layer
17-15A	14.65 ± 0.54	82.96 ± 0.63	2.38 ± 0.3				-1.64	-6.02	detrital layer
13-9	69.7 ± 0.69	26.55 ± 0.69	3.75 ± 0.36				-5.61	-7.76	detrital layer
17-5	45.67 ± 0.84	47.35 ± 0.84	3.03 ± 0.33		3.17 ± 0.99	0.77 ± 0.16	-3.49	-7.04	mixed sample
12-9	52.1 ± 1.11	35.17 ± 0.93	4.67 ± 0.39	3.91 ± 1.29	4.15 ± 0.9		-4.96	-7.63	mixed sample
12-10	96.41 ± 0.54	3.06 ± 0.48	0.53 ± 0.28				-6.94	-9.15	mixed sample
12-3	97.54 ± 0.57	2.09 ± 0.54	0.37 ± 0.17				-7.11	-8.89	endogenic calcite
12-6	97.58 ± 0.54	1.97 ± 0.51	0.44 ± 0.17				-7.16	-9.11	endogenic calcite
17-2D	95.96 ± 0.57	3.43 ± 0.51	0.61 ± 0.29				-6.53	-9.20	endogenic calcite

Tab. 5.1: XRD data for 12 samples. Data and their error are expressed as percentages. Oxygen and carbon isotope values for the same samples are also reported.

DOI: 10.2312/GFZ.b103-07065

A relationship can be observed between mineralogical composition and isotope values (Fig. 5.10). The correlation coefficient (n=12) between the $\delta^{18}O$ values and the amount of dolomite in the samples (expressed as percentage) is 0.88. Heavier $\delta^{18}O$ and $\delta^{13}C$ values correspond to higher percentages of dolomite in single samples. Two detrital layers have $\delta^{18}O$ values in the range of dolomite $\delta^{18}O$ while the samples dominated by endogenic calcite have lighter $\delta^{18}O$ values. In these samples the amount of dolomite is always below 3.5%.

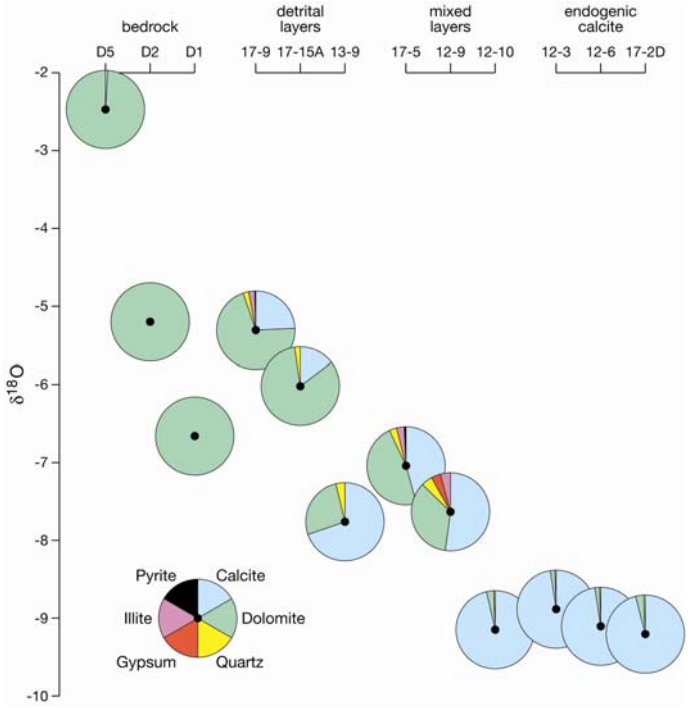

Fig. 5.10. XRD data plotted against the individual $\delta^{18}O$ values. The black dot in the middle of each circle marks the $\delta^{18}O$ value. Data divided by isotope samples classification.

In the mixed samples, a clear correlation between the amount of dolomite in a sample and its D value exists (Tab. 5.2). Samples including 35-47% dolomite have D of 1.46-2.35. The mixed sample which includes only 3% of dolomite has negative D value of –0.05.

sample code	amount of dolomite (%)	D
17-5	47.35	2.35
12-9	35.17	1.46
12-10	3.06	-0.05

Tab. 5.2: Amount of dolomite (%) and D for the three mixed samples analysed for XRD.

5.5. Discussion

Thin section analyses of varved sediments from the Piànico interglacial lake sediments provide information on the depositional processes and mineralogical composition of sediment intervals selected for stable isotope analyses. By this method it is possible to identify detrital layers as thin as 0.03 mm intercalated in the sequence of calcite varves. These detrital layers have been transported into the lake by surface runoff (Mangili et al., 2005) and thus are predominantly composed of dolomite from the Triassic Dolomia Principale Formation that forms the catchment of the lake. In addition, some scattered, probably wind-transported detrital dolomite and quartz grains occasionally occur in some but not all winter layers (Brauer et al., submitted; Fig. 5.4). In contrast, the fine calcite crystals forming the spring-summer layer are precipitated in the epilimnion of the lake during the warm and productive season (Kelts and Hsü, 1978). The isotopic signal at calcite precipitation is only reflected in the endogenic calcite component, whereas the detrital layers carry the isotopic signal of Triassic marine carbonates.

DOI: 10.2312/GFZ.b103-07065

This is confirmed by isotope measurements from the pure dolomite boulders revealing $\delta^{18}O$ values between –6.66‰ and –2.47‰ and $\delta^{13}C$ from –0.77‰ to +1.16‰, which is in good agreement with the published $\delta^{18}O$ mean for Triassic dolomite in the Alps (between –7‰ and +4‰; Degens and Epstein, 1964; Keim et al., 2006). Consequently, contamination with detrital carbonate in the Piànico lake record must result in heavier $\delta^{18}O$ values. This is demonstrated by the isotope composition of discrete detrital layers ($\delta^{18}O$ between –8.07‰ and –4.35‰). Most of these samples have $\delta^{18}O$ values within the range of the analysed dolomite boulders, but 9 detrital layer samples have $\delta^{18}O$ values in between the values of dolomite and endogenic samples. Microscopic inspection and XRD analyses show that this is due to a certain amount of endogenic calcite that has been reworked by erosion and incorporated in the detrital layers.
Mixed samples are generally lighter than samples from discrete detrital layers and plot in between detrital layer and endogenic calcite samples from the same interval (Fig. 5.7). It seems that the detritus-induced deviation D towards more positive $\delta^{18}O$ values is dependent from the portion of detrital matter included in a sample (Fig. 5.8). This is clearly supported by the quantitative data obtained from XRD analyses (Tab. 5.2). The highest D values occur when detrital layer amount to >20% of a sample, resulting in a bias in the isotope rising up to 3.51‰. However, the large amplitude of these $\delta^{18}O$ deviations is already an indication of possible contamination of these samples by detrital carbonate. All mixed samples with a detrital layer contribution from 5 to 20% have 0.1‰ - 1‰ heavier $\delta^{18}O$ values than the endogenic calcite $\delta^{18}O$ mean. These heavy $\delta^{18}O$ values significantly affect the isotope record and they could be interpreted as indicating climate warming, if the $\delta^{18}O$ changes were interpreted in terms of temperature shifts.
The mixed sample that showed negative D contains less than 3.5% of dolomite. In this and in those samples where the amount of detrital layers is below 5%, the effect of detrital material on $\delta^{18}O$ values is not always significant (D values –0.29‰ to +0.62‰). The maximum $\delta^{18}O$ difference between one endogenic calcite sample and the next one is 0.71‰. This value refers, however, to endogenic calcite shifts in the whole records, while mixed samples are coming from discrete intervals; the maximum $\delta^{18}O$ difference between two endogenic calcite samples neighbouring a mixed sample is 0.45‰ and should represent the maximum $\delta^{18}O$ shifts due to climate changes in the selected samples. The random behaviour of some mixed samples with D values included between ± 0.23‰ could be therefore due to climate changes.

It is likely that presence of detrital carbonate in bulk carbonate samples from alpine lakes in catchments formed by marine dolomite generally will result in positive isotope shifts. A review of $\delta^{18}O$ values in Late Quaternary alpine lakes shows that $\delta^{18}O$ values commonly vary between –6.5 and –12‰ (Mangili et al., submitted) therefore only slightly overlapping with the Triassic dolomite in the Alps ($\delta^{18}O$ mean between –7‰ and 3‰; Degens and Epstein, 1964). A first and simple indication of contamination effects might be, therefore, the total $\delta^{18}O_{carb}$ amplitude within a record. In the studied interglacial interval from the Piànico record, the $\delta^{18}O_{carb}$ amplitude is more than three times wider when all samples are included compared to the data only from endogenic calcite. This effect of detrital matter has certain implications for palaeoclimatic interpretation of isotope records from bulk lake carbonates. First of all, positive $\delta^{18}O_{carb}$ fluctuations might derive from contamination with marine dolomite. Increasing amounts of detrital matter in lake records are more likely to occur during colder and harsher climate regimes with sparser vegetation cover and increased erosion in the catchment. Thus, if samples containing detrital material would be used, a negative $\delta^{18}O_{carb}$ oscillation may result in a weakened signal (i.e. the negative swing in $\delta^{18}O$ in the record of Pianico at 1200 cm depth), or in a total overprint of the signal (i.e. Kolstrup and Buchardt, 1982).

In addition to the influence on palaeoclimatic interpretation, the mixture of detrital carbonate with an endogenic component can also affect covariance calculations, which might be used to infer palaeo-hydrological conditions (i.e. Talbot, 1990). Calculating the correlation coefficient of the

DOI: 10.2312/GFZ.b103-07065

entire studied interval reveals a strong covariance (r=0.76; n=393, Fig. 5.9), apparently indicating a hydrologically closed lake basin (Talbot, 1990; Leng and Marshall, 2004). However, covariance disappears and a negative correlation coefficient (r=-0.43; n=293, Fig. 5.9) is obtained after removing all samples which include detrital carbonate, suggesting a hydrologically open lake which is in agreement with geological data (Moscariello et al., 2000). Thus the application of the common interpretation to the entire Piànico data set would have caused substantial misinterpretation.

5.6. Conclusions

The effect of detrital carbonates on stable isotope analyses of bulk carbonates has been clearly demonstrated and quantified. If the amount of detrital material in a sample is higher than 3.5%, the isotope signal of bulk carbonates samples is biased. In our case study from the Piánico palaeolake, detrital carbonate resulted in heavier isotope values reflecting the isotope signature of the dolomitic catchment. Detrital matter contamination of endogenic calcite samples can further influence calculations of covariance with serious consequences.
Microscopic control of the depositional processes and mineralogy of analysed sample intervals provides a valuable tool for precise sample selection, thereby aiding interpretation of isotope records.

5.7. Acknowledgements

We thank G. Arnold, D. Berger and M. Köhler (GFZ Potsdam) for preparing high-quality thin sections and M. Dziggel and A. Hendrich (GFZ Potsdam) for drawing some of the figures.

DOI: 10.2312/GFZ.b103-07065

6. Centennial-scale oscillations in stable oxygen and carbon isotopes of endogenic calcite from the 15 500 varve year record of the Piànico interglacial (400 ka BP)

Clara Mangili[a], Achim Brauer[a], Birgit Plessen[a], Andrea Moscariello[b]

[a]*GeoForschungsZentrum (GFZ), Section 3.3 - Klimadynamik und Sedimente, Telegrafenberg, D-14473 Potsdam, Germany*
[b]*Cambridge Quaternary, Department of Geography, University of Cambridge, Downing Street, Cambridge CB2 3EN, United Kingdom*

Submitted to Quaternary Science Reviews

Abstract - *The palaeolake record from Piànico (Southern Alps) comprises a sequence of 15 500 continuous calcite varves formed during peak interglacial conditions around 400 ka BP. The varved nature of these deposits allows precise subsampling of five varve year intervals for stable isotope analyses. All samples consist of calcite precipitated in the epilimnion of the lake with contents of detrital carbonate below 4%. Four significant negative $\delta^{18}O$ oscillations occurred during the upper half of the interglacial. The most prominent of these oscillations has an amplitude of -1.07‰ and lasted 780 varve years. The three other oscillations are shorter (125 – 195 varve years) and of lower amplitude (0.40 – 0.87‰). An additional major drop in $\delta^{18}O$ occurs 275 varve years before the end of continuous calcite precipitation in the lake. This shift marks the end of long interglacial conditions and the beginning of harsher climate conditions and glacier advances in the Southern Alps. In contrast, the four $\delta^{18}O$ oscillations within the period of continuous formation of calcite varves reflect natural intra-interglacial climate dynamics.*

Keywords: oxygen isotopes, carbon isotopes, calcite varves, Southern Alps

6.1. Introduction

Stable isotope analysis of calcite precipitated within the annual cycle in the epilimnion of lakes ($\delta^{18}O_{carb}$) is a valuable tool for reconstructing climatic changes, provided that samples are not contaminated with allochtonous detrital carbonates. Previous works mainly focussed on Holocene and Lateglacial sediment records from present lakes (e.g. Siegenthaler et al., 1984; Siegenthaler and Eicher, 1986; McKenzie and Hollander, 1993; Kuc et al., 1998; Leng et al., 1999; Schwander et al., 2000; von Grafenstein et al., 2000; Hilfinger IV et al., 2001; Teranes and McKenzie, 2001; Kirby et al., 2002). Although these studies have demonstrated the great potential of $\delta^{18}O_{carb}$ as climate proxy, comparable data from palaeolakes from previous interglacials are still rare (e.g. Binka and Nitychoruk, 1995; Drescher-Schneider and Papesch, 1998; Boettger et al., 2000; Nitychoruk, 2000; Nitychoruk et al., 2005). In particular, surprisingly little is known about terrestrial isotope records correlating with Marine Isotope Stage (MIS) 11, although this interglacial is considered as a good analogue to the Holocene with respect to orbital forcing (e.g. Berger and Loutre, 2002; Loutre, 2003). Many efforts have been undertaken to study long marine records (e.g. McManus et al., 1999) and Antarctic ice cores (Petit et al., 1999; EPICA community members, 2004) that demonstrated a 27-30 ka interglacial at around 400 ka BP, including a period of 16-18 ka of full or peak interglacial conditions (de Abreu et al., 2005). The only available stable isotope data from a lacustrine record of this period is from Ossówka in Eastern Poland (Nitychoruk, 2000; Nitychoruk et al., 2005). Thus the sediment record from the Piànico palaeolake provides complementary data for the Southern Alps at sub-decadal resolution allowing resolving natural climatic variability during peak interglacial conditions 400 ka ago, a period for which any kind of human interference can be excluded.

DOI: 10.2312/GFZ.b103-07065

6.2. Study site and sediments

Deposits of the Piànico palaeolake outcrop at an altitude between 280 m and 350 m a.s.l. in the Borlezza Valley (45° 48' N, 10° 2' E; Fig. 6.1), a northwestern tributary to recent Lake Iseo, Southern Alps. The Piànico palaeolake is ca 3 km long and 500-800 m wide (Casati, 1968). The presence of varves indicates meromictic deep water conditions. The catchment of the palaeolake forming the lower part of the Borlezza Valley (Fig. 6.2) is constituted mainly by Upper Triassic dolomitic rocks (Dolomia Principale) and subordinately by limestones belonging to the Calcare di Zorzino Unit (Provincia di Bergamo, 2000).

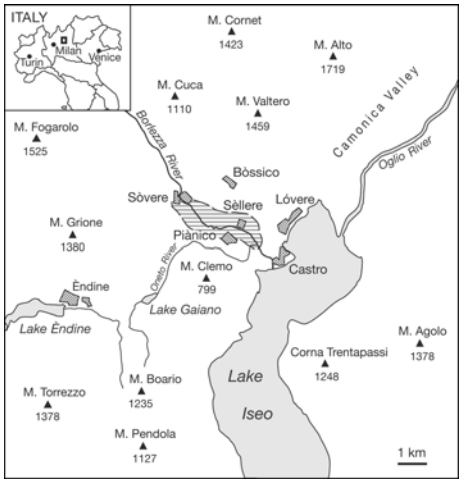

Fig. 6.1: Location of the Piànico-Sèllere Basin and reconstructed extension of the palaeolake (dashed area; modified after Casati, 1968).

The 48 m thick sequence of lacustrine sediments of the Piànico Formation (Moscariello et al., 2000) is subdivided into four units of partly finely laminated sediments: in this paper only the upper two units labelled as BVC (Banco Varvato Carbonatico; Fig. 6.3) and MLP (Membro di La Palazzina; Fig. 6.3) are considered. These units are exposed in several outcrops which have been microscopically correlated on a varve-to-varve basis (Mangili et al., 2005; Brauer et al., submitted). A composite lithological log was established through the stratigraphic combination of three outcrops: Main Section, Wall Section and Deer Section (Figs 6.2 and 6.3; Brauer et al., submitted).

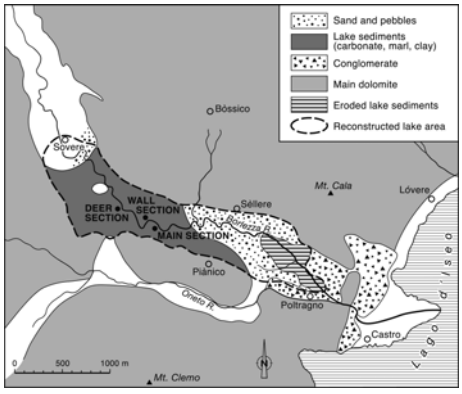

Fig. 6.2: Distribution of the Pleistocene sediments in the basin of the Piànico palaeolake during the early stages of lacustrine sedimentation (modified after Casati, 1968). The sampled outcrops are indicated (Main Section, Wall Section and Deer Section).

The BVC unit represents a long period of 15 500 years of interglacial climate as revealed by the continuous formation of calcite varves and by vegetation reconstructions (e.g. Amsler, 1900; Maffei, 1924; Moscariello et al., 2000; Rossi, 2003). The varves of this unit (Fig. 6.4) are composed of two laminae: a spring-summer light lamina formed by biochemically precipitated calcite with crystal sizes of 2-15 μm, and an autumn-winter dark lamina composed by organic matter, diatom frustules and few scattered detrital grains (Brauer et al., submitted). Summer layers (Fig. 6.4b) consist up to 98% of calcite and constitute 69-98% of the total varve thickness.

DOI: 10.2312/GFZ.b103-07065

Intercalated detrital layers (Fig. 6.4a) reflect surface runoff episodes caused by extreme precipitation events (Mangili et al., 2005).

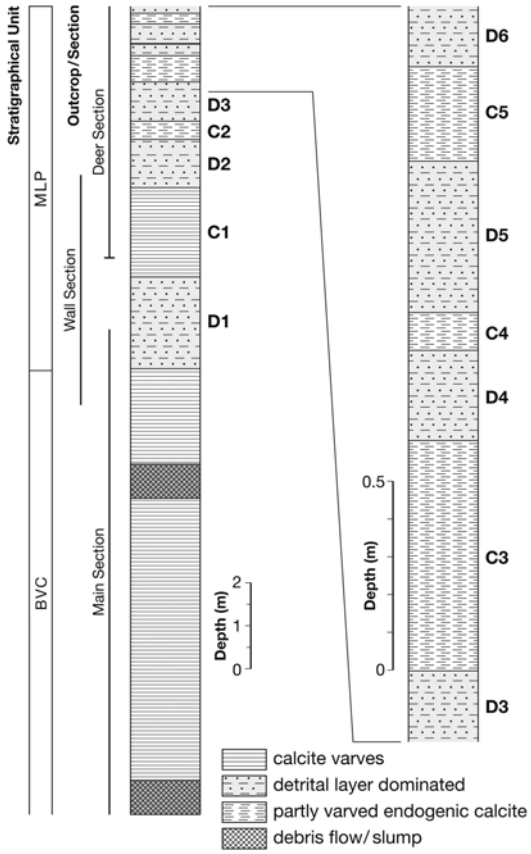

Fig. 6.3: Simplified composite stratigraphic column of the BVC and MLP units. Isotope data are obtained from samples taken at different outcrops as indicated by bars on the left side of the lithological column. The MLP unit exhibits a succession of five intervals of predominantly endogenic calcite sediments (10-185.5 cm thick; C1 to C5) intercalated with six intervals of detrital sediments (16-205.5 cm thick; D1 to D6).

The MLP unit exhibits a succession of six intervals of detrital sediments (each 16 - 205.5 cm thick; D1 to D6 in Fig. 6.3) intercalated by five intervals of predominantly endogenic calcite sediments (each 10 - 185.5 cm thick; C1 to C5 in Fig. 6.3). Thickness of both detrital and endogenic dominated sediment sections generally decreases towards the top of the profile. Calcite varves similar as in the BVC unit only formed in the lowermost section of endogenic calcite (C1 in Fig. 6.3). The lithological variations of predominantly autochthonous and allochthonous sediment deposition correlate well with vegetation changes (Moscariello et al., 2000; Rossi, 2003), both indicating millennial-scale climatic oscillations.

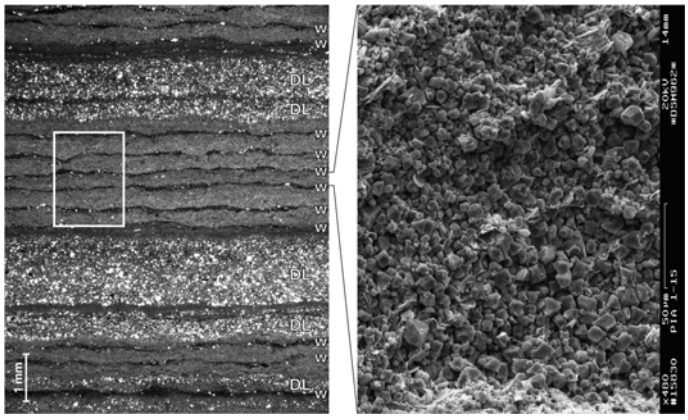

Fig. 6.4: (a) Thin section image of varves and detrital layers (crossed polarised light). Winter layers (w) and detrital layers (DL) are indicated. The rectangle marks a typical sample interval of five varves excluding detrital layers for isotope analyses. (b) S.E.M. picture proving that summer layers are composed of pure endogenic calcite crystals of different sizes.

DOI: 10.2312/GFZ.b103-07065

6.3. Methods

6.3.1. Field sampling

A composite stratigraphic profile was established for the studied interval in order to avoid sampling disturbed by local slump deposits. The BVC unit was sampled for isotope analyses in the Main and Wall Sections; the MLP unit was sampled in the Wall and Deer Sections (Fig. 6.2).

After cleaning the outcrop with a sharp knife to obtain a smooth and vertical surface, sediment blocks of 33 x 5 cm were carved out from the sediments with 5 cm overlap each. The sample boxes of stainless steel have removable side walls in order to extract the sediment blocks in the laboratory without breakage. After drying at room temperature, the sample blocks were covered with a transparent epoxy resin (Araldite® 2020) for further fixation. The epoxy impregnated up to ca 1-2 mm from the surface of the sediment blocks. The sample blocks then were sufficiently stable to be cut into three parallel ca 2 cm thick slices of which one was used for thin sectioning and another one for isotope sub-sampling.

6.3.2. Sub-sampling for isotope analyses

Isotope sub-samples were selected on the base of lithological data from thin section inspection. This enabled both to select sample intervals comprising precisely five varves and to ensure that these samples contain only endogenic calcite in order to exclude a bias through contamination with detrital carbonates.

In total, 387 samples were carefully scratched from fresh cut surfaces of the sediment blocks with a sharp scalpel. From all samples, 14 were obtained from two of the non-varved intervals in the MLP unit (C2 and C3 in Fig. 6.3) preventing from precise time control. Thickness of these samples was in the same range (2-4 mm) like in the varved part. In the detrital intervals of the MLP no samples have been taken because high amounts of detrital carbonates prevented from selecting endogenic calcite samples.

The time intervals between subsequent samples varied between the upper part of the BVC spanning 9350 varve years between 0 (continuous samples) and 100 varve years. The lower part of the BVC (~ 6150 varve years) was sampled at lower resolution between ~10 and 700 varve years. Sample resolution in the MLP varied between 0.5 and 20 cm.

6.3.3. Isotope analyses

The stable-isotope composition of the sediments was analysed in continuous flow mode with a Finnigan GasBench II connected with a DELTAplusXL mass spectrometer. From each sample, 0.25 ± 0.05 mg were loaded into 10 ml Labco Exeteiner® vials. Two sub-samples were analysed for each sample. After automatically flushing with He, the isotope samples were reacted in phosphoric acid (100%, density 1.93) at 75° C for 60 minutes in a Finnigan Gas Bench preparation system. Isotope compositions of the sediments were given relative to the VPDB standard in the conventional δ-notation and were calibrated against three international reference standards (NBS 19, CO1, CO8). The standard deviation (1 sigma) was < 0.1‰ for $\delta^{18}O$ and $\delta^{13}C$.

6.4. Chronology

A floating chronology has been established for the studied interval based on varve counting in the BVC unit with well preserved varves and sedimentation rate estimates and in the MLP unit with only few varved intervals.

The chronology for the upper 9350 years of the BVC was based on varve counting in thin sections using a petrographic microscope. Due to the exceptional preservation of varves, the error estimate of varve counting for this interval amounts to not more than 1-2%. For the lower part of the BVC a preliminary chronology (ca 6150 varve years) has been established through varve counting with a 10-times magnification lens in the outcrop. The counting error in this part of the chronology is slightly higher (~ 5%) due to the less precise counting technique.

DOI: 10.2312/GFZ.b103-07065

The duration of the studied part of the MLP unit has been determined to ca 8500 years based on a combination of varve counting and calculation of sedimentation rates using micro-facies data (Brauer et al., submitted). This is considered as a minimum estimate because of the high possibility of erosion caused by numerous thick detrital layers intercalated within this interval.
The floating chronology has been anchored to an absolute time scale by means of tephrochronology. A 0.7 mm thick volcanic ash layer has been geochemically and mineralogically correlated with the Roccamonfina Brown Leucitic Tuff (Brauer et al., in press) dated from near-vent deposits at 393 ± 12 ka BP. Using the estimated length of the MLP (8500 years) and the varve count from the BVC unit (15 500 years), the studied interval comprised the time span between about 415.1 ± 12 ka BP (bottom of the BVC unit) and 391.1 ± 12 ka BP (top of the studied sequence) with the BVC/MLP boundary at 399.6 ± 12 ka BP.

6.5. Results

The $\delta^{18}O$ values of endogenic calcite in the studied interval of the Piànico record range between –10.06‰ and –8.01‰ (Fig. 6.5a and 6.6a). Both the lightest and the heaviest $\delta^{18}O$ values occur in the BVC unit. $\delta^{18}O$ values of three endogenic calcite intervals of the MLP unit (C1-C3, Fig. 6.5a and Tab. 6.1) fell in the range –8.29‰ - –9.15‰. The smaller amplitude in these sections might be a consequence of the low number of samples from this interval (n=41).

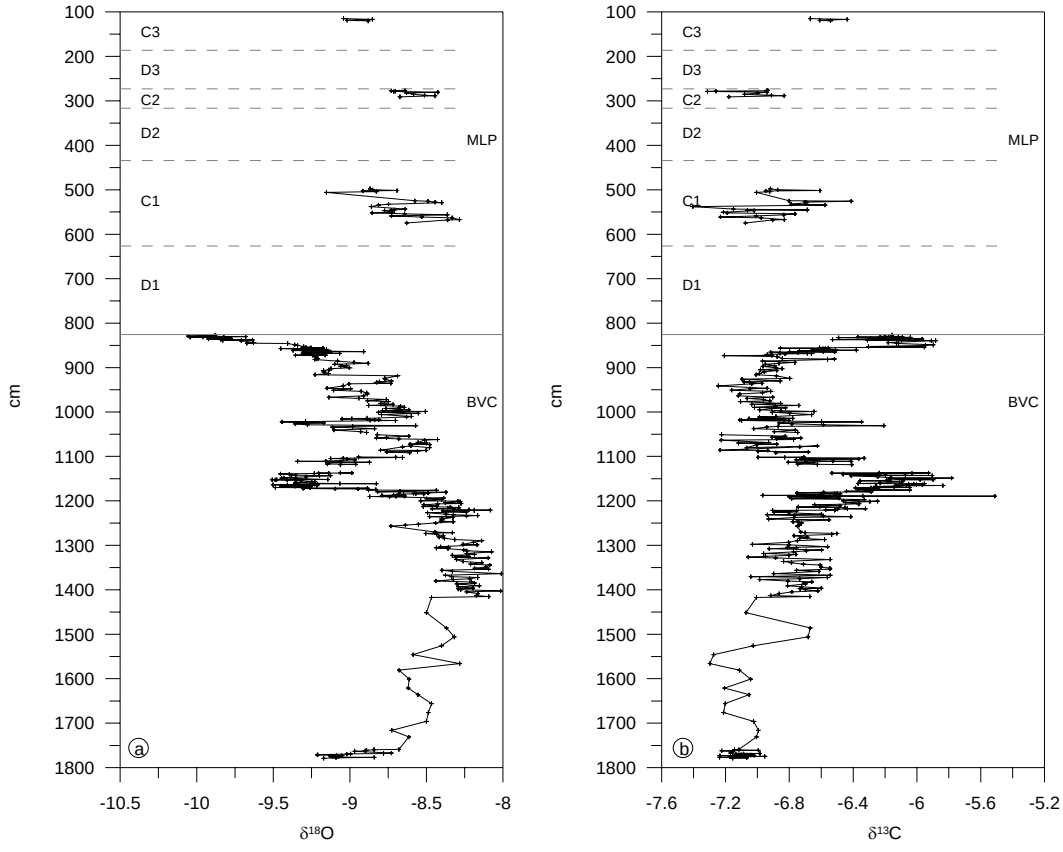

Fig. 6.5: $\delta^{18}O$ (a.) and $\delta^{13}C$ (b.) records for the BVC and MLP units. The '0'-point of the depth scale is at the top of the studied sequence (see Fig. 6.3). C1-C3 are the endogenic calcite-dominated sediment intervals within the MLP unit. No isotope data are obtained for the intercalated D1-D3 intervals which are dominated by detrital carbonated not allowing to sample pure endogenic calcite.

The general structure of the $\delta^{18}O$ curve from the peak interglacial (BVC unit) is tripartite (Fig. 6.5 and Tab. 6.1): from 1779 cm to 1415 cm (ca 5750 varve years) $\delta^{18}O$ gradually rises, from –9.21‰ to –8.28‰. Short-term oscillations might not be detected in this part of the record due to the low

DOI: 10.2312/GFZ.b103-07065

sampling resolution. From 1415 to 1173 cm depth, $\delta^{18}O$ values remain relatively stable except two short-term oscillations of 165 and 195 varve years duration. Despite these negative oscillations the mean $\delta^{18}O$ value in this ca 4350 years long period reached the most positive value in the BVC unit (–8.37‰). The end of this phase is marked by a sharp drop of –0.88‰ in $\delta^{18}O$ at 1173 cm depth. The ~4950 varve year long period from 1173 cm to 827 cm starts with a 780 varve year long period of negative values (mean: –9.30‰) followed by a shift to more positive values (–8.43‰). The further course of the curve is characterised by a general decrease of $\delta^{18}O$ towards the BVC/MLP boundary with superimposed two prominent short-term negative fluctuations. About 275 varve years before the upper limit of the BVC unit, a major fall in $\delta^{18}O$ marks the beginning of the final decline with lightest $\delta^{18}O$ values directly before the prominent lithological shift at the BVC/MLP boundary. This shift to detrital-dominated sedimentation prevented from continuation of isotope analses because endogenic calcite was not sufficiently available. The $\delta^{18}O$ values of the varved interval (C1) after the first detrital dominated interval (D1) again are 1.1-1.2‰ heavier than in the uppermost part of the BVC.

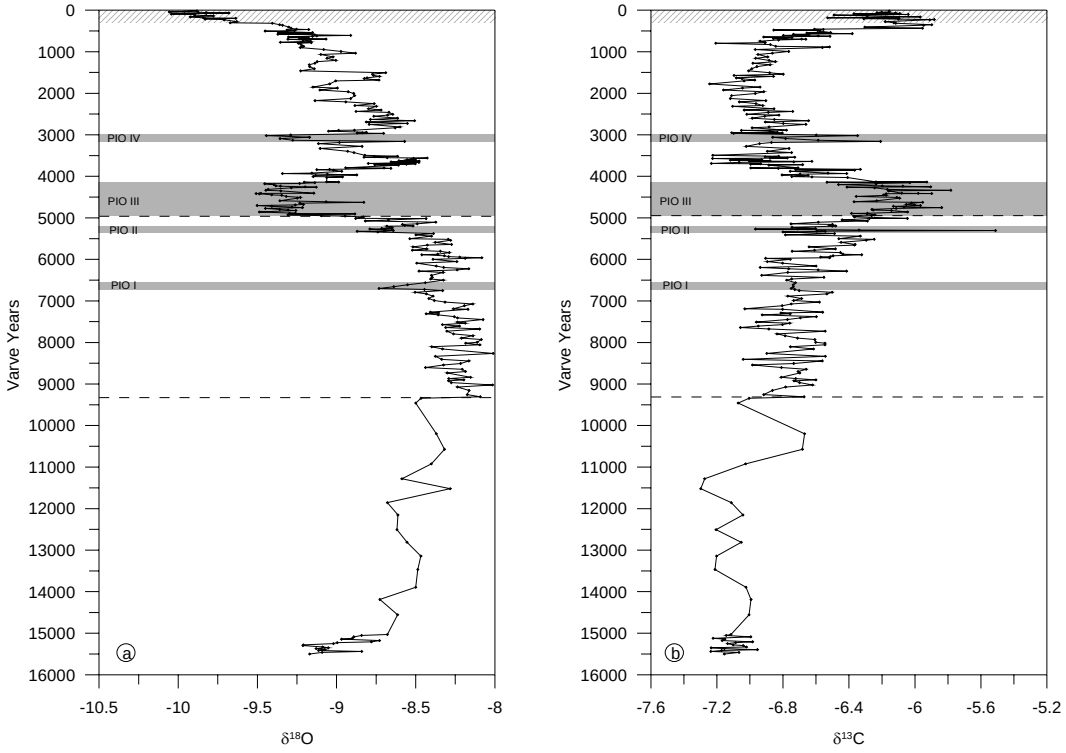

Fig. 6.6: $\delta^{18}O$ and $\delta^{13}C$ record only for the peak interglacial (BVC unit) plotted against the floating varve chronology with the '0' year marking the end of the peak interglacial (=top of BVC unit). Dashed lines mark the three-partition of the isotope record as discussed in the text.

Particularly remarkable are the four prominent $\delta^{18}O$ short-term oscillations (labelled as Pianico Isotope Oscillations, PIO; Fig. 6.6 and Tab. 6.2) within the BVC unit. The most prominent of these oscillations (PIO III) lasted 780 varve years and thus was clearly longer than PIO I, II and IV which spanned 165, 195 and 125 varve years, respectively (Tab. 6.2). The onset of PIO III is marked by a sudden drop in $\delta^{18}O$ of 1.07‰ to a mean value of –9.30‰ during this oscillation. From the three shorter oscillations, only PIO IV exhibits a $\delta^{18}O$ decrease in about the same range (-0.87‰) whereas the amplitudes of PIO I and II are much smaller (0.40-0.48‰).

DOI: 10.2312/GFZ.b103-07065

zone	number of samples	$\delta^{18}O$			$\delta^{13}C$		
		max	min	mean	max	min	mean
MLP - C3	4	-8.85	-9.04	-8.95	-6.44	-6.67	-6.56
MLP - C2	10	-8.42	-8.73	-8.61	-6.83	-7.31	-7.04
MLP - C1	27	-8.29	-9.15	-8.66	-6.41	-7.40	-6.91
BVC	346	-8.01	-10.06	-8.84	-5.51	-7.30	-6.66

Tab. 6.1: $\delta^{18}O$ and $\delta^{13}C$ maximum, minimum, mean values and overall amplitude of the isotope shifts for each carbonate interval in the MLP, for the whole BVC and for the three different parts recognisable in the $\delta^{18}O$ of the BVC unit.

The $\delta^{13}C$ values of the BVC unit range between –5.51‰ and –7.30‰ (Figs 6.5b and 6.6b; Tab. 6.1). The $\delta^{13}C$ curve shows an increasing trend from the base of the BVC until the end of PIO III when $\delta^{13}C$ drops by about 0.88‰. During PIO III, $\delta^{13}C$ reach a maximum of about -5.78‰, thus exhibiting an inverse oscillation than the $\delta^{18}O$ curve. Positive $\delta^{13}C$ oscillations were also recorded for PIO IV and the uppermost part of the BVC where oxygen isotopes finally decline. In contrast, for PIO I $\delta^{13}C$ decreases parallel to the drop in $\delta^{18}O$, while PIO II shows a complex behaviour with first rising and then declining $\delta^{13}C$ values.

zone	duration (years)	number of samples	$\delta^{18}O$				$\delta^{13}C$			
			max	min	mean	drop	max	min	mean	drop
final decline	275	18	-9.18	-10.06	-9.68	-0.88	-5.88	-6.61	-6.18	+0.67
PIO IV	125	5	-9.17	-9.44	-9.31	-0.87	-6.35	-6.86	-6.64	+0.65
PIO III	780	40	-8.83	-9.51	-9.30	-1.07	-5.78	-6.46	-6.15	+0.97
PIO II	195	14	-8.49	-8.87	-8.66	-0.48	-5.51	-6.97	-6.54	+1.27
PIO I	165	5	-8.44	-8.73	-8.56	-0.40	-6.72	-6.75	-6.74	-0.25

Tab. 6.2: $\delta^{18}O$ and $\delta^{13}C$ maximum, minimum and mean values for the Pianico Isotopic Oscillations (PIO). The correlation coefficient between $\delta^{18}O$ and $\delta^{13}C$ for PIO I-IV has been calculated for each fluctuation separately.

6.6. Interpretation and discussion

Palaeoclimatic interpretation from $\delta^{18}O$ of lacustrine carbonates from palaeolakes is a particular challenge, because direct calibration with temperature or $\delta^{18}O$ in precipitation ($\delta^{18}O_{precip}$) is hardly possible. Nevertheless, comparing present day $\delta^{18}O_{precip}$ for sites close to the palaeolake sediments at least provides a general idea about the order of magnitude of $\delta^{18}O_{carb}$ that might be expected. The mean $\delta^{18}O_{precip}$ in the village of Darfo Boario (ca 14 km NE of Pianico) for the period 1992-1999 is –7.66‰ (Longinelli and Selmo, 2003), and thus similar to the values measured from the Pianico calcite.

An additional approach to evaluate the $\delta^{18}O_{carb}$ record from Pianico is an indepth comparison with carbonate isotope records from other old interglacials but also from Holocene and Lateglacial lake sediments (Tab. 6.3; Fig. 6.7). The general similarity of $\delta^{18}O_{carb}$ from the Pianico record and many recent as well as palaeo lake sediments suggests comparable processes of carbonate formation. Nevertheless, some distinct differences appear comparing the minimum $\delta^{18}O$ values, commonly interpreted as indication of colder climate. All other $\delta^{18}O$ records revealed more negative minimum values than Pianico, except Ossówka in eastern Poland (Nitychoruk et al., 2005), the only other record corresponding to MIS 11. This might indicate a general difference between Holocene and MIS 11 climates but regional isotope effects may also play a role. The $\delta^{18}O_{carb}$ records from last interglacial lake sediments are more similar to those from Pianico and Ossówka than to Holocene records except the minimum value of ca 12‰ from the Mondsee record (Drescher-Schneider and Papesch, 1998). This negative value, however, occurred during the penultimate deglaciation period and thus is not representative for interglacial conditions. Interestingly, the reason for the greatest difference of minimum $\delta^{18}O_{carb}$ (>1‰) between Holocene

DOI: 10.2312/GFZ.b103-07065

(Lake Greifen and Lake Gosciaz) and MIS 11-age lake sediments (Piànico and Ossówka) are data from the most recent sediments of the last century. Interpretation of these negative $\delta^{18}O_{carb}$ in very young sediments includes changes in air mass circulation (McKenzie and Hollander, 1993).

Fig. 6.7: Location of the $\delta^{18}O$ carbonate records (circles) and of three stations with $\delta^{18}O$ data from modern precipitation (squares) discussed in the text and in Tab. 6.3.

Evaluation of the most positive $\delta^{18}O_{carb}$ values in the compared sediment sequences is additionally complicated because of a possible bias through contamination with detrital carbonate that for most records can not be excluded. Detailed isotope analyses of endogenic calcite with varying amounts of detrital dolomite of marine Mesozoic origin in the Pianico demonstrated a clear relation between the degree of contamination and the deviation towards more positive $\delta^{18}O$ values (Mangili et al., unpublished data). For this study only data from samples with detrital contamination <4% are shown so that a measurable bias through detrital material can be excluded. Presumably, this explains why the heaviest $\delta^{18}O_{carb}$ from Piànico are lighter than in all compared records (Tab. 6.3) thus resulting in the lowest amplitude of $\delta^{18}O_{carb}$ (~ 2‰) for the Piànico record. Although unlikely, it can also not be fully excluded that this low amplitude of $\delta^{18}O_{carb}$ variations is due to either a lower degree of climatic variability at Piànico or a lower sensitivity of this lake system to climate variations.

Site	Elevation (m a.s.l.)	Location	$\delta^{18}O$ max (‰)	$\delta^{18}O$ min (‰)	$\delta^{18}O$ amplitude	Time interval	Lenght of the record (years)
Pianico	350	45° 48' N 10° 02' E	-8.01	-10.06	2.05	MIS 11	16 000
Baldeggersee[1]	423	47° 11' N 8° 15' E	-8	-10.5	2.5	1885 AD - 1993 AD	108
Lake Greifen[2]	435.3	47° 20' N 8° 40' E	-7.6	-11.3	3.7	1750-1986	236
Ammersee[3]	520	48° 00' N 11° 07' E	~ -4.7[a]	~ -5.7[a]	~ 1	8.2 ka event	180
Gerzensee[4]	600	46° 49' N 7° 32' E	-6.5	-10.2	3.7	Lateglacial	~ 6000
Gerzensee[5]	600	46° 49' N 7° 32' E	~ -5.9[b]	~ -10.0[b]	4.1	Lateglacial	1850
Lake Gosciaz[6]	64.3	52° 35' N 19° 21' E	-7.5	-11	3.5	~ 11.500 to 1.200 cal BP	10 300
Lake Gosciaz[7]	64.3	52° 35' N 19° 21' E	-7.5	-10.5	3	Lateglacial	~ 1700
Gröbern[8]	~ 100	51° 40' N 12° 26' E	~ -2	~ -10	~ 8	Eemian	-
Mondsee[9]	481	47° 48' N 13° 23' E	~ -7.8	~ -12	~ 4.2	Eemian	-
Ossowka[10]	~ 150	52° 06' N 23° 08' E	~ -3.8	~ -8.8	~ 5	MIS 11	~35-39 000
Ossowka[10] climatic optimum	~ 150	52° 06' N 23° 08' E	-4.5	-7	2.5	MIS 11	16 000

[a] record from Cytherissa lacustris
[b] calcite from encrustation of Characeae

Tab 6.3: Compilation of different isotope records of lacustrine carbonates in Europe. $\delta^{18}O$ and $\delta^{13}C$ maximum, minimum and the amplitude recorded in the different sequences are reported. Where $\delta^{18}O$ values are not available from the original publications they were graphically obtained from the figures and here reported as 'ca-values'. Data from: (1) Teranes and McKenzie, 2001; (2) McKenzie and Hollander, 1993; (3) von Grafenstein et al., 1998; (4) Siegenthaler et al., 1984; (5) von Grafenstein et al., 2000; (6) Różański et al., 1998; (7) Rozanski et al., 1992; (8) Boettger et al., 2000; (9) Drescher-Schneider and Papesch, 1998; (10) Nitychoruk et al., 2005.

DOI: 10.2312/GFZ.b103-07066

Nevertheless, $\delta^{18}O_{carb}$ variations of ~2 ‰ for the peak interglacial at Piànico clearly indicate the presence of climate change. In particular, the four negative oscillations in $\delta^{18}O_{carb}$ (PIO I-IV) as well as the decline at the end of peak interglacial conditions indicate pronounced short-term climatic changes within a period of 10 000 years of generally relative stable interglacial climate conditions (Fig. 6.6). Since isotope fractionation during calcite precipitation in the epilimnion is inversely dependent on water temperature (–0.23‰/°C; Epstein et al., 1953), a negative shift in $\delta^{18}O_{carb}$ should be expected to reflect warmer water in the epilimnion. However, comparable negative shifts in $\delta^{18}O_{carb}$ from Holocene and Lateglacial lake records are commonly interpreted as indication for climatic cooling (Siegenthaler and Eicher, 1986; Kuc et al., 1998; von Grafenstein et al., 1998) because of the superimposed effect of $\delta^{18}O_{precip}$ which, in turn, is mainly controlled by air temperature. The relationship between $\delta^{18}O_{precip}$ and annual mean air temperature, known as Dansgaard relationship, amounts to +0.6‰/°C at mid and high latitudes (Dansgaard, 1964; Różański et al., 1992; Różański et al., 1993). Subtracting the fractionation effect of calcite formation (–0.23‰/°C) from this value results in a relation between air temperature and lake $\delta^{18}O_{carb}$ of ~0.37‰/°C for open lakes (Leng and Marshall, 2004). Applying the same factor to the Piànico record, the strongest negative shifts of –1.07‰ for PIO III and –0.43‰ at the end of the peak interglacial suggest temperature decreases of ca 2.9°C and 1.16°C.

These values are regarded as maximum estimates because additional factors as (1) seasonal effects, (2) changes in atmospheric circulation and (3) variations of the moisture source might have contributed to the drops in $\delta^{18}O_{carb}$. (1) A shift of the dominant amount of annual rainfall into the winter season could have also shifted oxygen isotopic compositions to more negative values. (2) Precipitation at Piànico can originate from either Atlantic or Mediterranean sources. The averages of the mean monthly $\delta^{18}O_{precip}$ in Genoa (Mediterranean source) and Groningen (Atlantic source) differ by 2.6‰ for the decade 1985-1995 (data from IAEA/WMO, 2004). Therefore, a shift, for example, caused by more frequent invasions of Atlantic air masses would have resulted in changes of isotope composition of precipitation towards lighter values.

(3) In addition, sea surface temperatures in the moisture source region might have also contributed to the observed negative shifts in $\delta^{18}O$. Most of the present day precipitation in the Southern Alps originates from Mediterranean low pressure systems generated over the Gulf of Genoa (H.M.S.O., 1962) through southerly flows of warm and moist Mediterranean air into northern Italy (e.g. Brunetti et al., 2000). Thus, a lowering of SST in the Gulf of Genoa also could have caused more negative $\delta^{18}O_{precip}$. Although from this region no high resolution SST data for MIS 11 are published, data from the Iberian Margin indicate a SST decrease of ca 2.5-3° C during the warmest part of the MIS 11 interglacial (de Abreu et al., 2005).

The most striking oscillation is PIO III mainly because of its long duration of 780 years. This cooling occurred after more than 10 000 varve years of warm interglacial conditions, and is even seen in a sudden change in vegetation from broad-leaved to conifer dominated taxa. Compared to well-known Holocene cold climatic oscillations, which lasted no longer than 2-3 centuries, the duration of PIO III is exceptional. In contrast, the amplitude of 1.07‰ compares well with that of 1‰ reported for the so-called '8.2 ka event' in the Holocene (von Grafenstein et al., 1998) that, however, was significantly shorter (180-200 years; Prasad et al., 2006). Longer lasting cold phases like the Younger Dryas are only reported from the Lateglacial, but this period was characterized by a much more pronounced negative oxygen isotope swing (Kuc et al., 1998). Discussing the triggering mechanisms for PIO III is difficult and requires additional high resolution data from marine cores in order to better understand changes in thermohaline circulation during this period. Nevertheless, it can be assumed that the potential triggers for Holocene climate deterioration, i.e. changes in thermohaline circulation and solar radiation (Bond et al., 1997; 2001) are the most likely candidates also for explaining PIO III. This would imply, however, that either the sun had a longer weak period during MIS 11 than experienced during the Holocene so far, or that longer and/or stronger inflow of freshwater into the North Atlantic had changed the thermohaline

DOI: 10.2312/GFZ.b103-07065

circulation lastingly. Potential sources for freshwater can be either enhanced circum-Atlantic river runoff or glacial meltwater from Greenland.

The changes in $\delta^{13}C_{carb}$ during the four cold oscillations are difficult to understand because they are not always in the same direction. A likely explanation for the positive shifts of $\delta^{13}C_{carb}$ during PIO II-IV and the final decline in $\delta^{18}O_{carb}$ during the end of the peak interglacial is a change in isotopic composition of water inflow (McKenzie, 1985; Leng and Marshall, 2004). $\delta^{13}C_{carb}$ values are thought to correspond to the isotopic composition of dissolved inorganic carbon (DIC) in the lake water body (McKenzie, 1985). Heavier $\delta^{13}C$ values of DIC thus might be due to enhanced carbonate solubility in colder water and/or to increased dissolution of carbonates with more positive $\delta^{13}C$ values (mean $\delta^{13}C$ values of the measured dolomites: +0.3‰; Mangili et al., unpublished data) in the catchment.

6.6.1. Comparison with other 400 ka old records

On the basis of the tephrochronological match of the distal volcanic ash layer with the Roccamonfina Brown Leucitic Tuff (BLT), the stratigraphic position of the Piànico interglacial is assumed to correspond to MIS 11. This calls for a tentative correlation with marine and ice records from this time interval (Fig. 6.8). Although a precise correlation is not possible due to the rather large dating errors of the BLT (Giannetti et al., 2001), it appears likely that the 15.5 kyrs long interglacial sequence from Piànico correlates with the ca 18 kyrs "full interglacial" period during MIS 11, as defined by de Abreu et al. (2005) in a marine core from the Iberian Margin. Taken into consideration a major hiatus at the base of the Piànico interglacial through a major slump deposit including reworked varved intervals (Brauer et al., submitted), the length of the period of interglacial warmth as indicated by the continuous formation of calcite varves is in good agreement with the peak interglacial in core MD01-2443. Interestingly, the length of the 'climatic optimum' reported from the Ossówka site in Poland is about the same (16 ka; Nitychoruk et al., 2005), also suggesting a correlation with the peak interglacial at Piànico. Accepting this correlation led us to further speculate on possible links even of more detailed features of these proxy records. During the full interglacial period in core MD01-2443 a drop in SSTs of ca 2.3 °C is recorded (de Abreu et al., 2005) which might reflect the same climatic fluctuation like PIO III (Fig. 6.8) and a ca 1‰ drop in $\delta^{18}O_{carb}$ observed in the Ossówka record at ca 37 m depth (Nitychoruk et al., 2005).

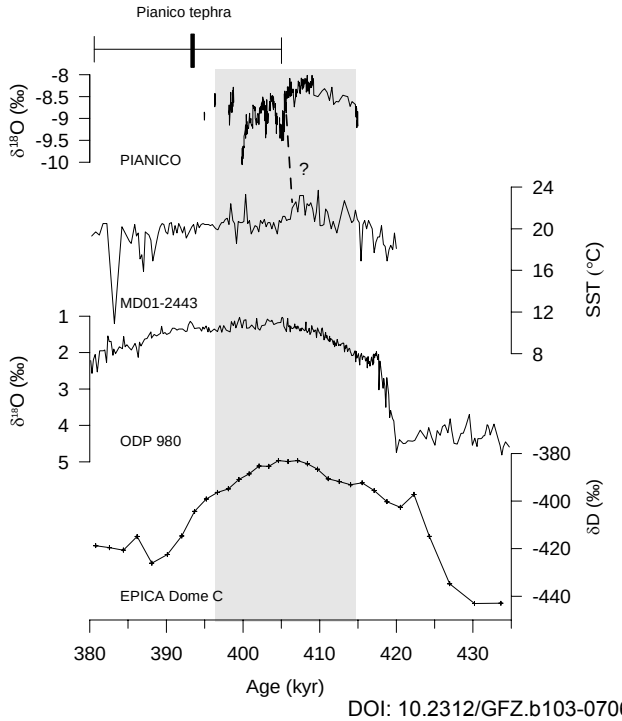

Fig. 6.8: Comparison of the $\delta^{18}O$ record from Pianico interglacial with the SST record of MD01-2443, the ODP 980 record (McManus et al., 1999) and the δD EPICA record (EPICA community members, 2004). The 18 ka long 'full interglacial' as defined by de Abreu et al. (2005) is indicated by the grey bar. The dashed line indicates possible correlation of PIO III with a drop in the SST record. The position of the distal deposit of the Roccamonfina Brown Leucitic Tuff is indicated as 'Piànico Tephra' with error bars of the dated near vent deposits (393 ± 12 ka BP; Giannetti, 2001).

DOI: 10.2312/GFZ.b103-07065

As mentioned before these correlations are speculative, in particular, because marine records from the North Atlantic (Oppo et al., 1998; McManus et al., 1999) and the Antarctic ice core (EPICA community members, 2004) do not show such short-term intra-interglacial climate oscillations (Fig. 6.8). Possible explanations for these differences include regional climate differences, sensitivity of proxies, and, last but not least, time resolution of the data series. Despite the present uncertainties of correlation, the clear indication of a centennial-scale interglacial climate oscillation at Piànico calls for further high-resolution studies and efforts to improve the dating precision.

6.7. Conclusions

The $\delta^{18}O$ record from the Piànico sediments represents a 15 500 years long time series of natural interglacial climate variability. The varved nature of the sediments allowed to sub-sample in well-defined and precise 5-year intervals and provides information about short-term climatic fluctuations at decadal resolution. Four negative $\delta^{18}O_{carb}$ fluctuations reflect rapid climate shifts during peak interglacial conditions at about 400 ka BP. Most of these oscillations are comparable in amplitude and duration with Holocene climate changes except the most prominent period of climatic deterioration which occurred after 10 000 years of relative climatic stability and lasted for 780 varve years, thus much longer than known Holocene cold periods. This cold period is expressed by a drop of 1.07‰ in $\delta^{18}O_{carb}$ and a rapid change in vegetation and might be linked to a drop in SSTs recorded at the Iberian margin. Three shorter cold oscillations with durations between 125 and 195 varve years have smaller $\delta^{18}O$ amplitudes. Another 0.88‰ decline of $\delta^{18}O_{carb}$ occurred 285 varve years before the end of peak interglacial conditions which is marked also by a distinct change from an autochthonous to an allochthonous sedimentation regime. Most striking, however, is the long period of climate deterioration reflected by PIO III that exceeds Holocene cold phases thus suggesting that the present interglacial did not yet experienced the full range of potential natural interglacial climate variability. Therefore, a better knowledge of the triggering mechanism of this oscillation is crucial for evaluating possible future changes.

6.8. Acknowledgements

We wish to thank G. Arnold, D. Berger and M. Köhler for preparing high-quality thin sections. M. Dziggel and A. Hendrich helped with the lay out of the figures.
We are grateful to Lucia de Abreu for providing the data from core MD01-2443 used in Fig. 6.8. Data of isotopic composition of recent precipitation are from the IAEA/WMO database. We acknowledge the Centre for Isotope Research, Groningen, The Netherlands and the Istituto Internazionale per le Ricerche Geotermiche, Pisa, Italy.

DOI: 10.2312/GFZ.b103-07065

7. Main results

The tephrochronological dating of the Piànico sequence fixes the varve floating chronology to the interglacial centred at 400 ka BP and corresponding to Marine Isotope Stage 11 (MIS 11). This interglacial period is considered to be the best analogue to the Holocene, on the basis of similar Earth orbital parameters and, in particular, on similar eccentricity values (e.g. Berger and Loutre, 2003; Loutre and Berger, 2003; McManus et al., 2003; Fig. 7.1).

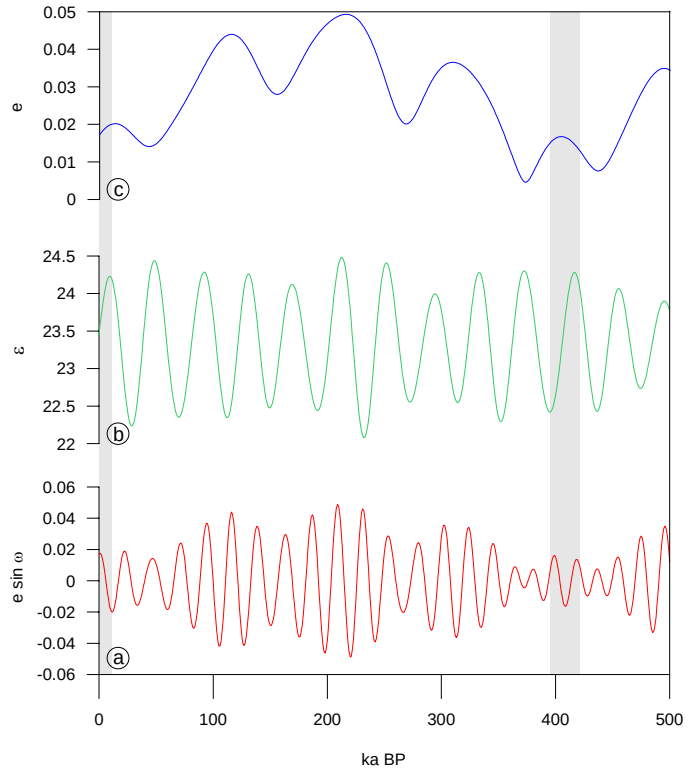

Fig. 7.1: Earth's orbital parameters for the last 500 ka (data from Berger and Loutre, 1991). a) Precession; b) obliquity; c) eccentricity. Holocene and MIS 11 are marked by grey bars.

MIS 11 has been usually described as a stable 27-30 ka long interglacial (e.g. McManus et al., 1999; EPICA community members, 2004) and used to forecast the remnant length of the Holocene (e.g. EPICA community members, 2004; Ruddiman, 2005a). Even including the hiatus at the onset of interglacial, the length of the Piànico interglacial is much shorter than 27 ka. However, from our chronology and from the varve counting, the length of the interglacial interval of Piànico is in agreement with the new finding from site MD01-2443 (de Abreu et al., 2005) and Ossówka (Nitychoruk et al., 2005). In these sequences, both correlating to MIS 11, a 16-18 ka period characterised by peak interglacial conditions has been recently highlighted within the 27 ka interglacial period of MIS 11 (de Abreu et al., 2005; Nitychoruk et al., 2005). The interglacial sequence of Piànico would then correspond to the climatic optimum within MIS 11 (Chapter 6).
The high-resolution of the Piànico record enables, therefore, to study short-term climate changes within the climatic optimum of MIS 11. So far, four climatic oscillations and a period of climate deterioration at the very end of the 15.5 ka interval have been recorded.
The climatic deterioration at the end of the 15.5 ka interval started within a decade and was characterised by cold conditions and increase in extreme summer precipitation events (Chapters 2, 4 and 6; Fig. 7.2).

DOI: 10.2312/GFZ.b103-07065

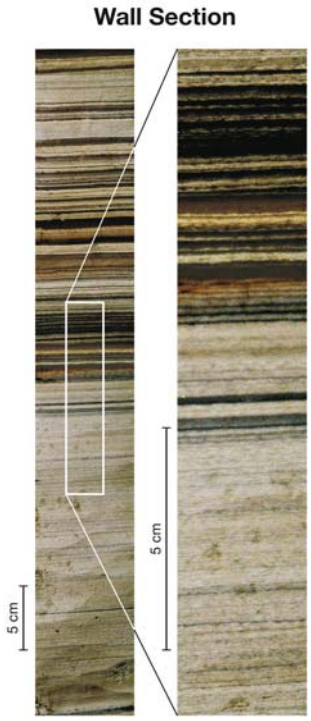

Fig 7.2: At the end of the 15,500 years characterised by interglacial conditions, climate rapidly deteriorated. This 430 years period is characterised by strong increase in extreme precipitation events as indicated by high frequency of detrital layers.

The high resolution used for this study enables also to highlight a 1000 years intra-interglacial cold phase (Chapters 4 and 6) that was characterised by reduction in lake productivity associated with colder climate (Fig. 7.3).

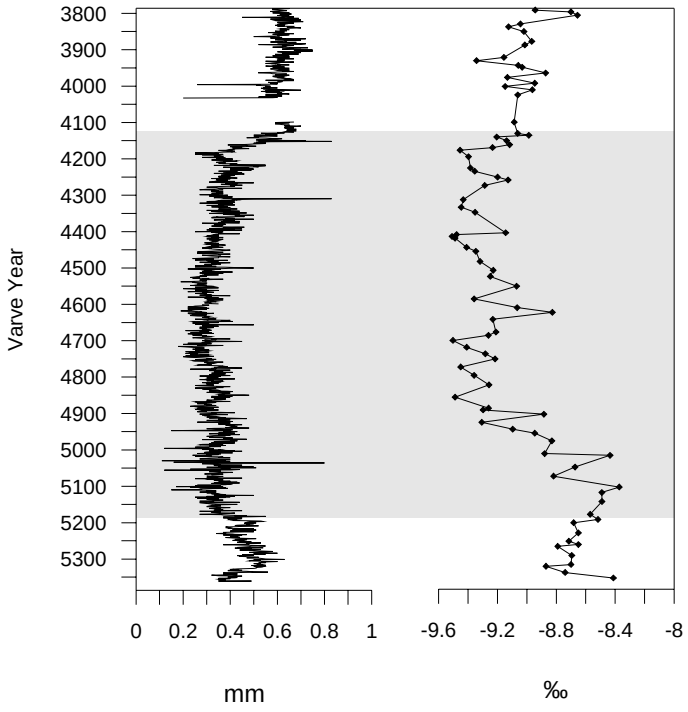

Fig. 7.3: intra-interglacial cold phase (grey bar): reduction in thickness of summer varve layers indicating reduction in lake productivity (left) and drop in d18O values probably indicating colder temperature (right).

What observed in the interglacial sequence of Piànico constitutes the first report of a cold intra-interglacial period within MIS 11. However, some evidences of sudden changes during MIS 11 can be found also in other records. For example, a drop in SSTs of ca 2.3 °C is recorded in MD01-2443 within the 18 ka period of full interglacial conditions (de Abreu et al., 2005). This drop in SSTs is associated with a drop of $\delta^{13}C$ and $\delta^{18}O$ of benthic foraminifera indicating an episode of reduced ocean ventilation and changes in deepwater production/circulation. The $\delta^{18}O$ drop in

DOI: 10.2312/GFZ.b103-07065

benthic foraminifera of MD01-2443 was correlated to a similar drop in ODP 980 (McManus et al., 1999; de Abreu et al., 2005). Drastic reduction in $CaCO_3$ content and drop in $\delta^{13}C$ of benthic foraminifera were also observed in ODP 1063 and linked to a reduction of NADW production (Poli et al., 2000).

A cold oscillation similar to the cold phase observed in Piànico has not been so far observed in the Holocene. This implies that the Holocene has not experienced the whole range of natural climate variability.

8. Conclusions

The Piànico sequence represents a valuable archive that enables the reconstruction of past climate variability. For the first time seasonal resolution and multi proxy approach were applied to study a varved interglacial sequence. Through this approach, new findings were possible. The main of these findings is represented by the intra-interglacial cold period that constitutes a new type of climate change not experienced by the Holocene yet. This implies that the intra-interglacial climate variability can be wider than expected, and that new and more high-resolution researches are required.

9. Future work

Future work on the Piànico sequence will focus on:
- extending the data set by completing the varve counting of the whole 15,500 years sequence;
- studying the decadal and centennial variability;
- understanding of leads and lags in proxies;
- possible understanding of the trigger(s) of the cold oscillations recorded.

The multi proxy approach and the new procedures developed for the sequence of Piànico will be applied to study other varved sequences at seasonal resolution.

DOI: 10.2312/GFZ.b103-07065

10. References

Alley, R.B., Mayewski, P.A., Sowers, T., Stuiver, M., Taylor, K.C., Clark, P.U. (1997) Holocene climatic instability: A prominent, widespread event 8200 years ago. Geology, 25, 483-486.

Amsler, M. (1900) Flore interglaciaire de Pianico. Compte Rendu des travaux de la Soc. Helvetique de Sc. nat. reunie a Thusis, 44-46.

Anderson, R.Y. (1993) The varve chronometer in Elk Lake: Record of climatic variability and evidence for solar-geomagnetic-14C-climate connection. In: Bradbury, J.P., and Dean, W.E., eds., Elk Lake, Minnesota: Evidence for Rapid Climate Change in the North-Central United States, Volume 276, Geological Society of America Special Paper, Boulder, Colorado, 45-67.

Anderson, N.J., Leng, M.J. (2004) Increased aridity during the early Holocene in West Greenland inferred from stable isotopes in laminated-lake sediments. Quaternary Science Reviews 23, 841-849.

Baltzer, A. (1896) Beiträge zur Kenntniss der Interglacialen Ablagerungen. Neue Jahrbuch für Mineralogie, Geologie und Mineralogie 1, 159-186.

Barlow, L.K. (2001) The time period A.D. 1400-1980 in Central Greenland ice cores in relation to the North Atlantic Sector. In: Ogilvie, A.E.J., and Jonnson, T., eds., The icebergs in the mist: northern research in pursuit of a "Little Ice Age". Dordrecht, Kluwer Academic Publishers, 101-119.

de Beaulieu, J.L., Reille, M. (1995) Pollen records from the Velay craters. A review and correlation of the Holsteinian Interglacial with isotope stage 11. Mededelingen Rijks Geologische Dienst 52, 59-70.

de Beaulieu, J.L., Andrieu-Ponel, V, Reille, M, Grüger, E, Tzedakis, C, Svobodova, H. (2001) An attempt at correlation between the Velay pollen sequence and the Middle Pleistocene stratigraphy from central Europe. Quaternary Science Reviews 20, 1593-1602.

Bellucci, F, Lirer, L, Munno, R. (1999) Geology of Ponza, Ventotene and Santo Stefano islands (with a 1:15,000 scale geological map). Acta Vulcanologica 11, 197-222.

Berger, A., Loutre, M.F. (1991) Insolation values for the climate of the last 10 million years: Quaternary Science Reviews 10, 297-317.

Berger, A., Loutre, M.F. (2002) An exceptionally long interglacial ahead?. Science 297, 1287-1288.

Berger, A., Loutre, M.F. (2003) Climate 400,000 Years ago, a key to the Future ? In: Unique and Exceptionally Long Interglacial Marine Isotope Stage 11: Window into Earth Warm Future Climate, Volume 137, American Geophysical Union, 17-26.

Bertini, A. (2000) Pollen record from Colle Curti and Cesi. Early and Middle Pleistocene mammal sites in the Umbro-Marchean Apennine Mountains (central Italy). Journal of Quaternary Science 15, 825-840.

Bertuletti, C., **Carollo, A.** (1973) Climatologia del bacino idrografico del Torrente Borlezza. Amministrazione provinciale di Bergamo, Bergamo, 94 pp.

Binka, K., **Nitychoruk, J.** (1995) Mazovian (Holsteinian) lake sediments at Woskrzenice near Biala Podlaska. Geological Quarterly 39(1), 109-120.

Blikra, L.H., Nemec, W. (1998) Postglacial colluvium in western Norway: depositional processes, facies and palaeoclimatic record. Sedimentology 45, 909-959.

Blikra, L.H., Nemec, W. (2000) Reply to "Bertran, P. and Jomelli, V. 2000. Post-glacial colluvium in western Norway: depositional processes, facies and palaeoclimatic record. Sedimentology 47, 1058-1068.

DOI: 10.2312/GFZ.b103-07065

Boettger, T., Junge, F.W., Litt, T. (2000) Stable climatic conditions in central Germany during the last interglacial. Journal of Quaternary Science 15(5), 469-473.

Boivin, P, Camus, G, De Goer, A, Gourgaud, A, Kieffer, G, Mergoil, J, Vincent, P. (1994) Volcanology of the Chaine des Puys. Parc Naturel Régional des Volcans d'Auvergne.

Bond, G., Showers, W., Cheseby, M., Lotti, R., Almasi, P., deMenocal, P., Priore, P., Cullen, H., Hadjas, I., Bonani, G. (1997) A Pervasive Millennial-Scale Cycle in North Atlantic Holocene and Glacial Climates. Science 278, 1257-1266.

Bond, G., Kromer, B., Beer, J., Muscheler, R., Evans, M.N., Showers, W., Hoffmann, S., Lotti-Bond, R., Hajdas, I., Bonani, G. (2001) Persistent Solar Influence on North Atlantic Climate During the Holocene. Science 294, 2130-2136.

Borchardt, G.A., Aruscavage P.J., Millard H.T. Jr. (1972) Correlation of the Bishop ash, a Pleistocene marker bed, using instrumental neutron activation analysis. Journal of Sedimentary Petrology 42, 301-306.

Brauer, A. (2004) Annually laminated lake sediments and their palaeoclimatic relevance. In: The climate in Historical Times. Towards a Synthesis of Holocene Proxy Data and Climate Models (Eds H. Fischer, T. Kumke, G. Lohmann, G. Flöser, H. Miller, H. von Storch and J.F.W. Negendank), pp. 109-128. Springer, Berlin.

Brauer, A., Hajdas, I., Negendank, J.F.W., Vos, H., Rein, B. Zolitschka, B. (1994) Warvenkronologie. Eine Methode zur absoluten Datierung und Rekonstruktion kurzer und mittlerer solarer Periodizitäten. Geowissenschaften 12, 325-332.

Brauer, A., Endres, C., Negendank, J.F.W. (1999) Lateglacial calendar year chronology based on annually laminated sediments from Lake Meerfelder Maar, Germany. Quaternary International 61, 17-25.

Brauer, A., Endres, C., Günter, C., Litt, T., Stebich, M., Negendank, J.F.W. (1999) High resolution sediment and vegetation responses to Younger Dryas climate change in varved lake sediments from Meerfelder Maar, Germany. Quaternary Science Reviews 18/3, 321-329.

Brauer, A., Litt, T., Negendank, J.F.W., and Zolitschka, B. (2001) Lateglacial varve chronology and biostratigraphy of lakes Holzmaar and Meerfelder Maar, Germany. Boreas 30, 83-88.

Brauer, A., Wulf, S., Mangili, C., Moscariello, A. (2006) Tephrochronological dating of varved interglacial lake deposits from Piànico-Sèllere (Southern Alps, Italy) to about 400 ka. Journal of Quaternary Science, in press.

Brauer, A., Mangili, C., Moscariello, A. (submitted) Palaeoclimatic implications from micro-facies data of a 5900 varve time series from the Pianico interglacial sediment record, Southern Alps. Submitted to Palaeogeography, Palaeoclimatology, Palaeoecology.

Briot, D. (1990) Magma mixing versus xenocryst assimilation: The genesis of trachyandesites in Sancy volcano, Massif Central, France. Lithos 25, 227-241.

Briot, D., Cantagrel, J.M., Dupuy, C., Harmon, R.S. (1991) Geochemical evolution in crustal magma reservoirs: Trace-element and Sr-Nd-O isotopic variations in two continental intraplate series at Monts Dore, Massif Central, France. Chemical Geology 89, 281-303.

Brunetti, M., Buffoni, L., Maugeri, M., Nanni, T. (2000) Precipitation intensity trends in Northern Italy. International Journal of Climatology 20, 1017-1031.

Brunskill, G.J. (1969) Fayetteville Green Lake, New York. II. Precipitation and sedimentation of calcite in a meromictic lake with laminated sediments. Limnol. Oceanogr. 14, 830-847.

Cantagrel, J.M., Baubron, J.C. (1983) Chronologie des éruptions dans le massif volcanique des Monts-Dore (K-Ar): Implications volcanologiques. Géologie de la France (2) 1, 1-2, 123-142. BRGM Orleans.

DOI: 10.2312/GFZ.b103-07065

Casati, P. (1968) Alcune osservazioni sul bacino lacustre pleistocenico di Pianico (Lombardia). Geologia - Istituto Lombardo (Rend. Sc.) A102, 575-595.

Chardon, M. (1969) Les formationes quaternaires du Bassin de Clusone (Prealpes Lombardes). Recherches mediterraneennes 1, 93-108.

Cioni, R, Sbrana, A, Bertagnini, A, Buonasorte, G, Landi, P, Rossi, U, Salvati, L. (1987) Tephrostratigraphic correlations in the Vulsini, Vico and Sabatini volcanic successions. Periodico di Mineralogia 56, 137-155.

Civetta, L., Innocenti, F., Manetti, P., Peccerillo, A., Poli, G. (1981) Geochemical characteristics of potassic volcanics from Mts. Ernici (Southern Latium, Italy). Contributions to Mineralogy and Petrology 78, 37-47.

Civetta, L., Cornette, Y., Crisci, G., Gillot, P.Y., Orsi, G., Requejo, C.S. (1984) Geology, geochronology and chemical evolution of the island of Pantelleria. Geological Magazine 121, 541-562.

Civetta, L., D'Antonio, M., Orsi, G., Tilton, G.R. (1998) The Geochemistry of volcanic rocks from Pantelleria Islands, Sicily Channel: petrogenesis and characteristics of the mantle source region. Journal of Petrology 39, 1453-1491.

Clayton, R.N., Jones, B.F., Berner, R.A. (1968) Isotope studies of dolomite formation under sedimentary conditions. Geochimica et Cosmochimica Acta 32, 415-432.

Conticelli, S., Francalanci, L., Manetti, P., Cioni, R., Sbrana, A. (1997) Petrology and geochemistry of the ultrapotassic rocks from the Sabatini Volcanic District, central Italy: the role of evolutionary processes in the genesis of variably enriched alkaline magmas. Journal of Volcanology and Geothermal Research 75, 101-136.

Corti, B. (1895) Di alcuni depositi quaternari di Lombardia. Atti della Societa´ Italiana di Scienze Naturali 35, 41-131.

Crisci, G.M., De Rosa, R., Esperanca, S., Mazzuoli, R., Sonnino, M. (1991) Temporal evolution of a three component system: the island of Lipari (Aeolian Arc, southern Italy). Bulletin of Volcanology 53, 207-221.

Curioni, G. (1877) Geologia applicata delle province Lombarde. Milano.

Damon, P.E., Peristykh, A.N. (2000) Radiocarbon calibration and application to geophysics, solar physics, and astrophysics. Radiocarbon 42/1, 137-150.

Dansgaard, W. (1964) Stable isotopes in precipitation. Tellus XVI(4), 436-468.

Dansgaard, W., Johnsen, S.J., Clausen, H.B., Dahl-Jensen, D., Gundestrup, N.S., Hammer, C.U., Hvidberg, C.S., Steffensen, J.P., Sveinbjörnsdottir, A.E., Jouzel, J., Bond, G. (1993) Evidence for general instability of past climate from a 250-kyr ice-core record: Nature 364, 218-220.

de Abreu, L., Abrantes, F., Shackleton, N.J., Tzedakis, P.C., McManus, J.F., Oppo, D.W., Hall, M.A. (2005) Ocean climate variability in the eastern North Atlantic during interglacial marine isotope stage 11: A partial analogue to the Holocene?. Paleoceanography 20, doi:10.1029/2004PA001091.

Dean, W.E., Stuiver, M. (1993) Stable carbon and oxygen isotope studies of the sediments of Elk Lake, Minnesota. In: Bradbury, J.P., Dean, W.E. (Eds.), Elk Lake, Minnesota: Evidence for Rapid Climate Change in the North-Central United States. Geological Society of America Special Paper, Boulder, Colorado, Vol. 276, pp. 163-180.

De Astis, G., La Volpe, L., Peccerillo, A., Civetta, L. (1997) Volcanological and petrological evolution of Vulcano island (Aeolian Arc, southern Tyrrhenian Sea). Journal of Geophysical Research 102, 8021 - 8050.

DOI: 10.2312/GFZ.b103-07065

De Fino, M., La Volpe, L., Piccarreta, G. (1982) Magma evolution at Mount Vulture (Southern Italy). Bulletin of Volcanology 45, 115-126.

de Geer, G. (1912) A geochronology of the last 12000 years. In "11th International Geological Congress". Stockholm, pp. 241-253.

Degens, E.T., Epstein, S. (1964) Oxygen and carbon isotope ratios in co-existing calcites and dolomites from recent and ancient sediments. Geochimica et Cosmochimica Acta 28, 23-44.

De Rita, D., Funiciello, R., Corda, L., Sposato, A., Rossi, U. (1993) Volcanic Units. In Sabatini Volcanic Complex. Di Filippo M (ed.). Consiglio Nazionale delle Ricerche Quaderni de 'La ricerca scientifica' 114/11, 33-79.

Ding, Z.L., Rutter, N.W., Sun, J.M., Yang, S.L., Liu, T.S. (2000) Re-arrangement of atmospheric circulation at about 2.6 Ma over northern China: evidence from grain size records of loess-palaeocol and red clay sequences: Quaternary Science Reviews 19, 547-558.

Drescher-Schneider, R., Papesch, W. (1998) A contribution towards the reconstruction of Eemian vegetation and climate in central Europe: first results of pollen and oxygen-isotope investigations from Mondsee, Austria. Veget Hist Archaeobot 7, 235-240.

Drohmann, D., **Negendank, J.F.W.** (1993) Turbidites in the sediments of Lake Meerfelder Maar (Germany) and the explanation of suspension sediments. In: Palaeolimnology of European Maar Lakes (Eds J.F.W. Negendank and B. Zolitschka), Lect. Notes in Earth Sci. 49, 196-208. Springer-Verlag, Berlin Heidelberg.

Droop, G.T.R. (1987) A general equation for estimating Fe3+ concentrations in ferromagnesian silicates and oxid from microprobe. Mineralogical Magazine 51, 431-437.

Dykoski, C.A., Edwards, R.L., Cheng, H., Yuan, D., Cai, Y., Zhang, M., Lin, Y., Qing, J., An, Z., Revenaugh, J. (2005) A high-resolution, absolute-dated Holocene and deglacial Asian monsoon record from Dongge Cave, China: Earth and Planetary Science Letters, 233, 71-86.

Edwards, K.J., Langdon, P.G., Sugden, H. (in press) Separating climatic and possible human impacts in the early Holocene: biotic response around the time of the 8200 cal. yr BP event: Journal of Quaternary Science, p. doi: 10.1002/jqs.1018.

Emmert-Straubinger, E. (1991) Die Interglazialflora von Pianico (Prov. Bergamo, Italien). In Proceedings of the Pan-European Palaeobotanical Conference. Kovar-Eder J (ed.). Museum of Natural History, Vienna, 15-18.

EPICA community members (2004) Eight glacial cycles from an Antarctic ice core. Nature 429, 623-628.

Epstein, S., Buchsbaum, R., Lowenstam, H.A., Urey, H.C. (1953) Revised carbonate-water isotopic temperature scale. Bulletin of the Geological Society of America 64, 1315-1326.

Epstein, S., Graf, D.L., Degens, E.T. (1964) Oxygen isotope studies on the origin of dolomites. In: Craig, H., Miller, S.L., Wasserburg, G.J. (Eds.), Isotopic and Cosmic Chemistry. North-Holland Pub Co., Amsterdam, pp. 169-180.

Fagan, B. (2000) The Little Ice Age. Basic Books, pp. 246.

Ferrari, L., Conticelli, S., Burlamacchi, L., Manetti, P. (1996) Volcanological evolution of the Monte Amiata, southern Tuscany: new geological and petrochemical data. Acta Vulcanologica 8, 41-56.

Filippi, M.L., Lambert, P., Hunziker, J.C., Kübler, B. (1998) Monitoring detrital input and resuspension effects on sediment trap material using mineralogy and stable isotopes ($\delta^{18}O$ and $\delta^{13}C$): the case of Lake Neuchâtel (Switzerland). Palaeogeography, Palaeoclimatology, Palaeoecology 140, 33-50.

DOI: 10.2312/GFZ.b103-07065

Folk, R.L. (1974) The natural history of cristalline calcium carbonate: effect of magnesium content and salinity. Journal of Sedimentary Petrology 44, 40-53.

Follieri, M., Magri, D., Sadori, L. (1988) 250,000-year pollen record from Valle di Castiglione (Roma). Pollen et Spores XXX, 329-356.

Foster, G. (1996) Wavelets for period analysis of unevenly sampled samples time series. The Astronomical Journal 112, 1709-1729.

Freda, C., Gaeta, M., Palladino, D.M., Trigila, R. (1997) The Villa Senni eruption (Alban Hills, central Italy): the role of H_2O and CO_2 on the magma chamber evolution and on the eruptive scenario. Journal of Volcanology and Geothermal Research 78, 103-120.

Frogley, M.R., Griffiths, H.I., Heaton T.H.E. (2001) Historical biogeography and Late Quaternary environmental change of Lake Pamvotis, Ioannina (north-western Greece): evidence from ostracods. Journal of Biogeography 28, 745-756.

Geyh, M.A., Müller, H. (2005) Numerical 230Th/U dating and a palynological review of the Holsteinian/Hoxnian Interglacial. Quaternary Science Reviews 24, 1861-1872.

Geyh, M.A., Merkt, J., Müller, H. (1971) Sediment- Pollen- und Isotopenanalysen an jahreszeitlich geschichteten Ablagerungen im zentralen Teil des Schleinsees. Archiv für Hydrobiologie 69, 366-399.

Giannetti, B. (2001) Origin of the calderas and evolution of Roccamonfina volcano (Roman Region, Italy). Journal of Volcanology and Geothermal Research 106, 301-319.

Giannetti, B., Luhr, J.F. (1983) The White Trachytic Tuff of Roccamonfina Volcano (Roman Region, Italy). Contributions to Mineralogy and Petrology 84, 235-252.

Gleissberg, W. (1944) A table of secular variations of the solar cycle. Terrestrial Magnetism and Atmospheric Electricity 49/4, 243-244.

Goslar, T. (1998) Late-Glacial sediments of Lake Gosciaz - Chronological Background. In: Ralska-Jasiewiczowa, M., Goslar, T., Madeyska, T., and Starkel, L., eds., Lake Gosciaz, Central Poland A monographic study, Volume Part 1: Krakow, W.Szafer Institute of Botany Polish Academy of Sciences, 119-124.

Goslar, T., Arnold, M., Tisnerat-Laborde, N., Hatte, C., Paterne, M., Ralska-Jasiewiczowa, M. (2000) Radiocarbon calibration by means of varves versus 14C ages of terrestrial macrofossils from Lake Gosciaz and Lake Perespilno, Poland. Radiocarbon 42/3, 335-348.

Govi, M., Sorzana, P.F. (1980) Landslide susceptibility as a function of critical rainfall amount in Piedmont Basin (North-western Italy). Studia Geomorphologica Carpatho-Balcanica XIV, 43-61.

Grootes, P.M., Stuiver, M., White, J.W.C., Johnsen, S.J., Jouzel, J. (1993) Comparison of oxygen isotope records from the GISP 2 and GRIP Greenland ice cores. Nature 366, 552-554.

Gruber, N., Wehrli, B., Wüest, A. (2000) The role of biogeochemical cycling for the formation and preservation of varved sediments in Soppensee (Switzerland). Journal of Paleolimnology 24/3, 277-291.

Gupta, A.K., Fyfe, W.S. (1975) Leucite survival: the alteration to analcime. Canadian Mineralogist 13, 361-363.

Hilfinger IV, M.F., Mullins, H.T., Burnett, A., Kirby, M.E. (2001) A 2500 year sediment record from Fayetteville Green Lake, New York: evidence for anthropogenic impacts and historic isotope shift. Journal of Paleolimnology 26, 293-305.

H.M.S.O. (Her Majesty's Stationery Office) (1962) Weather in the Mediterranean. Her Majesty's Stationery Office, London.

Hsü, K.J., Kelts, K.R. (1985) Swiss lakes as a geological laboratory. Naturwissenschaften 72, 315-321.

DOI: 10.2312/GFZ.b103-07065

Hunt, J.B., Hill, P.G. (1996) An inter-laboratory comparison of the electron probe microanalysis of glass geochemistry. Quaternary International 34-36, 229-241.

IAEA/WMO (2004) Global Network of Isotopes in Precipitation. The GNIP Database. Accessible at: http://isohis.iaea.org

IPCC (2001) Climate Change 2001: The Scientific basis [Houghton, J.T., Ding, Y., Griss, D.J., Noguer, M., van der Linden, P.J., Dai, X., Maskell, K., Johnson, C.A. (eds.)]. Cambridge University Press, Cambridge, U.K.

Kashiwaya, K., Ochiai, S., Sakai, H., Kawai, T. (2001) Orbit-related long-term climate cycles revealed in a 12-Myr continental record from Lake Baikal. Nature 410, 71-74.

Keim, L., Spötl, C., Brandner, R. (2006) The aftermath of the Carnian carbonate platform demise: a basinal perspective (Dolomites, Southern Alps). Sedimentology 53, 361-386.

Keller, J. (1980). The island of Salina. Rendiconti Società Italiana di Mineralogia e Petrologia 36, 489-524.

Kelts, K.R., Hsü, K.J. (1978) Freshwater carbonate sedimentation. In: Lakes - Chemistry, Geology, Physics (Ed. A. Lerman), pp. 295-323. Springer-Verlag, New York.

Kelts, K.R., **Hsü, K.J.** (1980) Resedimented facies of 1875 Horgen slumps in Lake Zurich and a process model of longitudinal transport of turbidity currents. Eclogae Geol. Helv. 73, 271-281.

Khursevich, G.K., Karabanov, E.B., Prokopenko, A.A., Williams, D.F., Kuzmin, M.I., Fedenya, S.A., Gvozdkov, A.A. (2001) Insolation regime in Siberia as a major factor controlling diatom production in Lake Baikal during the past 800,000 years. Quaternary International 80-81, 47-58.

Kienel, U., Schwab, M.J., Schettler, G. (2005) Distinguishing climatic from direct anthropogenic influences during the past 400 years in varved sediments from Lake Holzmaar (Eifel, Germany). Journal of Paleolimnology 33, 327-347.

Kirby, M.E., Patterson, W.P., Mullins, H.T., Burnett, A.W. (2002) Post-Younger Dryas climate interval linked to circumpolar vortex variability: isotopic evidence from Fayetteville Green Lake, New York. Climate Dynamics 19, 321-330.

Kitagawa, H., van der Plicht, J. (1998) Atmospheric radiocarbon calibration to 45,000 yr BP: Late Glacial fluctuations and cosmogenic isotope production. Science 279, 1187-1190.

Kolstrup, E., Buchardt, B. (1982) A pollen analytical investigation supported by an ^{18}O-record of a Late glacial lake deposit at Graenge (Denmark). Review of Palaeobotany and Palynology 36, 205-230.

Koschel, R.H. (1997) Structure and function of pelagic calcite precipitation in lake ecosystems. Verhandl. Internat. Verein. Limnologie 26, 343-349.

Koschel, R.H., Benndorf, J., Proft, G., Recknagel, F. (1983) Calcite precipitation as a natural control mechanism of eutrophication. Archiv für Hydrobiologie 98, 380-408.

Kraml, M. (1997) Laser-$^{40}Ar/^{39}Ar$-Datierungen an distalen marinen Tephren des jung-quartären mediterranen Vulkanismus (Ionisches Meer, METEOR-Fahrt 25/4). PhD thesis, Albert-Ludwigs-Universität: Freiburg.

Kuc, T., Różański, K., Duliński, M. (1998) Isotopic indicators of the Late-Glacial/Holocene transition recorded in the sediments of Lake Gościąż. In: Ralska-Jasiewiczowa, M., Goslar, T., Madeyska, T., Starkel, L. (Eds.), Lake Gościąż, Central Poland A monographic study. W. Szafer Institute of Botany and Polish Academy of Sciences, Krakow, Part 1, pp. 158-162.

Kuenen, P.H. (1950) Turbidity currents of high-density. In: Reports of the 18th International Congress (1948), pt. 8, The Geology of Sea and Ocean Floors, pp. 44-52, London.

DOI: 10.2312/GFZ.b103-07065

Kuenen, P.H. (1951) Properties of turbidity currents of high density. In: Turbidity Currents and the Transportation of Coarse Sediments to Deep Water, a Symposium (Ed J.L. Hough), 2, 14-33. Society of Economic Palaeontologists and Mineralogists, Special Publication.

Lambert, A., Hsü, K.J. (1979) Non-annual cycles of varve-like sedimentation in Walensee, Switzerland. Sedimentology 26, 453-461.

Lambert, A.M., Kelts, K.R., Marshall, N.F. (1976) Measurements of density underflows from Walensee, Switzerland. Sedimentology 23, 87-105.

Lavina, P. (1985) Le volcan du Sancy et le "Massif adventif". Etudes volcanologiques et structurales. Thèse de IIIème cycle, Clermont Fd.

Lawson, I., Frogley, M.R., Bryant, C., Preece, R., Tzedakis, P. (2004) The Lateglacial and Holocene environmental history of the Ioannina basin, north-west Greece. Quaternary Science Reviews 23, 1599-1625.

Le Bas, M.J., Le Maitre, R.W., Streckeisen, A., Zanettin, B. (1986) A chemical classification of volcanic rocks based on the Total Alkali-Silica diagram. Journal of Petrology 27, 745-750.

Leng, M.J., Marshall, J.D. (2004) Palaeoclimate interpretation of stable isotopes data from lake sediment archives. Quaternary Science Reviews 23, 811-831.

Leng, M.J., Roberts, N., Reed, J.M., Sloane, H.J. (1999) Late Quaternary palaeohydrology of the Konya Basin, Turkey, based on isotope studies of modern hydrology and lacustrine carbonates. Journal of Paleolimnology 22, 187-204.

Le Roy Ladurie, E. (1971) Times of Feast, Times of Famine: a history of climate since the year 1000. Allen & Unwin Ltd, London, pp. 428.

Linke, G. (1993) Das Holstein-Projekt des Geologischen Landesamtes Hamburg - Hintergrund und Ablauf. Geologisches Jahrbuch A 138, 3-7.

Lisiecki, L.E., Raymo, M.E. (2005) A Pliocene-Plesitocene stack of 57 globally distributed benthic $\delta^{18}O$ records. Paleoceanography 20, doi: 10.1029/2004PA001071.

Livingstone, D.M., Hajdas, I. (2001) Climatically relevant periodicities in the thicknesses of biogenic carbonate varves in Soppensee, Switzerland (9740-6870 calendar yr BP). Journal of Paleolimnology 25, 17-24.

Lona, F. (1952) Revisione della flora fossile insubrica attraverso i resti microscopici. Nuovo Giornale Botanico Italiano LIX, 506-509.

Lona, F., Venzo, S. (1956) La station interglaciaire de Pianico-Sellere. Sediments lacustres a microvarves avec phyllites et pollens, de Pianico en province de Bergamo. In: Guide de la Onzieme Excursion Phytogeographique Internationale Alpes Orientales, pp. 39-46. Istituto Botanico, Firenze.

Longinelli, A., Selmo, E. (2003) Isotopic composition of precipitation in Italy: a first overall map. Journal of Hydrology 270, 75-88.

Lotter, A.F. (1989) Evidence of annual layering in Holocene sediments of Soppensee, Switzerland. Aquatic Science 51, 19-30.

Lotter, A.F., Birks, H.J.B. (1997) The separation of the influence of nutrients and climate on the varve time-series of Baldeggersee, Switzerland. Aquatic Science 59, 362-375.

Lotter, A.F., Lemcke, G. (1999) Methods for preparing and counting biochemical varves. Boreas 28, 243-252.

Loutre, M.F. (2003) Clues from MIS 11 to predict the future climate - a modelling point of view. Earth and Planetary Science Letters 212, 213-224.

Loutre, M.F., Berger, A. (2003) Marine Isotope Stage 11 as an analogue for the present interglacial: Global and Planetary Change 36, 209-217.

DOI: 10.2312/GFZ.b103-07065

Ludlam, S.D. (1969) Fayetteville Green Lake, New York, U.S.A. VII. The laminated sediments. Limnol. Oceanogr. 14/6, 848-857.

Ludlam, S.D. (1974) Fayetteville Green Lake, New York; 6, The role of turbidity currents in lake sedimentation. Limnol. Oceanogr. 19**,** 656-664.

Lücke, A., Brauer, A. (2004) Biogeochemical and micro-facial fingerprints of ecosystem response to rapid Late Glacial climatic changes in varved sediments of Meerfelder Maar (Germany). Palaeogeography, Palaeoclimatology, Palaeoecology 211/1-2, 139-155.

Luhr, J.F., Giannetti, B. (1987) The Brown Leucitic Tuff of Roccamonfina volcano, Roman Region, Italy. Contributions to Mineralogy and Petrology 95, 420-436.

Maffei, L. (1924) Contributo allo studio della flora fossile del deposito lacustre di Pianico: Atti Istituto Botanico Universitá di Pavia, v. Serie III, p. 47-69.

Mangili, C., Brauer, A., Moscariello, A., Naumann, R. (2005) Microfacies of detrital event layers deposited in Quaternary varved lake sediments of the Piànico-Sèllere Basin (northern Italy). Sedimentology 52, 927-943.

Mangili, C., Brauer, A., Plessen, B., Moscariello, A. (submitted) Centennial-scale oscillations in stable oxygen and carbon isotopes of endogenic calcite from the 15 500 varve year record of the Piànico interglacial (400 ka BP). Submitted to Quaternary Science Reviews.

Mangili, C., Brauer, A., Plessen, B., Moscariello, A. (unpublished data) Effects of detrital carbonate on the interpretation of stable oxygen and carbon isotopes from the interglacial lake record of Piànico. To be submitted to Quaternary Science Reviews.

Martinetto, E., Ravazzi, C. (2002) The Late Pliocene and Early-Middle Pleistocene floral history of Northern Italy as reconstructed by pollen and macroflora. In 6th European Paleobotany-Palynology Conference. Athens, Greece, pp. 228-229.

McKenzie, J.A. (1985) Carbon isotopes and productivity in the lacustrine and marine environment. In: Stumm, W. (Editor), Chemical processes in lakes. John Wiley & sons, New York, pp. 99-118.

McKenzie, J.A., Hollander, D.J. (1993) Oxygen-Isotope Record in Recent Carbonate Sediments from Lake Greifen, Switzerland (1750-1986): application of continental isotopic indicator for evaluation of changes in climate and atmospheric circulation patterns. In: Swart, P.K., Lohmann, K.C., McKenzie J., Savin, S. (Eds.), Climate Change in Isotopic Records. American Geophysical Union, Geophysical Monograph, vol. 78, pp. 101-111.

McManus, J.F., Oppo, D.W., Cullen, J.L. (1999) A 0.5-Millon-Year Record of Millennial-Scale Climate Variability in the North Atlantic. Science 283, 971-975.

McManus, J.F., Oppo, D.W., Cullen, J.L., Healey, S. (2003) Marine Isotope Stage 11 (MIS 11): Analog for Holocene and Future Climate?, Unique and Exceptionally Long Interglacial Marine Isotope Stage 11: Window into Earth Warm Future Climate, Volume 137: Geophysical Monograph, American Geophysical Union 69-85.

Müller, H. (1974) Pollenanalytische Untersuchungen und Jahresschichtenzaehlung an der eem-zeitlichen Kieselgur von Bispingen/ Luhe: Geologisches Jahrbuch A 21, 149-169.

Menzies, J., Taylor, J. (2003) Seismically induced soft-sediment microstructures (seismites) from Meikleour, western Strathmore, Scotland. Boreas 32, 314-327.

Merkt, J. (1971) Zuverlässige Auszählungen von Jahresschichten in Seesedimenten mit Hilfe von Groß-Dünnschliffen. Arch. Hydrobiol. 69, 145-154.

Minder, L. (1922) Über biogene Entkalkung im Zürichsee. Verh. Int. Verein Limnol. 1, 20-23.

Miyoshi, N., Fujiki, T., Morita, Y. (1999) Palynology of a 250-m core from Lake Biwa: a 430,000-year record of glacial-interglacial vegetation change in Japan: Review of Palaeobotany and Palynology 104, 267-283.

DOI: 10.2312/GFZ.b103-07065

Morimoto, N., Fabries, J., Ferguson, A.K., Ginzburg, I.V., Ross, M., Seifert, F.A., Zussman, J., Aoki, K., Gottardi, G. (1988) Nomenclature of pyroxenes. Mineralogical Magazine 52, 535-550.

Mörner, N.-A. (1996) Liquefaction and varve deformation as evidence of paleoseismic events and tsunamis. The autumn 10,430 BP case in Sweden. Quaternary Science Reviews 15/8-9, 939-948.

Moscariello, A., Deganutti, A.M. (2000) Sedimentary and hydrologic processes of a debris-flow dominated alluvial fan (Moscardo Fan, Italy). In: Debris-flow hazards mitigation: mechanics, prediction and assessment (Eds G.F. Wieczorek and N.D. Naeser), pp. 301-309. Balkema, Rotterdam.

Moscariello, A., Schneider, A.M., Filippi, M.L. (1998) Late glacial and early Holocene palaeoenvironmental changes in Geneva Bay (Lake Geneva, Switzerland). Palaeogeogr. Palaeoclimatol. Palaeoecol. 140, 51-73.

Moscariello, A., Ravazzi, C., Brauer, A., Mangili, C., Chiesa, S., Rossi, S., Beaulieu, d. J.-L. and **Reille, M.** (2000) A long lacustrine record from the Piànico-Sèllere Basin (Middle-Late Pleistocene, Nothern Italy). Quatern. Int. 73/74, 47-68.

Müller, H. (1965) Eine pollenanalytische Neubearbeitung des Interglazial-Profils von Bilshausen (Unter-Eichsfeld). Geologisches Jahrbuch 83, 327-352.

Müller, H. (1974) Pollenanalytische Untersuchungen und Jahresschichtenzählungen an der eemzeitlichen Kieselgur von Bispingen/Luhe. Geologisches Jahrbuch A21, 149-169.

Nappi, G., Antonelli, F., Coltorti, M., Milani, L., Renzulli, A., Siena, F. (1998) Volcanological and petrological evolution of the Eastern Vulsini District, Central Italy. Journal of Volcanology and Geothermal Research 87, 211-232.

Nielsen, C.H., Sigurdsson, H. (1981) Quantitative methods for electron microprobe analysis of sodium in natural and synthetic glasses. American Mineralogist 66, 547-552.

Nipkow, F. (1920) Vorläufige Mitteilungen über Untersuchungen des Schlammabsatzes in Zürichsee. Zeitschrift für Hydrologie 1, 100-122.

Nitychoruk, J. (2000) Climate reconstruction from stable-isotope composition of the Mazovian Interglacial (Holsteinian) lake sediments in eastern Poland. Acta Geologica Polonica 50(2), 247-294.

Nitychoruk, J., Binka, K., Hoefs, J., Ruppert, H., Schneider, J. (2005) Climate reconstruction for the Holsteinian Interglacial in eastern Poland and its comparison with isotopic data from Marine Isotope Stage 11. Quaternary Science Reviews 24, 631-644.

North Greenland Ice Core Project members (2004) High-resolution record of Northern Hemisphere climate extending into the last interglacial period. Nature 431, 147-151.

Ohlendorf, C., Sturm, M. (2001) Precipitation and Dissolution of Calcite in a Swiss High Alpine Lake. Arctic Antarctic and Alpine Research 33/4, 410-417.

Oppo, D.W., McManus, J.F., Cullen, J.L. (1998) Abrupt climates events 500,000 to 340,000 years ago: evidence from Subpolar North Atlantic sediments. Science 279, 1335-1338.

Orombelli, G. (1974) Alcune date C^{14} per il Quaternario lombardo. Studi Trentini di Scienze Naturali 51, 125-127.

Palladino, D.M., Agosta, E. (1997) Pumice fall deposits of the western Vulsini Volcanoes (central Italy). Journal of Volcanology and Geothermal Research 78, 77-102.

Pastre, J.F., Cantagrel, J.M. (2001) Téphrostratigraphie du Mont Dore. Quaternaire 12, 249-267.

Paterne, M., Guichard, F., Labeyrie, J. (1988) Explosive activity of the South Italian volcanoes during the past 80,000 years as determined by marine tephrochronology. Journal of Volcanology and Geothermal Research 34, 153-172.

DOI: 10.2312/GFZ.b103-07065

Penck, A., Brückner, A. (1909) Die Alpen im Eiszeitalter. 3. Bd. Her. Tauchnitz, Leipzig. 481 pp.

Perrotta, A., Scarpati, C., Giacomelli, L., Capozzi, A.R. (1996) Proximal depositional facies from a caldera-forming eruption: the Parata Grande Tuff at Ventotene Island (Italy). Journal of Volcanology and Geothermal Research 71, 207-228.

Petit, J.-R., Jouzel, J., Raynaud, D., Barkov, N.I., Barnola, J.-M., Basile, I., Bender, M., Chappellaz, J., Davis, M., Delaygue, G., Delmotte, M., Kotlyakov, V.M., Legrand, M., Lipenkov, V.Y., Lorius, C., Pepin, L., Ritz, C., Saltzman, E., Stievenard, M. (1999) Climate and atmospheric history of the past 420,000 years from the Vostok ice core, Antarctica. Nature 399, 429-436.

Pfister, C. (1994) Switzerland: The time of icy winters and chilly springs.In: Frenzel, B., Pfister, C., and Gläser, B., eds., Climatic trends and anomalies in Europe 1675-1715, Volume 13, Palaeoclimate Research. Stuttgart, Gustav Fischer, p. 205-224.

Poli, M.S., Thunell, R.C., Rio, D. (2000) Millennial-scale changes in North Atlantic Deep Water circulation during marine isotope stages 11 and 12: Linkage to Antarctic climate. Geology 28, 807-810.

Prasad, S., Brauer, A., Rein, B., Negendank, J.F.W. (2006) Rapid climate change during the early Holocene in western Europe and Greenland. The Holocene 16, 153-158.

Phillips, E.R., Auton, C.A. (2000) Micromorphological evidence for polyphase deformation of glaciolacustrine sediments from Strathspey, Scotland. In: *Deformation of Glacial Materials* (Eds A.J. Maltman, B. Hubbard and M.J. Hambrey), Geological Society London, Special Publication 176, pp. 279-292.

Picozzi, A. (1859) Sulla scoperta d'alcune ossa fossili nella marna bianca farinacea di Piànico presso Sovere. Atti Società Geologica residente in Milano 1, 78-80.

Pinti, D.L., Quidelleur, X., Chiesa, S., Ravazzi, C., Gillot, P.Y. (2001) K-Ar dating of an early Middle Pleistocene distal tephra in the interglacial varved succession of Pianico-Sellere. Earth Planet. Sci. Lett. 5819, 1-7.

Pinti, D.L., Quidelleur, X., Lahitte, P., Aznar, C., Chiesa, S., Gillot, P.Y. (2003) The Piànico tephra: an early Middle Pleistocene record of intraplate volcanism in the Mediterranean. Terra Nova 15, 176-186.

Pouclet, A., Horvath, E., Gabris, G., Juvigné, E. (1999) The Bag Tephra, a widespread tephrochronological marker in Middle Europe: chemical and mineralogical investigations. Bulletin of Volcanology 60, 265-272.

Prasad, S., Brauer, A., Rein, B., Negendank, J.F.W. (2006) Rapid climate change during the early Holocene in western Europe and Greenland. The Holocene 16, 153-158.

Provincia di Bergamo (2000) Carta Geologica della Provincia di Bergamo. Note illustrative. Provincia di Bergamo, Bergamo.

Rapp, A. (1985) Extreme rainfall and rapid snowmelt causes of mass movements in high latitude mountains. In: Field and theory Lectures in Geocryology (Eds M. Church and O. Slaymaker), pp. 36-56. University of British Columbia Press, Vancouver.

Rapp, A., Nyberg, R. (1981) Alpine debris flows in northern Scandinavia. Geogr. Ann. 63 A, 183-196.

Ravazzi, C., Pini, R., Breda, M., Martinetto, E., Muttoni, G., Chiesa, S., Confortini, F., Egli, R. (2005) The lacustrine deposits of Fornaci di Ranica (late Early Pleistocene, Italian Pre-Alps): stratigraphy, palaeoenvironment and geological evolution. Quaternary International 131, 35-58.

DOI: 10.2312/GFZ.b103-07065

Raynal, J.P., Lefèvre, D., Vernet, G., Pilleyre, T., Sanzelle, S., Fain, J., Miallier, D., Montret, M. (1998) Sedimentary dynamics and tecto-volcanism in the Venosa Basin (Basilicata, Italia). Quaternary International 47/48, 97-105.

Ralska-Jasiewiczowa, M., Goslar, T., Madeyska, T., Starkel, L. (1998) Lake Gosciaz, Central Poland A monographic study. W. Szafer Institute of Botany and Polish Academy of Sciences, Krakow, Part 1.

Rasmussen, S.O., Andersen, K.K., Svensson, A.M., Steffensen, J.P., Vinther, B.M., Clausen, H.B., Siggaard-Andersen, M.-L., Johnsen, S.J., Larsen, L.B., Dahl-Jensen, D., Bigler, M., Röthlisberger, R., Fischer, H., Goto-Azuma, K., Hansson, M.E., Ruth, U. (2006) A new Greenland ice core chronology for the last glacial termination: Journal of Geophysical Research 111, doi:10.1029/2005JD006079.

Reille, M., de Beaulieu, J.L., Svobodova, H., Andrieu-Ponel, V., Goeury, C. (2000) Pollen analytical biostratigraphy of the five last climatic cycles from a long continental sequence from the Velay region (Massif Central, France). Journal of Quaternary Sciences 15, 665-685.

Richards, D.A., Smart, P.L. (1991) Potassium-argon and argon-argon dating. In Quaternary dating methods; a user's guide. Smart PL, Frances PD, (eds). Quaternary Research Association, Technical Guide 4, 37-44.

Ringberg, B., Erlström, M. (1999) Micromorphology and petrography of Late Weicheslian glaciolacustrine varves in southeastern Sweden. Catena 35, 147-177.

Ringrose, P.S. (1989) Palaeoseismic (?) liquefaction event in late Quaternary lake sediment at Glen Roy, Scotland. Terra Nova 1/1, 57-62.

Roberts, N., Reed, J.M., Leng, M.J., Kuzucuoglu, C., Fontugne, M., Bertaux, J., Woldring, H., Bottema, S., Black, S., Hunt, E. Karabiyikoglu, M. (2001) The tempo of Holocene climatic change in the eastern Mediterranean region: new high-resolution crater-lake sediment data from central Turkey. The Holocene 11(6), 721-736.

Rodriguez-Pascua, M.A., Calvo, J.P., De Vicente, G., Gomez-Gras, D. (2000) Soft-sediment deformation structures interpreted as seismites in lacustrine sediments of the Prebetic Zone, SE Spain, and their potential use as indicators of earthquake magnitudes during the Late Miocene. Sed. Geol. 135, 117-135.

Roger, S. (2000) Datations 40Ar/39Ar de niveaux volcaniques intercales dans des sequences sedimentaires lacustres et marines, Pleistocenes a Messiniennes: Implications Paléoenvironnementales. PhD thesis, Universite de Droit: Marseille.

Rossi, S. (2003) Etude pollinique de la sequence lacustre Pleistocene de Piànico-Sèllere (Italie), Université de Droit, d´Economie et des Sciences d´Aix Marseille III, Marseille, 293 pp. Unpublished Ph.D. thesis.

Różański, K., Araguäs-Araguäs, L., Gonfiantini, R. (1992) Relation Between Long-Term Trends of Oxygen-18 Isotope Composition of Precipitation and Climate. Science 258, 981-985.

Różański, K., Araguäs-Araguäs, L., Gonfiantini, R. (1993) Isotopic patterns in modern global precipitation. In: Swart, P.K., Lohmann, K.C., McKenzie, J., and Savin, S., (Editors), Climate Change in Continental Isotopic Records. Geophysical Monograph, American Geophysical Union, v. 78.

Różański, K., Kuc, T., Duliński, M., Wachniew, P. (1998) Oxygen and carbon isotope composition of authigenic carbonates in the Holocene part of the lake Gościąż sediments. In: Ralska-Jasiewiczowa, M., Goslar, T., Madeyska, T., Starkel, L. (Editors), Lake Gościąż, Central Poland A monographic study. W. Szafer Institute of Botany and Polish Academy of Sciences, Krakow, Part 1, 229-232.

DOI: 10.2312/GFZ.b103-07065

Ruddiman, W.F. (2003) The anthropogenic greenhouse era began thousands of years ago. Climatic Change 61/3, 261-293.

Ruddiman, W.F. (2005a) Cold climate during the closest Stage 11 analog to recent Millennia. Quaternary Science Reviews 24, 1111-1121.

Ruddiman, W.F. (2005b) Plows, Plagues, and Petroleum. Princeton University Press, Princeton, pp. 202.

Schwander, J., Eicher, U., Ammann, B. (2000) Oxygen isotopes of lake marl at Gerzensee and Leysin (Switzerland), covering the Younger Dryas and two minor oscillations, and their correlation to the GRIP ice core. Palaeogeography, Palaeoclimatology, Palaeoecology 159, 203-214.

Shackleton, N.J., Berger, A., Peltier, W.R. (1990) An alternative astronomical calibration of the lower Pleistocene timescale based on ODP Site 677. Transactions of the Royal Society of Edinburgh. Earth Sciences 81, 251-261.

Shiki, T., Kumon, F., Inouchi, Y., Kontani, Y., Sakamoto, T., Tateishi, M., Matsubara, H., **Fukuyama, K.** (2000) Sedimentary features of the seismo-turbidites, Lake Biwa, Japan. Sed. Geol. 135, 37-50.

Siegenthaler, U., Eicher, U. (1986) Stable oxygen and carbon isotope analyses. In: Berglund, B.E. (Editor), Handbook of Holocene Palaeoecology and Palaeohydrology. John Wiley & Sons Ltd., pp. 407-422.

Siegenthaler, U., Eicher, U., Oeschger, H., Dansgaard, W. (1984) Lake sediments as continental $d^{18}O$ records from the glacial/post-glacial transition. Annals of Glaciology 5, 149-152.

Sordelli, F. (1873) Descrizione di alcuni avanzi vegetali delle argille plioceniche lombarde, coll' aggiunta di un Elenco delle piante fossili finora conosciute in Lombardia. Atti della Società Italiana di Scienze Naturali 16, fasc. II.

Sordelli, F. (1896) Flora Fossilis Insubrica. Studi sulla vegetazione di Lombardia durante i tempi geologici. Tip. Cogliati: Milano. 298 pp.

Stuiver, M., Grootes, P.M., Braziunas, T.F. (1995) The GISP2 $d^{18}O$ Climate Record of the Past 16,500 Years and the Role of the Sun, Ocean, and Volcanoes. Quaternary Research 44, 341-354.

Spötl, C., Vennemann, T.W. (2003) Continuous-flow isotope ratio mass spectrometric analysis of carbonate minerals. Rapid Commun. Mass Spectrom. 17, 1004-1006.

Stoppani, A. (1857) Studi geologici e paleontologici sulla Lombardia. Milano, Tip. Turati.

Stoppani, A. (1873) Corso di geologia, vol. II. Bernardoni, Milano.

Stoppani, A. (1880) L' Era Neozoica (Geologia d'Italia, P. II). Milano. 367 pp.

Stuiver, M., Braziunas, T.F. (1993) Sun, ocean, climate and atmospheric 14CO2: An evaluation of causal and spectral relationships. The Holocene 3(4), 289-305.

Sturm, M., **Matter, A.** (1978) Turbidites and varves in Lake Brienz (Switzerland): deposition of clastic detritus by density currents. Spec. Publs int. Ass. Sediment. 2, 147-168.

Talbot, M.R. (1990) A review of the palaeohydrological interpretation of carbon and oxygen isotopic ratios in primary lacustrine carbonates. Chemical Geology (Isotope Geoscience Section) 80, 261-279.

Teranes, J.L., McKenzie, J.A., Bernasconi, S.M., Lotter, A.F., Sturm, M. (1999) A study of oxygen isotopic fractionation during bio-induced calcite precipitation in eutrophic Baldeggersee, Switzerland. Geochimica et Cosmochimica Acta 63(13/14), 1981-1989.

Teranes, J.L., McKenzie, J.A. (2001) Lacustrine oxygen isotope record of 20^{th}-century climate change in central Europe: evaluation of climatic controls on oxygen isotopes in precipitation. Journal of Paleolimnology 26, 131-146.

DOI: 10.2312/GFZ.b103-07065

Thompson, J.B., Schultze-Lam, S., Beveridge, T.J., Des Marais, D.J. (1997) Whiting events: Biogenic origin due to the photosynthetic activity of cyanobacterial picoplankton. Limnol. Oceanogr. 42/1, 133-141.

Tinner, W., Lotter, A.F. (2001) Central European vegetation response to abrupt climate change at 8.2 ka. Geology 29, 551-554.

Torrence, C., Compo, G.P. (1998) A practical guide to wavelet analysis. Bulletin of the American Meteorological Society 79/1, 61-78.

Turner, C. (1998) Volcanic maars, long Quaternary sequences and the work of the INQUA Subcommission on European Quaternary Stratigraphy. Quaternary International 47/48, 41-49.

Tzedakis, P.C., Andrieu, V., de Beaulieu, J.L., Crowhurst, S., Follieri, M., Hooghiemstra, H., Magri, D., Reille, M., Sadori, L., Shackleton, N.J., Wijmstra, T.A. (1997) Comparison of terrestrial and marine records of changing climate of the last 500,000 years. Earth and Planetary Science Letters 150, 171-176.

van der Meer, J.J.M., Warren, W.P. (1997) Sedimentology of Late Glacial clays in lacustrine basins, Central Ireland. Quatern. Sci. Rev. 16, 779-791.

van der Meer, J.J.M., Menzies, J., Rose, J. (2003) Subglacial till: the deforming glacier bed. Quatern. Sci. Rev. 22, 1659-1685.

Venzo, S. (1955) Le attuali conoscenze sul Pleistocene lombardo con particolare riguardo al Bergamasco. Atti della Societa´ Italiana di Scienze Naturali 94, 155-200.

Vernet, G., Raynal, J.P., Fain, J., Maillier, D., Montret, M., Pilleyre, T., Sanzelle, S. (1998) Tephrostratigraphy of the last 160 ka in western Limagne (France). Quaternary International 47/48, 139-146.

Veski, S., Seppä, H., Ojala, A.E.K. (2004) Cold event at 8200 yr B.P. recorded in annually laminated lake sediments in eastern Europe. Geology 32, 681-684, doi: 10.1130/G20683.1.

von Grafenstein, U., Erlenkeuser, H., Kleinmann, A., Müller, J., Trimborn, P. (1994) High-frequency climatic oscillations during the last deglaciation as revealed by oxygen-isotope records of benthic organisms (Ammersee, southern Germany). Journal of Paleolimnology 11, 349-357.

von Grafenstein, U., Erlenkeuser, H., Müller, J., Jouzel, J., Johnsen, S. (1998) The cold event 8200 years ago documented in oxygen isotope records of precipitation in Europe and Greenland. Climate Dynamics 14, 73-81.

von Grafenstein, U., Erlenkeuser, H., Brauer, A., Jouzel, J., Johnsen, S.J. (1999) A Mid-European decadal isotope-climate record from 15,500 to 5000 years B.P. Science 284, 1654-1657.

von Grafenstein, U., Eicher, U., Erlenkeuser, H., Ruch, P., Schwander, J., Ammann, B. (2000) Isotope signature of the Younger Dryas and two minor oscillations at Gerzensee (Switzerland): palaeoclimatic and palaeolimnologic interpretation based on bulk and biogenic carbonates. Palaeogeography, Palaeoclimatology, Palaeoecology 159, 215-229.

Vos, H., Sanchez, A., Zolitschka, B., Brauer, A., Negendank, J.F.W. (1997) Solar activity variations recorded in varved sediments from the crater lake of Holzmaar - a maar lake in the Westeifel Volcanic Field, Germany. Surveys in Geophysics 18/2-3, 163-182.

Walters jr., L.J., Claypool, G.E., Choquette, P.W. (1972) Reaction rates and dO^{18} variation for the carbonate-phosphoric acid preparation method. Geochimica et Cosmochimica Acta 36, 129-140.

Wastegård, S., Rasmussen, T.L. (2001) New tephra horizons from Oxygen Isotope Stage 5 in the North Atlantic: correlation potential for terrestrial, marine and ice-core archives. Quaternary Science Reviews 20, 1587-1593.

DOI: 10.2312/GFZ.b103-07065

Wastegård, S., Björck, S., Greve, C., Rasmussen, T.L. (2005) A tephra-based correlation between the Faroe Islands and the Norwegian Sea raises questions about chronological relationships during the last interglacial. Terra Nova 17, 7-12.

Wijmstra, T.A., Smit, A. (1976) Palynology of the Middle part (30-78 metres) of the 120 m deep section in Northern Greece (Macedonia). Acta Bot. Neerl. 25, 297-312.

Windheuser, H., Brunnacker, K. (1978) Zeitstellung und Tephrostratigraphie des quartären Osteifel-Vulkanismus. Geol. Jb. Hessen 106, 261-271.

Witt, A., Schumann, A.Y. (2005) Holocene climate variability on millennial scales recorded in Greenland ice cores. Nonlinear Processes in Geophysics 11, 345-352.

Wulf, S., Kraml, M., Brauer, A., Keller, J., Negendank, J.F.W. (2004) Tephrochronology of the 100 ka lacustrine sediment record of Lago Grande di Monticchio (southern Italy). Quaternary International 122, 7-30.

Zagwijn, W.H. (1996) The Cromerian Complex Stage of the Netherlands and correlation with other areas in Europe. In: The early middle Pleistocene in Europe. Turner C (ed.). Balkema, Rotterdam; 145-172.

Zolitschka, B., Haverkamp, B., Negendank, J.F.W. (1992) Younger Dryas oscillation - varve dated microstratigraphic, palynological and palaeomagnetic records from Lake Holzmaar,

Zolitschka, B., Brauer, A., Negendank, J.F.W., Stockhausen, H., Lang, A. (2000) Annually dated late Weichselian continental paleoclimate record from the Eifel, Germany. Geolog 28, 783-786.

DOI: 10.2312/GFZ.b103-07065

Appendix 1

DOI: 10.2312/GFZ.b103-07065

Appendix 1

Microfacies, microstratigraphical classification and DLI values of all detrital layers (DL) in both the Wall and Main Section. Positions where varve years have been added to the WS chronology according to the correlation with the MS are marked with an asterisk (*). Codes for detrital layer types: SG = summer graded, GE = graded erosive, SS = summer silt, S = spring, MS = matrix supported, WS = winter silt.

			Wall Section		Main Section		
DL codes	**Varve nr.**	**nr. of varves between this DL and the one**	**DL thickness (mm)**	**DL type**	**DL thickness (mm)**	**DL type**	**DLI**
DL A137b	894	3	1.05	S G	0.12	S S	1.09
DL A137a	894	3	0.90	S G	0.15	S S	0.79
DL A136	890	2	20.15	G E	11.35	S	277.20
DL A135	887	0	2.40	S G	0.40	S G	5.60
DL A134	886	1	4.07	S G	1.55	S G	14.16
DL A133	884	0	0.22	S			
DL A132	883	5	0.70	S S	0.07	S S	0.49
DL A131	877	0	0.35	M S			
DL A130	876	2	1.15	S G	0.12	S S	1.31
DL A129	873	0	0.40	S S			
DL A128	872	5	0.20	S S			
DL A127	866	0	4.55	G E	0.95	S G	19.80
DL A126	865	0	0.25	S S			
DL A125	864	1*	14.65	G E	6.66	G E	170.27
DL A124b	862	1	0.40	S S	0.10	S S	0.15
DL A124a	862	1	0.50	S S	0.08	S S	0.24
DL A123	860	7	2.35	S G	0.12	S S	5.51
DL A122	852	27	3.95	S G	1.40	S G	13.64
DL A121	824	15	0.27	S S	0.45	S S	-0.13
DL A120	808	6	0.85	S G	0.25	S S	0.66
DL A119	801	0	1.40	S G	0.92	S G	1.11
DL A118	800	21	0.60	S S	0.04	S S	0.36
DL A117	778	5	1.45	S G	0.50	S G	1.85
DL A116b	772	0	0.20	S S			
DL A116a	772	0	2.40	S G	0.65	S G	5.34
DL A115	771	0	1.55	S	0.35	S	2.28
DL A114	770	3	3.80	S	0.43	S	14.26
DL A113	766	6	0.40	S S	0.10	S S	0.15
DL A112	759	1	1.40	S G	0.15	S S	1.94
DL A111	757	0	1.45	S G	0.25	S S	2.04
DL A110	756	0	0.20	S S			
DL A109	755	1	0.30	S S			
DL A108b	753	0	1.70	S G	0.10	S G	2.88
DL A108a	753	0	0.45	S S	0.05	S S	0.20
DL A107	752	0	5.43	S G	1.10	S G	28.27
DL A106	751	1	0.50	S S			
DL A105	749	0	0.50	S S	0.04	S S	0.25

DOI: 10.2312/GFZ.b103-07065

DL A104b	748	0	0.20	S			
DL A104a	748	0	0.40	S S	0.02	S S	0.16
DL A103	747	1	1.40	S G	0.10	S S	1.95
DL A102	745	1	1.05	S G	0.12	S G	1.09
DL A101	743	0	0.30	S			
DL A100	742	0	0.40	S G			
DL A99	741	0	4.83	S G	0.68	S G	22.87
DL A98	740	8	10.79	S G	1.58	S G	113.93
DL A97	731	0	1.10	S G	0.15	S S	1.19
DL A96	729	2	1.30	S G	0.05	S S	1.69
DL A95	727	0	0.30	S S	0.02	S S	0.09
DL A94	726	4	1.34	S G	0.05	S S	1.79
DL A93	721	1	6.75	S G	2.17	S G	40.85
DL A92	719	11	0.65	M S	0.50	M S	0.17
DL A91	707	20	1.93	S G	1.60	S G	1.16
DL A90	686	23	0.40	S S	0.15	S S	0.14
DL A89	662	4	0.90	S	0.20	S	0.77
DL A88	657	0	1.15	S G	0.23	S S	1.27
DL A87	656	1	3.25	S G	0.40	S G	10.40
DL A86	654	0	0.20	S S			
DL A85	653	0	0.35	S	0.10	S	0.11
DL A84	652	1	0.43	S	0.07	S	0.18
DL A83	650	0	2.20	S G	0.33	S S	4.73
DL A82	649	1	12.40	M S	10.57	M S	42.04
DL A81	647	9	5.35	S G	1.82	S G	25.31
DL A80	637	4	0.40	S S	0.04	S S	0.16
DL A79b	632	0	0.27	S S			
DL A79a	632	0	2.70	S G	1.10	M S	6.08
DL A78	631	0	0.90	S S	0.25	S S	0.75
DL A77	630	6	0.50	S			
DL A76	623	5	0.70	S G			
DL A75	617	0	3.95	S G	0.60	S S	15.24
DL A74	616	0	0.32	S G			
DL A73b	615	0	0.50	S S			
DL A73a	615	0	0.25	S S			
DL A72	614	0	0.90	S G			
DL A71	613	0	0.40	S W	0.05	S W	0.16
DL A70	612	12	2.85	S G	0.25	S S	8.06
DL A69b	599	0	0.25	S S			
DL A69a	599	0	0.80	S S	0.20	S S	0.60
DL A68	598	7	0.32	S			
DL A67	560	0	0.60	S G			
DL A66	589	2	0.30	S S	0.07	S S	0.09
DL A65	586	7	1.60	S	0.15	S	2.54
DL A64	578	4	6.00	S G	2.23	S G	31.03
DL A63	573	1	0.35	S			
DL A62c	571	2	3.35	M S			
DL A62b	571	2	0.37	S S	0.05	S S	0.13
DL A62a	571	2	3.08	S G	0.91	S G	8.66
DL A61	568	1	0.30	S S			
DL A60	566	1	0.27	S W			
DL A59	564	0			0.65	M S	
DL A58b	563	0			0.20	M S	

DOI: 10.2312/GFZ.b103-07065

DL A58a	563	0			0.20	M S	
DL A57	562	3	0.40	S S			
DL A56b	558	0	6.05	S G			
DL A56a	558	0	4.70	M S	2.42	M S	16.23
DL A55	557	0	1.30	S G	0.03	S S	1.69
DL A54	556	0	0.20	S S	0.02	S S	0.04
DL A53	555	1	0.30	S S			
DL A52	553	2	0.70	S G	0.03	S S	0.49
DL A51	550	0	1.25	S G			
DL A50	549	4	0.20	S S			
DL A49	543	2	0.90	M S	2.88	M S	7.48
DL A48	541	10	0.40	S S	0.07	S S	0.16
DL A47	530	2	0.50	S S	0.06	S S	0.25
DL A46b	527	1	0.55	S S			
DL A46a	527	1	1.75	S S	0.05	S S	3.06
DL A45	525	5	0.20	S S			
DL A44	519	3	0.70	S S	0.20	S S	0.45
DL A43	515	3	0.90	S G			
DL A42	510	1	2.50	S G	0.15	S S	6.23
DL A41	509	0	1.50	S S	0.06	S S	2.25
DL A40	508	1	1.78	S G	0.14	S S	3.15
DL A39	506	0	1.85	S G	0.05	S S	3.42
DL A38	505	0	0.37	S			
DL A37b	504	1	0.35	S S	0.05	S S	0.12
DL A37a	504	1	4.80	S	0.68	S	22.58
DL A36	502	2	0.32	S S	0.10	S S	0.09
DL A35	499	2	1.81	S G	0.10	S S	3.27
DL A34	496	0	0.28	S S	0.04	S S	0.08
DL A33	495	0	0.83	S			
DL A32	494	0	3.95	S G	0.60	S G	15.24
DL A31	492	4*	0.65	S S			
DL A30	488	1	0.70	S G			
DL A29	486	0	1.95	S G	0.09	S S	3.79
DL A28	485	3	0.70	S S			
DL A27	481	0	5.36	S G	0.50	S G	28.48
DL A26	480	2	0.62	M S			
DL A25	477	1	0.30	S S	0.02	S S	0.09
DL A24	475	1	0.30	S S			
DL A23	473	1	0.50	S S	0.12	S S	0.24
DL A22	471	1	0.50	S S			
DL A21	469	22	0.50	S S	0.10	S S	0.24
DL A20	446	2			0.36	S W	
DL A19	443	1	0.06	S S	0.30	S S	-0.09
DL A18	441	7			0.70	M S	
DL A17	433	5	1.50	S S	0.45	S S	2.05
DL A16b	427	3	1.83	S S	0.15	S S	3.33
DL A16a	427	3	0.60	S S	0.10	S S	0.35
DL A15	423	14	0.20	S W	0.37	S W	0.10
DL A14	408	15	0.05	S S	0.25	S S	-0.06
DL A13	392	36	0.05	S S	0.25	S S	-0.06
DL A12	355	14	0.13	S S	0.33	S S	-0.09
DL A11	340	16	0.15	S S	0.40	S S	-0.14
DL A10	323	14			0.20	S W	

DOI: 10.2312/GFZ.b103-07065

DL A9	308	77			0.35	M S	
DL A8	230	20*	0.06	S S	0.20	S S	-0.04
DL A7	209	8	0.05	S W	0.35	S W	-0.12
DL A6	200	32	1.50	M S			2.25
DL A5	167	53			0.70	M S	
DL A4	113	45	0.45	S S	0.90	S S	-0.61
DL A3	67	40	5.00	M S	13.27	M S	-151.09
DL A2	26	4			2.30	M S	
DL A1	21	20			0.40	M S	
TEPHRA	0		6.60		9.29		

DOI: 10.2312/GFZ.b103-07065